The Hong Kong Polytechnic University

Department of Applied Biology and Chemical Technology

Development of Novel Biodegradable Core-Shell Nanoparticles as Carriers for Gene Delivery

---

HETTI Mimi

A Thesis Submitted in Partial Fulfillment of the Requirements

for the Degree of Master of Philosophy

August 2009

CERTIFICATE OF ORIGINALITY

I hereby declare that this thesis is my own work and that, to the best of my knowledge and belief, it reproduces no material previously published or written, nor material that has been accepted for the award of any other degree of diploma, except where due acknowledgement has been made in the text.

_____

HETTI Mimi

August 2009

ABSTRACT

Highly uniform gelatin/poly(ethyleneimine) (gelatin/PEI) core-shell nanoparticles that are composed of biodegradable gelatin cores and cationic branched polyethylenimine (PEI) shells were designed and successfully synthesized. The highly uniform gelatin microgels were firstly prepared through thermal denaturation, followed by covalent linkage of the branched PEI polymer (Mw 25 kD) onto the preformed gelatin microgels via coupling reaction using *N*-ethyl-*N*′-(3-dimethylaminopropyl)carbodiimide (EDC). The gelatin core-to-PEI shells weight ratio was varied by adding different amount of PEI and changing the reaction pH. After purification by ultrafiltration, the gelatin/PEI nanoparticles were treated with an appropriate mixture of ethanol/water solution to generate gelatin/PEI nanoparticles with well-defined gelatin cores and PEI shells. The resultant nanoparticles had hydrodynamic sizes ranging from 196 to 424 nm in diameter with surface charges between +47 to +64 mV depending on the PEI content and ethanol concentration. By varying the reaction pH and amount of PEI added, the PEI contents of the nanoparticles could be controlled between 25 and 65%. Transmission electron microscopy images revealed that the nanoparticles had a well-defined core-shell nanostructure.

Application of the gelatin/PEI core-shell nanoparticle as a potential gene carrier was explored. It was found that the nanoparticles were able to completely condense plasmid DNA and siRNA at N/P ratios of 2 and 5, respectively. The condensed gene molecules could be effectively released from the nanoparticles through polyelectrolyte exchange reaction with poly(aspartic acid). The integrity of the gene molecules was preserved during these complexation and release processes. In addition, the nanoparticles were able to protect the condensed pDNA and siRNA from enzymatic degradations.

In vitro studies revealed that the gelatin/PEI nanoparticles could deliver argininosuccinate synthetase (ASS) gene targeting siRNA to the HeLa cells to perform gene silencing. After transfection of the siRNA/nanoparticle complexes to the cells for about one day, the percentage knock-down of ASS-mRNA level was as high as 70%. The confocal laser scanning microcopic studies indicated that the core-shell nanoparticles were effective in delivering siRNA to both the cytoplasm and nuclei of HeLa cells. The flow cytometry studies also suggested that the percentage of cellular uptake of the complexed siRNA was as high as 94.7% while the native siRNA were failed to enter to the cells. The results of MTT assay showed that cytotoxicity of the nanoparticles was lower than that of the native PEI polymer. Results from these

studies show that our gelatin/PEI core-shell nanoparticle is a promising candidate for non-viral gene delivery.

PUBLICATION LIST

1. Hetti Mimi, Aihua Wu, Pei Li. "Novel Biodegradable Gelatin/PEI Core-Shell Nanoparticles as Potential Gene Carriers". *Abstract of Papers*, 36thAnnual Meeting and Exposition of the Controlled Release Society, Copenhagen, Denmark, July 18-22, 2009.
2. Hetti Mimi, Aihua Wu, Pei Li. "Novel Biodegradable Core-Shell Nanoparticles as Carriers for Gene Delivery". *Abstract of Papers O-77*, the 16th Symposium on Chemistry Postgraduate Research in Hong Kong, Hong Kong Baptist University, April 18, 2009.
3. Hetti Mimi, Aihua Wu, Pei Li. "Novel Biodegradable Core-Shell Nanoparticles as Carriers for Gene and Drug Deliveries". *Abstract of Papers*, International Symposium of "Frontiers in Biomaterials-Based Drug and Gene Delivery", National Cheng Kung University, Tainan City, Taiwan, February 27, 2009.
4. Hetti Mimi, Aihua Wu, Pei Li. "Development of Novel Biodegradable Core-Shell Nanoparticles as Carriers for Gene and Drug Deliveries". *Abstract of Papers P-22*, the 15th Symposium on Chemistry Postgraduate Research in Hong Kong, The University of Hong Kong, Apr. 26, 2008.

ACKNOWLEDGMENTS

First and foremost, I would like to express my deepest gratitude to my chief supervisor, Dr. Pei Li, Associate Professor, Department of Applied Biology and Chemical Technology, The Hong Kong Polytechnic University, for her generous guidance, supervision and very useful advices throughout my study and her invaluable comments and revisions of this thesis. She also gave me chances to attend international conferences to widen my knowledge. It is a valuable experience for me under the supervision of Dr. Li.

I also like to deliver my thankfulness to Dr. Yung-chung Leung, Associate Professor, Department of Applied Biology and Chemical Technology, The Hong Kong Polytechnic University, and his research team members, especially Dr. Alan Lam and Miss Sandra Siu, for their valuable advices, discussion and technical support in biological area.

I also like to thank my group members, Dr. Kin-man Ho, Dr. Wei-ying Li, Dr. Ai-hua Wu and Mr. Lee Cheng-hao, for their useful suggestion and incessant discussion throughout the whole project and friendship. Especially, I thank Mr. Lee Cheng-hao

very much as he helped me to do all of the transmission electron microscopy.

I would also like to thank all of the technical staffs of the Department of Applied Biology and Chemical Technology at The Hong Kong Polytechnic University, especially Miss Sarah Yeung, who help me lots for the confocal laser scanning microscopy.

In addition, I would like to thank my entire family for their loves, meticulous nursing, encouragement and mental support throughout my study.

Finally and but the last, I gratefully Lo Ka Chung Centre for Natural Anti-Cancer Drug Development for the financial support of this project.

TABLE OF CONTENTS

ABBREVIATIONS AND SYMBOLS

Abbreviations

ASS	Argininosuccinate synthetase
ADI	Arginine deiminase
AGE	Agarose gel electrophoresis
cDNA	Complementary deoxyribonucleic acid
CLSM	Confocal laser scanning microscopy
DIC	Differential interference contrast
DMEM	Dulbecco's modified Eagle's medium
DNase 1	Deoxyribonuclease I
EDC·HCl	*N*-Ethyl-*N*′-(3-dimethylaminopropyl)carbodiimide hydrochloride
EDTA	Ethylene diaminetetraacetic acid
EtBr	Ethidium bromide
HCl	Hydrochloric acid
FBS	Fetal bovine serum
FITC	Fluorescein isothiocyanate
GAPDH	Glyceraldehyde 3-phosphate dehydrogenase
HeLa	Human cervix adenocarcinoma
MTT	(3-[4,5-dimethylthiazol-2-yl]-2,5-diphenyl tetrazolium bromide)
mRNA	Massager ribonucleic acid
N/P	Nitrogen-to-phosphate
NP	Nanoparticle
pAsp	Poly(L-aspartic acid)
PBS	Phosphate buffered saline
PDI	Poly dispersity index

pDNA	Plasmid deoxyribonucleic acid
P/S	Penicillin-streptomycin
PCR	Polymerase chain reaction
PEI	Polyethylenimine
PTA	Phosphotungstic acid
RNAi	Ribonucleic acid interference
rpm	Rate per minute
RT	Reverse transcriptase
SDS	Sodium dodecyl sulfate
SEM	Scanning electron microscopy
siRNA	Small interfering ribonucleic acid
TEM	Transmission electron microscopy
TGA	Thermogravimetric analysis
TNBS	2,4,6-trinitrobenzenesulfonic acid
UV/VIS	Ultra-violet/visible

Symbols

Å	Angstrom or 1×10^{-10} meter
D_v	The volume average of particle diameter
D_n	The number average of particle diameter
M	Molarity or mole/L
pI	Isoelectric point
T_g	Glass-rubber transition temperature
T_m	Thermal unfolding temperature
λ	Wavelength
ζ	Zeta
$Z_{average}$ (Z_{ave} in abbreviation)	Hydrodynamic diameter

1 Introduction

Nowadays, nanoparticles with different materials, sizes, morphologies, nanostructures etc, are developed and are widely applied in biomedical fields. Their applications include biodetections,[6] biomaterial coatings, bioimaging,[2] biosensing,[7] bioseparations, chromatography, diagnosis,[1,5] drug deliveries,[3-4] gene deliveries, immobilizing biocatalyst, protein analysis in microfluidic systems,[8] and remediation of overdosed toxins. In this study, a novel kind of core-shell nanoparticle, which is comprised of a biodegradable core and a branched polyethylenimine shell, has been developed and its application in gene delivery was systematically investigated.

1.1 Background of gene therapy

Haemophilia, Mendelian diseases, Huntington's disease, and Muscular Dystrophy are some of the examples of hereditary diseases due to genetic disorders of human genes.[9] The aim of gene therapy is to deliver therapeutic nucleic acids to correct a malfunctioning gene, non-expressed gene or to supplement the production of a natural occurring protein.[10,11] Effective new delivery strategies may provide permanent cures of the genetic diseases and greatly improve patients' satisfaction by preventing repeated injections of required proteins for prolonged period of time.

Traditional treatment methods of Severe Combined Immunodeficiency (SCID) are bone marrow transplantation and enzyme replacement therapy. The chance of having match donors for bone marrow transplantation is extremely rare. Alternatively, the cost of weekly injection of the polyethylene glycol adenine deaminase (PEG-ADA) to the patients' body to replace the abnormal enzymes is very expensive. Besides, it can only have temporary effects and have low efficiency. The first ADA gene therapy of curing SCID was performed in 1990.[12] In this therapy, five patients, who suffered from matastatic melanoma were treated through taking out the tumor-infiltrating lymphocytes and inserting with the missing gene by retrovirus. After putting the genetically modified cells into the patients' bodies, the cells were consistently found in the circulation of all patients with the absence of infectious virus.

Generally, there are two kinds of therapeutic genes according to their intracellular actions. The first kind is plasmid DNA. Plasmid DNA (pDNA) is a closed circular double strand DNA present in bacteria. It is usually inserted with a specific protein-encoded-gene, which is capable of expressing a specific gene upon successive localization (or even integration) at the nuclei. The administration of pDNA is to supply the particular protein-encoded-DNA, which is under-expressed in the patients' body so that the particular protein can be expressed in normal level in the patients' body. The genetically modified pDNA is firstly inserted into some micro-organisms, such as bacteria and yeast, to allow replications of the pDNA. After that, the pDNA is isolated and purified for gene delivery.

The second kind is RNA interference (RNAi) or antisense RNA, which are artificially synthesized with the sequences homologous to the silenced gene.[13] It can bind to the particular messenger RNA (mRNA) and down-regulate the protein level by mRNA degradation. It can be further divided into three categories, which are single-stranded antisense oligonucleotides (ODNs), ribozymes and small interfering ribonucleic acid (siRNA). [14-15] ODN is an 18 – 25 bps long single stranded nucleic acids.[16] It cleaves target mRNA by hybridizing to the corresponding mRNA through Watson-Crick binding. [17] Ribozymes compose of three RNA helices, which form three dimensional catalytically active RNA. It cleaves single stranded regions in RNA through trans-esterification or hydrolysis reaction.[17, 18] The siRNA is 19 – 25 bps long double stranded nucleic acids. It unwinds its duplex to enable recognition of the mRNA and incorporates with the RNA-induced silencing complex (RISC) to degrade the bound mRNA.[17, 19]

1.2 Gene delivery systems

Gene therapy requires successful cellular uptake of the gene, followed by high level of gene expression of the encoded proteins or gene silencing of the target gene. However, the gene therapy has several challenges: 1) The cellular uptake of the therapeutic entities is often very low as they are highly susceptible for enzymatic degradations. 2) Lack of specificity to target cells and intracellular compartments. 3) Poor in tissue penetration, resulting in low transfection efficiency. 4) Possible stimulation of non-specific immune response.[70] 5) The large molecular weight of therapeutic plasmid DNA and polyanionic nature of the nucleic acids also contribute to the barriers of cellular uptake. Therefore, an

effective gene delivery system is highly desirable and the prerequisites of ideal gene delivery systems are summarized below.

I. Safety concern is the first priority of all materials applied in human bodies. An ideal gene delivery vector should be non-immunogenic, non-mutagenic and biocompatible to prevent side effects related to the delivery vectors, such as immune response, cytotoxicity and causing mutagens to the host genome.

II. In addition, protection ability is also very important. The wide range of active substances in the bloodstreams, such as serum proteins, serum nucleases and organic and inorganic small ions, can damage the integrity of injected DNA substances. Naked DNA molecules can undergo rapid clearance in the presence of DNase I. Therefore, an ideal gene carrier should give efficient protection to the DNA molecules before the DNA molecules are internalized and reached target sites. The carrier itself should be stable in the bloodstream and are capable of preventing too early release of the protected DNA, resulting in a prolonged and sustained release of DNA molecules.

III. Other than the protection ability, an ideal gene carrier should play a role to overcome the intercellular and intracellular barriers and deliver specifically to the target sites to maximize the function of the therapeutic genes. Thus, the gene carriers should be optimized to give targeting ability for the target cells specifically, mask the anionic nature of DNA molecules, transport through the cell

membrane and be internalized, be degraded in the endosomes to release the trapped DNA molecules, guide intracellular trafficking of the exogenous DNA molecules to the nuclei or other target organelles, such as ER and mitochrondria[14] and finally can be removed from the cells by exocytosis to prevent accumulation of waste materials. The steps involved in cytosolic gene delivery by nanoparticular gene carrier are show in Figure 1.1.[15, 78]

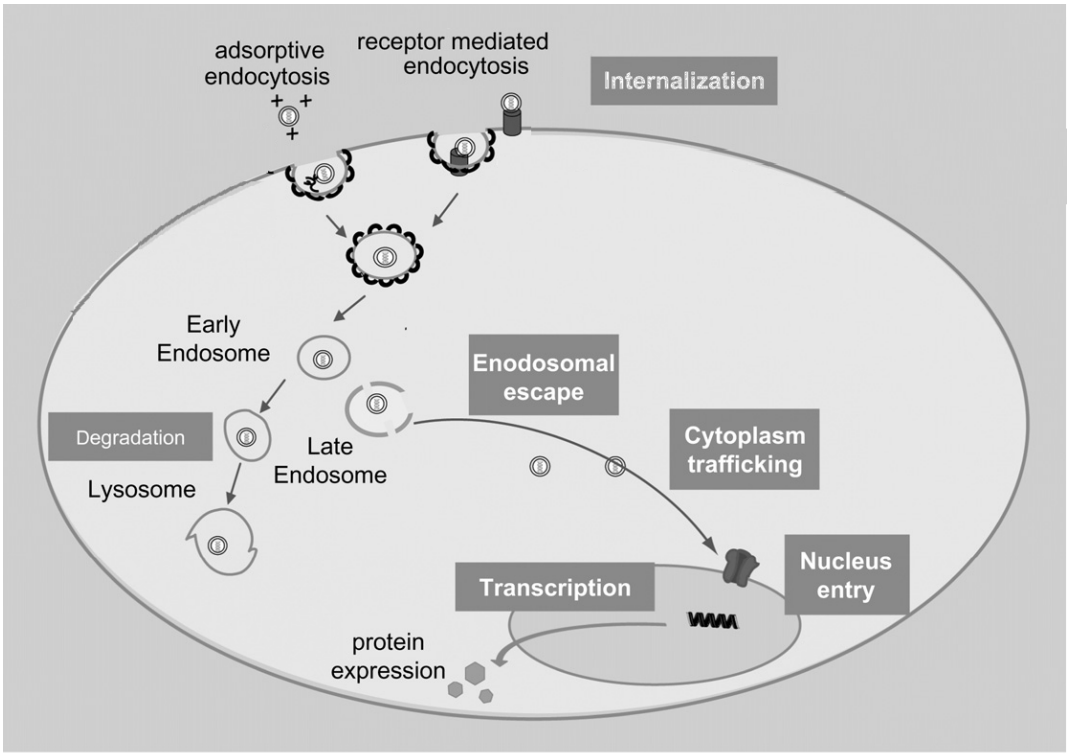

Figure 1.1. Schematic drawing of steps involved in cytosolic delivery of therapeutics using polymeric nanoparticles.[15, 78]

IV. Others included high level of gene expression of the protein or gene silencing of the RNAi, easy to handle, store, and manufacture in large scales.[16]

The current gene delivery systems include physical transfection systems, viral and non-viral gene carries.

Physical methods

Physical transfection involves transfer of exogenous nucleic acids into host genome via physical means and no gene carrier is involved. Gene gun, electroporation, iontophoresis, microinjection and ultrasound mediated gene transfer are some of the common transfection techniques.[21] Gene gun involves shooting gold or tungsten bullets conjugated with DNA molecules into target cells. However, there is a problem of waste accumulation of the used metal "bullets". Electroporation relies on application of short electric pulses to temporary destabilize cell membrane and generate pores for entry of the DNA materials. Iontophoresis makes use of a low density electric current to promote penetration of charged DNA molecules. This technique is non-invasive with lesser damage. But the transfection efficiencies of electroporation and iontophoresis depend on the size of the input DNA.

The advantages of physical transfection systems include low operating cost, easy to handle, non-immunogenic, and high transfer efficiency. They are also simple and straight forward methods to transfer DNA molecules. However, all of them can only be applied in *ex vivo* [22] way or in superficial tissues, such as ocular tissues.[21] In addition, several physical treatments can cause damage to the cells and their internal organelles.

Viral transduction systems

In preparing the viral vectors, the elements of the viral genome related to its infectivity are retained while those of replication and disease are removed, and the gene of interest is inserted. When the genetically modified viruses are put into the cell cultures or animal bodies, the viruses will infect target cells as the same way as its infection cycles: attach to the host cell surface that are presence of specific receptor, insert the viral genome and make use of the materials of host cell for the expression of the therapeutic gene.[22,23] Several kinds of viruses that are commonly applied in *in vivo* tests and clinically used involve retrovirus, adenovirus, adeno-associated virus, herpes simplex virus and lentivirus.

Gene transfer using viral vectors is regarded as a very effective way compared with the non-viral ones due to the sophisticated mechanisms that viruses developed to overcome the intracellular barriers and deliver the gene to cell nuclei.[24] Although viral vectors are more efficient in gene transfer, and have much high levels of sustained transgene expression, they are expensive to produce. In addition, there is a potential risk that the viral vectors are mutagenic to the host genome and cause inflammatory responses.

Non-viral transfection systems

With respect to the safety and production concerns of the viral vectors, non-viral transfection systems have been receiving increasing attention in gene therapy, and have

become attractive alternatives. A wide range of non-viral gene transfection systems, constructed of different materials with different sizes, morphologies, properties and interactions, have been developed up to now. Protein, polycations, liposomes, nanoparticles and synthetic agents are some of the examples. [21]

Although viral vectors can overcome the intracellular barriers for effective gene delivery, they generally have low gene transfection efficiency and short duration of expression. To address thesis drawbacks, the non-viral vectors should be specially designed to overcome the intracellular barriers, to maximize the level of gene expression or gene silencing, cells and nucleus targeting abilities and biocompatibility while to minimize cytotoxicity, immunogenicity, accumulation of waste materials and other adverse effects to the patients.

1.3 Current designs of different non-viral gene carriers and their functions

The development of gene delivery vectors began with viral types owing to the high transduction efficiency by the infection mechanism of virus. However, the focus is switching to non-viral types at later stage mainly due to safety concern. The non-viral gene carriers are free of viral genome, biologically and immunogenetically safe. Since the transfection efficiency is lower than the viral vectors, current designs and developments of non-viral vectors focus on improving the transfection efficiency. Besides, some of the candidates have high functionality and have high potential to be modified with targeting ligands for target specific delivery or stabilizing components to improve their *in vivo* stability. Some of the materials themselves are also external stimuli responsive for

controlled gene release and endosomal escape. Other advantages of the particles included low cost, ease of production and possible for large scale production in clinic use.

There are large varieties of non-viral vectors which have been successfully developed. Some of them even showed promising results *in vivo*. Examples included liposomes, block copolymer micelles, nanoparticles, dendrimers and nanocapsules. The materials, such as natural biopolymers, synthetic cationic polymers, acid- or bio-degradable polymers, neutral non-condensing polymers, surfactants, polysaccharides and peptides are often used for the synthesis.

1.3.1 Liposomes

Cationic lipid based liposomes relies on electrostatic interactions between negatively charged DNA molecules and cationic groups of lipid molecules to form stable liposome/DNA complex, named lipoplex. The cationic lipids facilitate fusion of the lipoplexes with the cell membranes and resulting in cellular uptake. After internalization, endosomal membrane is destabilized by the liposomes and is resulted in anionic phospholipid flip-flop. (Step 3, Figure 1.2) The anionic lipids diffuse into the complex and form a charge neutral ion pair with cationic lipids. Thus, the DNA molecules are escaped from the endosome and into cytoplasm. [25, 26, 75] The schematic illustration of cell internalization and endosomal escape is shown in Figure 1.2.

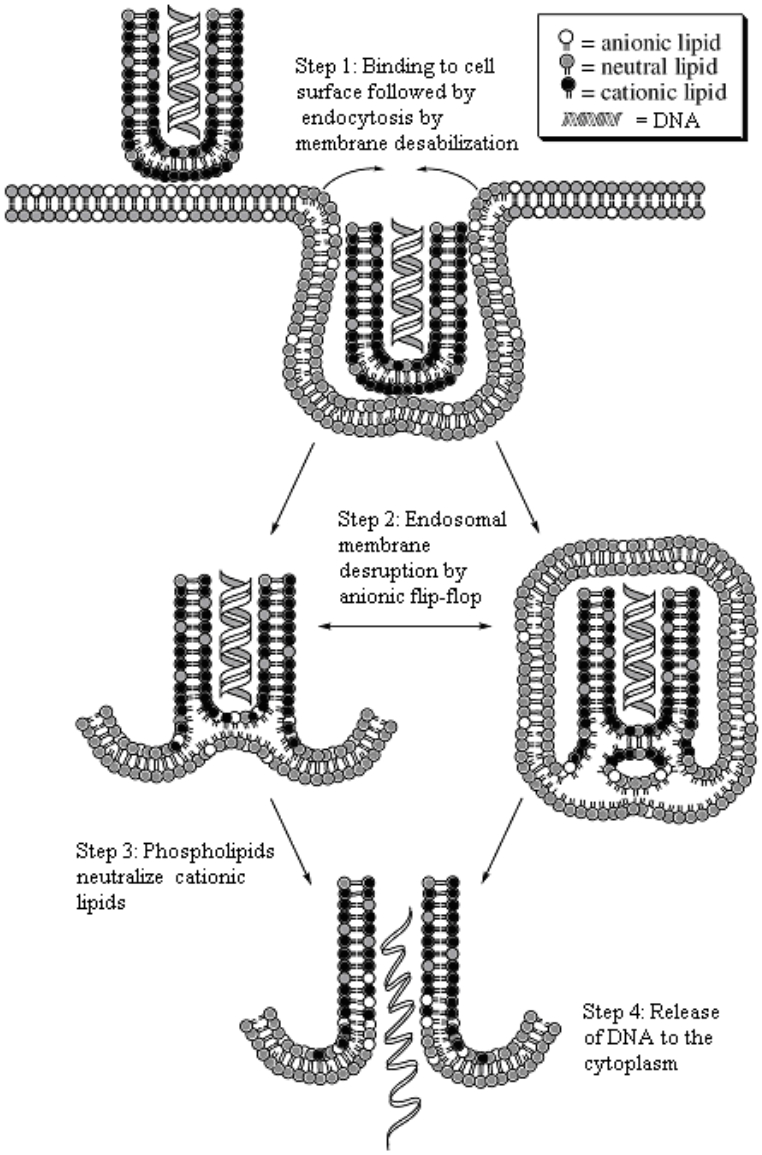

Figure 1.2. Mechanism of uptake and release of plasmid DNA from the lipoplex.[26, 75]

The liposomes offer biocompatibility, low toxicity and possibility of large-scale production for clinical applications. Lipofectamine® and Lipofectin® are two of the commercially available liposomes. Figure 1.3 shows the structures of some of the cationic lipids.

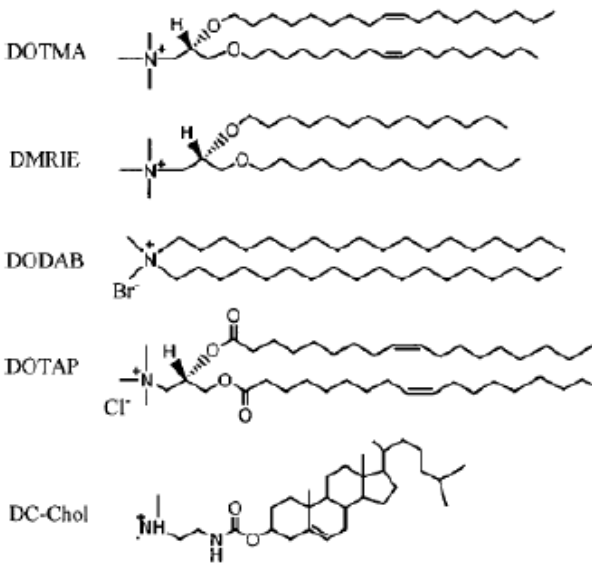

Figure 1.3. Chemical structures of some cationic lipids used in gene delivery.

Felgner *et al* have performed DOTMA-mediated transfection of cells, called lipofection.[27] The cationic lipid, *N*-[1[(2,3,-dioleyloxy)propyl]-*N,N,N*-trimethylammonium chloride (DOTMA) was synthesized by mixing of 3-(dimethylamino)-1,2-propanediol, potassium *tert*-butoxide and oleyl *p*-toluenesulfonate in xylene and refluxing (140^{o}C) for 3 h, followed by concentrating by chromatography over silica gel.[27] DNA condensation was achieved by mixing the lipids and pDNA to form stable lipoplex. And fusion of the liposomes with cell membrane of two monkey kidney cell lines, CV-1 and COS-7 cells, was observed by Fluorescence microscopy.

However, many reports have pointed out that the injected liposome/DNA complexes are instable *in vivo* and form large aggregates with blood components, like serum proteins, and are instable in high liposome concentrations.[28, 29] To overcome this, non-ionic surfactants or lipids are added in the liposome formulation.

Seok *et al* developed a cationic lipid-based emulsion (CLE) prepared by an oil-in-water (O/W) emulsion method, aiming to reduce aggregation with blood components and enhance *in vivo* stability by addition of natural oil as the core.[28] After dissolving in chloroform and drying into a film, the cationic emulsifier 1,2-dioleoyl-*sn*-glycero-3-trimethylammonium-propane (DOTAP) was dissolved in aqueous solution and added into squalene oil to form the oil-in-water emulsion. Upon simple mixing, the plasmid DNA molecules were condensed on the cationic surface of the emulsion. The liposomes are able to fully complex the pDNA at cationic lipid to DNA (C/D) ratio of 2. The pDNA loaded liposomes with C/D ratio of 4 have about 200 nm hydrodynamic diameters and about +50 mV of zeta potential were dictated for *in vitro* and *in vivo* gene transfections.

Obata *et al* have designed amino acid based lipids for plasmid DNA delivery. Three types of cationic head groups, including lysine, histidine and arginine, were synthesized in a series of complicated procedures summarized in Scheme 1.1.[25] Briefly, glutamates with different length of hydrophobic moieties were synthesized, followed by conjugation of the cationic head groups of lysine, histidine or arginine.

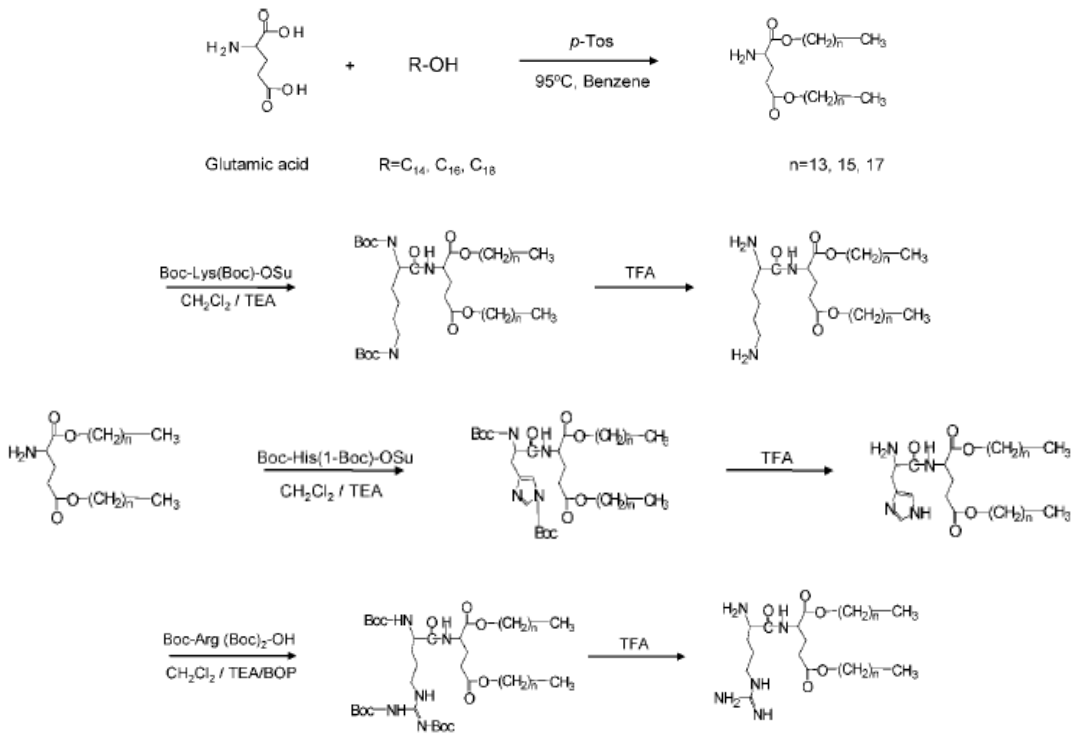

Scheme 1.1. Synthesis of amino acid amino acid based lipids for plasmid DNA delivery.[25]

The lysine- and arginine type lipid assemblies appeared as unilamellar vesicles of about 100 nm in diameter observed by the TEM, while histidine are in tube-like nanostructure. In addition, the condensation ability and gene expression efficiency of the lysine- and arginine-type lipids are better than that of histidine (the cationic lipid-to-DNA (C/D) ratio for fully complexation of lysine- and arginine-type were 3, while that of histidine was 5). The arginine type lipids form complex with pDNA to generate lipoplexes with hydrodynamic diameter of about 150 nm, and surface charge of about +25 mV at a C/D ratio of above 5. Although the zeta potentials of the lysine-type lipoplexes are higher (+25 to 40 mV at C/D ratio of 5-50), the large particle sizes (>400 nm) at low C/D ratios (below 20) show that the lipoplexes have certain degree of aggregation. It was also

observed that the membrane fusogenic ability of the lipids increased with decreasing of the length of the alkyl chains. Besides, the synthetic lipids showed much low cytotoxicity and higher gene expression comparing with Lipofectamine 2000.

1.3.2 Copolymer micelles

The block or graft copolymers that are composed of a cationic segment and a non-ionic hydrophilic segment have a distinct feature of associating anionic DNA molecules to form polyion complex micelles. The cationic segments of the copolymer interact with the ionic DNA molecules by electrostatic interaction to form the core of polyion complex while the hydrophilic segments are extended to form the shells (Figure 1.4). The extended hydrophilic polymers at the outer layer of the micelles give protection to the entrapped DNA molecules and maintain high colloidal stability while the neutral surface charge reduces interaction with the blood components.[30, 79]

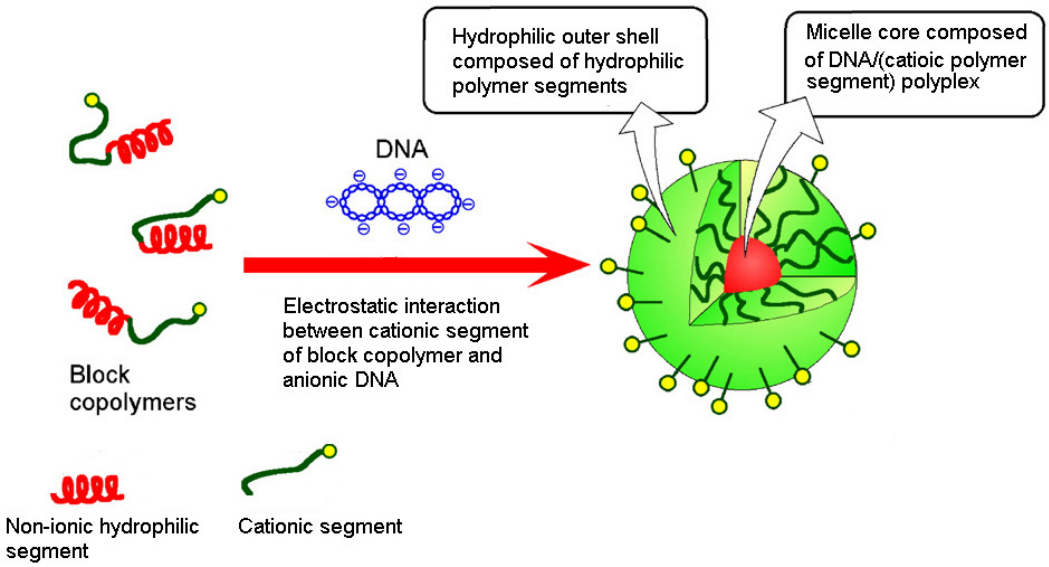

Figure 1.4. Formation of polyion complex micelles [79]

A typical example is copolymer of polyethylenimine and poly(ethylene glycol) copolymer (PEI-*co*-PEG). The monomethoxy PEG derivatized with *N*-hydroxysuccinimidyl ester group (PEG-NHS) was reacted with branched PEI by PEGylation to obtain the graft copolymers of PEI-PEG. [31] For the block copolymers, the heterotelechelic PEG macroinitiator (acetal-PEG-SO_2CH_3) was used. The methanesulgonyl end of the heterotelechelic PEG initiates oxazline polymerization.[30] After alkaline deprotection, the block form of PEG-PEI was formed with linear PEI segments. The synthetic method is shown in Figure 1.5.

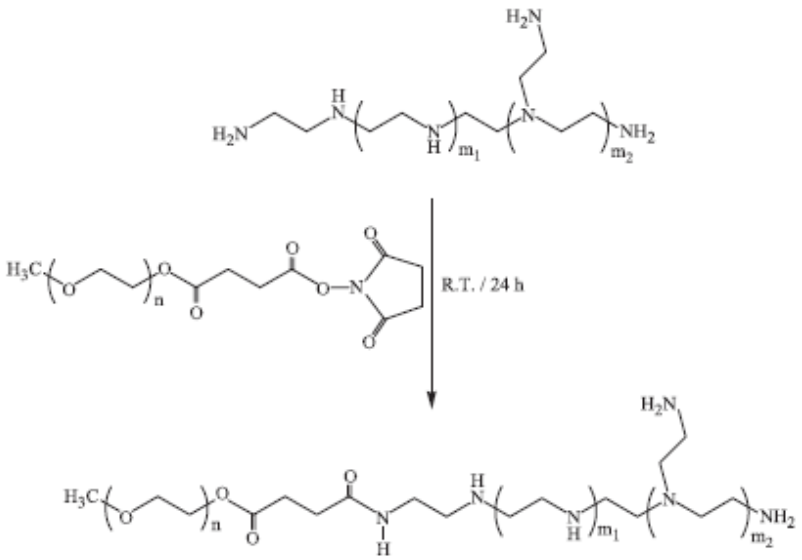

Figure 1.5. Synthesis of PEGlyated-PEI. [31]

The present of PEG reduced the zeta potentials of the polymer/DNA micelles from +19 mV to +10-17 mV at N/P ratio of 7, indicating mild shielding effect of PEG on positive surface. However, the condensation capacity is not as high as the original cationic polymers. The N/P ratio for complete pDNA condensation is above 7 (comparing with the N/P ratio of PEI of 2). On the other hand, the PEGylated PEIs showed significantly lower

cytotoxicity and higher transfection activity in COS-1 cells than PEI, because the corporation with PEG reduces the positive charge density of PEI and results in reduction of cell membrane disruption.

Pluronic® block copolymers are commercially available amphiphilic tri-block copolymer, consisting of hydrophilic ethylene oxide (EO) and hydrophobic propylene oxide (PO) blocks arranged in a triblock structure: EO_x-PO_y-EO_x. The chemical structure of is shown in Figure 1.6a. The molecular weight and degree of hydrophilicity can be altered by the number of EO and PO blocks.[27]

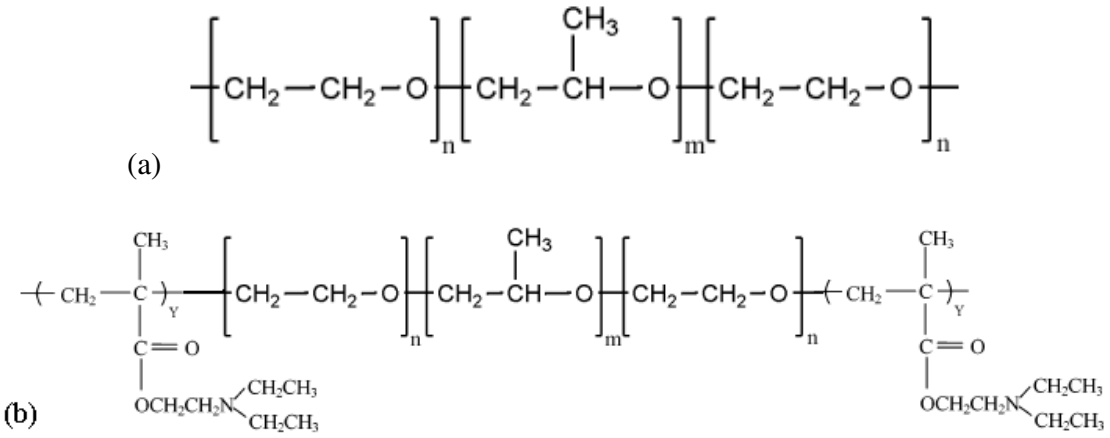

Figure 1.6. Chemical structure of (a) Pluronic® block copolymers and (b) PDEAM-PEO-PPO-PEO-PDEAEM pentablock copolymers.

Several groups have designed copolymer micelles by covalently attaching polycations onto Pluronic® chains. For example, Agarwal *et al* have developed cationic pentablock copolymers with short poly(diethylamino ethyl methacrylate) (PDEAEM) blocks covalently attached to Pluronic® block copolymers for long-termed sustained release of plasmid DNA for the SKOV3 human ovarian carcinoma cell line.[32] The pentablock

copolymer $PDEAM_8$-PEO_{100}-PPO_{65}-PEO_{100}-$PDEAEM_8$ was synthesize by an Atom Transfer Radical Polymerization (ATRP) via growing of DEAEM chains on both PEO ends of Pluronic F127. The chemical structure is shown in Figure 1.6b. It is reported that the pentablock copolymer exist as micelles in aqueous solution with Pluronic segments as the core and cationic PDEAEM segments as corona. For the preparation of hydrogel formulation, the pentablock copolymers were mixed with pDNA at an N/P ratio of 25 to form nanoplex by electrostatic attraction. Upon injecting the nanoplexes into tissue culture at 37^{o}C, the temperature sensitive nanoplexes self-assemble reversibly to form localized hydrogels in situ in response to the temperature increase. Slow dissolve of the hydrogels was observed (15 wt% of copolymers dissolved to release the nanoplex up to 5 days *in vitro*) and the electrostatically bound DNA molecules were released in nanoplex form, preserving the integrity of supercoiled pDNA. The neutral surface charge of the nanoplexes was measured, indicating that the cationic surface charge was shielded by the non-ionic Pluronic coating to prevent interaction with serum proteins. The procedures of nanoplexes and hydrogel formations and release of nanoplexes were summarized in Figure 1.7.

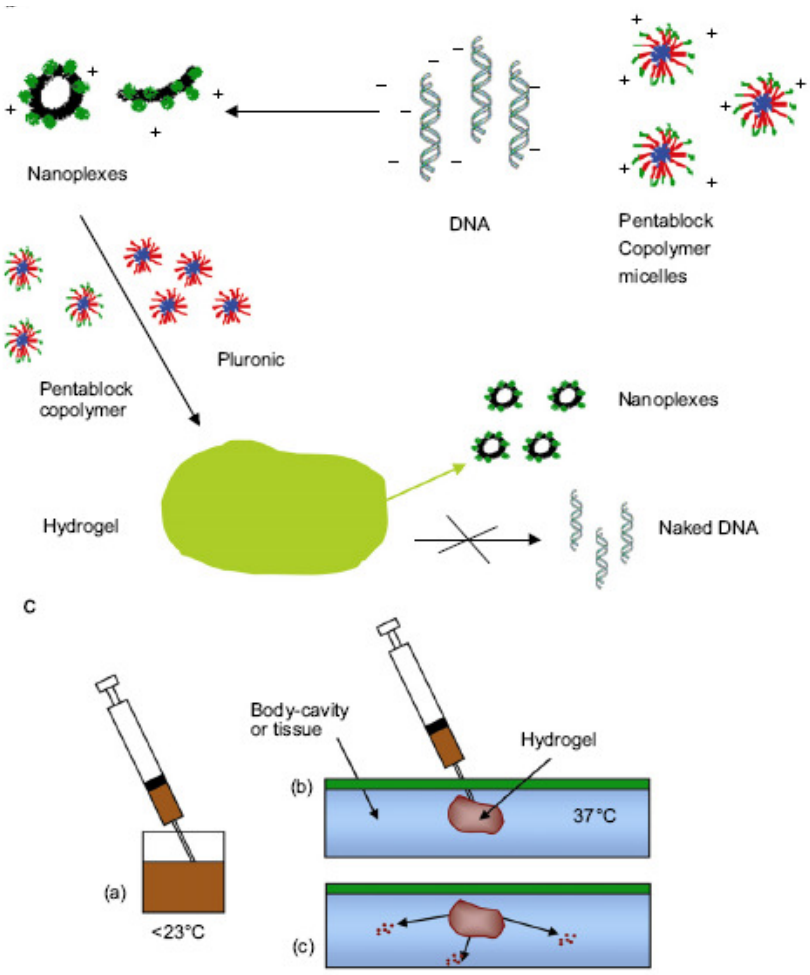

Figure 1.7. Schematic illustrations of nanoplex and hydrogel formations followed by release of complex form of pDNA by hydrogel dissolve. [32]

However, as the cationic segments are only a very small portion in the copolymer, larger amount of polymer is required to completely complex the pDNA. In addition, even though the pentablock copolymers have relatively narrow molecular weight distribution (M_w/M_n = 1.14), the resulting hydrodynamic diameter of the nanoplexs showed a large size distributions (150 – 650 nm).

Xu's group also designed another kind of pentablock copolymers of P(HEMA)-*b*-P(DMAEMA)-*b*-PEG-*b*-P(DMAEMA)-*b*-P(HEMA) (in which HEMA = 2-hydroxyethyl mathacrylate, DMAEMA = (2-dimethyl amino) ethyl methacrylate and EG = ethylene glycol) via consecutive atom transfer radical polymerization (ATRP) techniques. [33] Briefly, polymerization of DMAEMA was started on both ends of di-2-bromoisobutyryl-terminated PEG (Br-PEG-Br) to form P(DMAEMA)-*b*-PEG-*b*-P(DMAEMA) tri-block copolymers. After that, polymerization of HEMA was followed on bother ends of P(DMAEMA) chains to form the penta-block copolymers. The synthesis method and structure of the copolymers is illustrated in Figure 1.8. The cationic P(DMAEMA) segments are used to condense DNA molecules. The PEG segments reduce the surface charge density of the polymer/DNA complex to give anti-fouling effects and reduction of cytotoxicity. And P(HEMA) can provide biocompatibility to the polymer as its physical properties are similar to those of living tissues. Different from the pentablock copolymer micelles/pDNA nanoplexes prepared by the Agarwal's group, this kind of pentablock copolymers form micelles only when forming complex with pDNA. The copolymers have been applied in *in vitro* gene transfection of HEK 293 and COS7 cell lines.

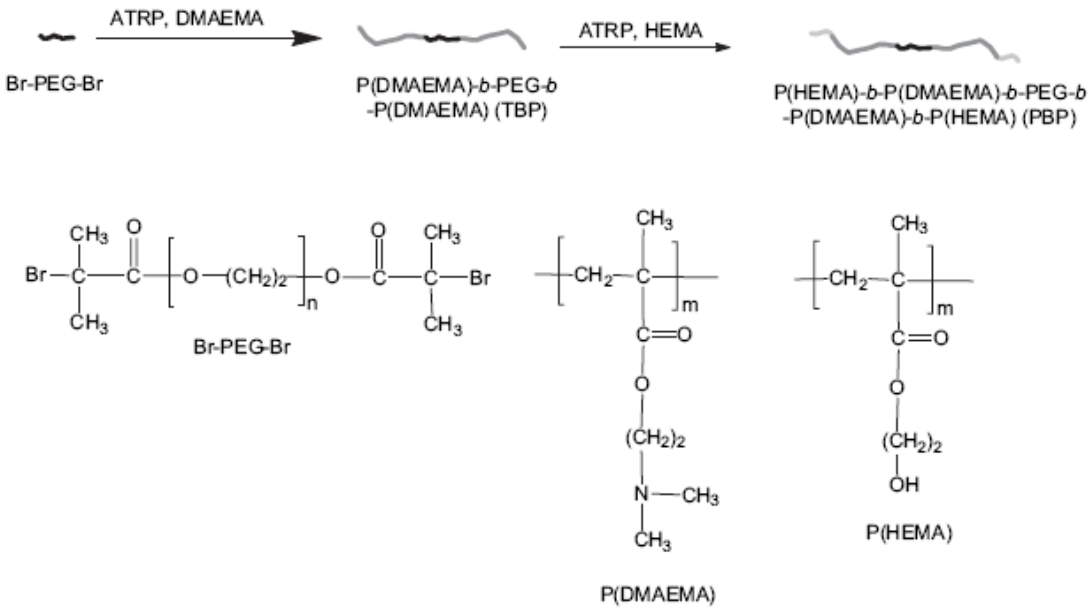

Figure 1.8. Schematic illustrations of the synthesis and structure of P(HEMA)-*b*-P(DMAEMA)-*b*-PEG-*b*-P(DMAEMA)-*b*-P(HEMA) (in which HEMA = 2-hydroxyethyl mathacrylate, DMAEMA = (2-dimethyl amino) ethyl methcarylate and EG = ethylene glycol) copolymers. [33]

The polydispersity index of the copolymers increases with molecular weight and number of blocks. Though the block copolymers can effectively complex with plasmid DNA with small particle sizes (hydrodynamic diameter of 100-160 nm) and high positive surface charges (zeta potentials of +25 to 35 mV) at polymer to pDNA weight ratio of 5 to 25, the capability to condense with pDNA is not as high as that of PEI. The polymer to pDNA weight ratios to reach complete condensations was between 1.5 and 3 depending on DMAEMA density in comparison with 0.5 for the PEI.

1.3.3 Synthetic cationic polymers

Synthetic cationic polymers, such as polyethylenimine, poly(L-lysine)[34, 35], poly(disulfide amine),[36] poly(L-histidine),[37] polyamidoamine (PAMAM)[38] and poly(ester amide)[39] have very high positive charge densities among various non-viral gene carriers. Thus, they have high capability to condense DNA or RNA molecules by electrostatic interactions to form polyplexes. Besides, they are safe to use with a reasonable production cost, allowing large scale production. The cationic polymers also have the functionality that can be used to conjugate with different site targeting ligands, for example folate, sucrose and surface antigen for cell specific bindings.

However, one of the major problems associated with the polyplexes is that they tend to form large aggregates with broad particle size distributions. In addition, they interact non-specifically with serum components in blood circulation.[40] The high positive charge density also cause destabilization of cell membranes and result in cytotoxicity. The most common way to tackle these problems is to conjugate the polycations with neutral non-condensing polymers, such as poly(ethylene glycol) (PEG) and poly(vinly alcohol). Studies show that most of the conjugated polycations had improved stability and reduced cytotoxicity. On the other hand, higher amounts of the conjugated polycations are required to completely condense the same amount of DNA comparing with the un-conjugated ones.

Branched-PEI based polycations

Polyethylenimine is one of the highest cationically charged polymers due to its high amine content. Each of the backbone repeating unit of PEI is constructed by two carbon atoms followed by one nitrogen atom. Its industrial applications include paper production, shampoo manufacturing and water purifications. Based on the different kind of monomers, PEI can be divided into linear and branched forms. The linear PEI is synthesized by cationic polymerization of 2-substituted 2-oxazoline to from linear poly(*N*-formalethylenimine) followed by hydrolysis. The branched form is produced from cationic polymerization of aziridine monomers through chain growth mechanism. The branch sites are generated by specific interaction between two growing chains.[41] The structures of the monomers and PEI polymers are shown in Figure 1.9.

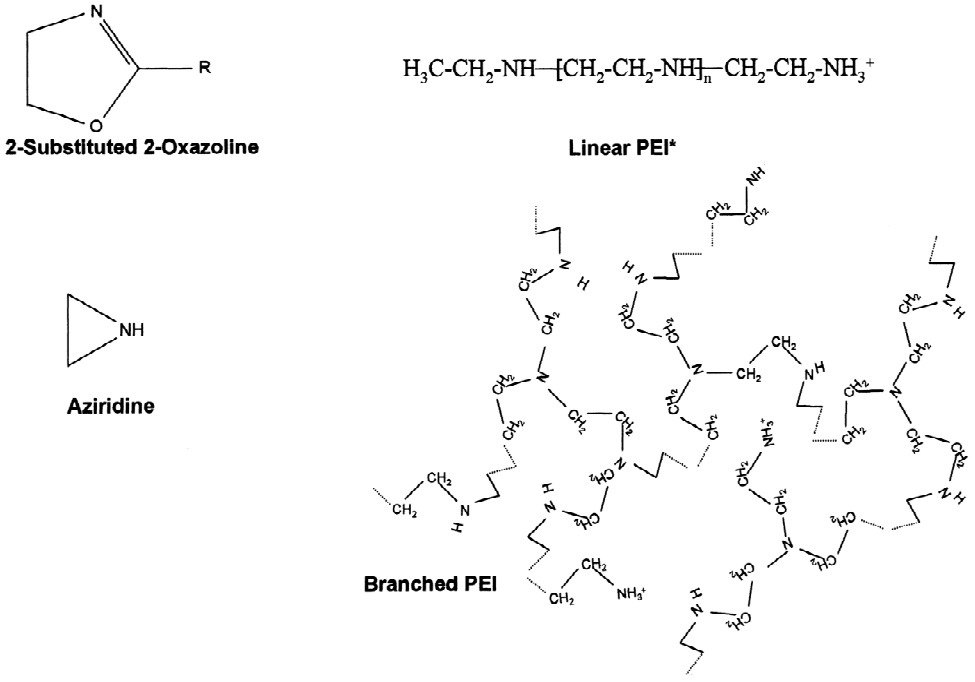

Figure 1.9. Structures of linear PEI with its monomer (2-substituted 2-oxazoline) and branched PEI with its monomer (aziridine).[41]

Besides above mentioned industrial applications, the branched form of PEI has received much interest in gene delivery than its linear form and has been considered as one of the most effective polymer-based gene carriers of a wide variety of cells.[41] This is because branched PEI contains primary (1^o), secondary (2^o) and tertiary (3^o) amine groups for proton sponge effect [43] while linear PEI mainly contains secondary amine groups. The proton sponge effect of the branched PEI plays an important role in efficient gene transfections. The mole ratio of 1^o, 2^o and 3^o amine groups is about 1:2:1.[41] Under physiological pH of 7.4, the 1^o amine groups are protonated and are responsible for DNA condensation while the other amines remain unprotonated. Upon internalized into cells, the pH inside the endosomes decreases to about 5. The secondary and tertiary amines then provide large buffering capacity and the protonation level increases from 20% to 45%.[44] The massive proton accumulation accompany with a passive chloride influx resulted in osmotic swelling and endosomal disruption. Therefore, the entrapped DNA materials are released.[42, 43, 78] Figure 1.10 illustrates the mechanism of this effect.

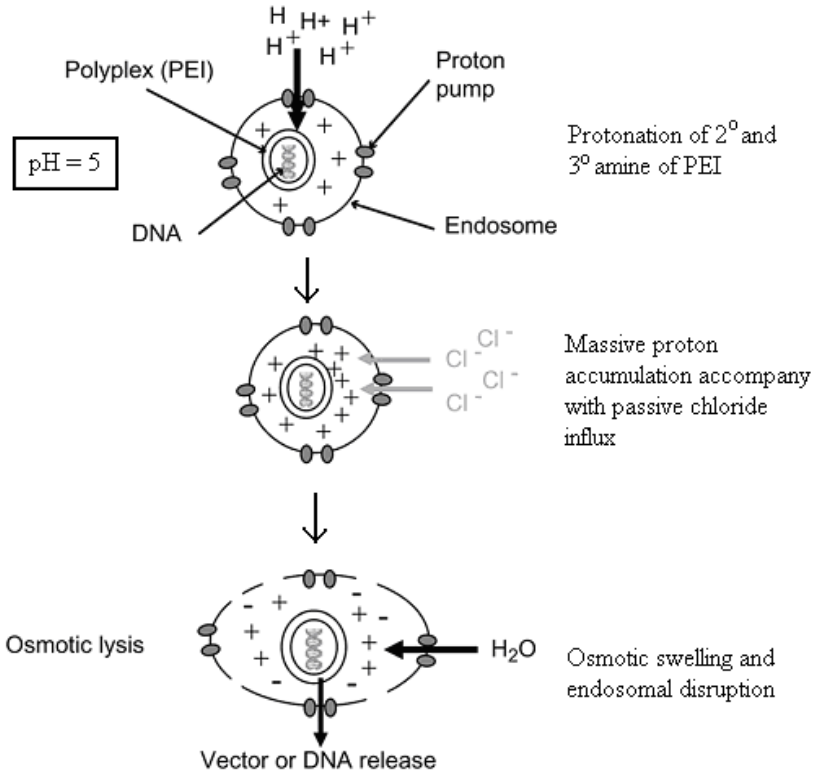

Figure 1.10. Mechanism of internalization and endosomal escape of PEI/DNA polyplex.[42, 78]

The cationic PEI molecules can effectively condense negatively charged DNA molecules by electrostatic interaction. In general, excess amount of PEI is needed so that the resultant polymer/DNA complex contains positive charge. Thus, they can be internalized by the cell via adsorptive endocytosis. It was found that both gene transfection efficiency and cytotoxicity increased as the molecular weight of PEI increased.[44, 40] For example, PEI and modified PEI with molecular weight between 25 to 800 kDa have been successfully used for in vitro and in vivo gene delivery. However, PEI with molecular weight lower than 2000 Da failed to have protein expression.[44]

Biodegradable poly(lactic-co-glycolic acid) (PLGA) based polymers

Poly(lactic-co-glycolic aicd) (PLGA) is a biodegradable polymer synthesized through random ring-opening co-polymerization of glycolic acid and lactic acid. It is commonly investigated as a biodegradable gene carrier, making use of its hydrolysable ester linkages.[45-48] PLGA nanoparticles have advantages such as high stability in the blood stream, ease of cellular uptake by endocytosis, and high functionality to conjugate with ligands for specific tissues or organs targeting.[46]

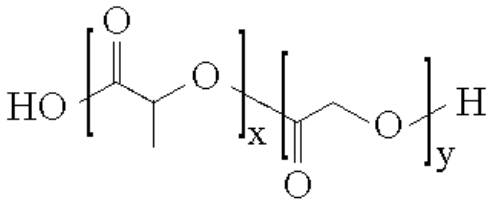

Figure 1.11. Chemical structure of poly(lactic-co-glycolic aicd) PLGA . x is number of units of lactic acid and y is number of units of glycolic acid.

Kang *et al* have evaluated the PLGA nanospheres as a vascular endothelical growth factor gene carrier and have studied the *in vivo* gene transfections.[46] The plasmid DNA encapsulated PLGA nanospheres were prepared using a double emulsion-solvent evaporation method. The pDNA was mixed with PLGA in methylene chloride by a homogenizer. Aqueous solution of polyvinyl alcohol was added to form a water-in-oil-in-water multiple emulsion. The resultant nanoparticles had a homogenous spherical nanostructure with hydrodynamic diameter range of about 120 -280 nm. After injecting the complex into the skeletal muscle of ischemic limb model of mice, prolonged gene expressions were observed after 12 days. Besides, the cytotoxicity was much lower than

that of PEI. One obvious drawback of the preparation method is that the pDNA molecules can be damaged by vigorous mixing during synthesis of PLGA nanoparticles/pDNA complex.

To reduce damage of DNA molecules during nanoparticles or nanoplexes formation, Oster *et al* have prepared a kind of biodegradable cationic nanoparticles, consisting of amine-modified poly(vinyl alcohol) (PVAL) backbones grafted with poly(lactic-co-glycolic aicd (PLGA) (Figure 1.12), by solvent displacement method. [45] Firstly, the PVAL backbones were amine modified by conjugation with 3-diethylamino-1-propylamine (DEAPA), 2-diethylamino-1-ethylamine (DEAEA) or 3-dimethylamino-1-propylamine (DMAPA) using N,N-carbonyldiimidazole as the coupling agent. After that, the amine-modified PVAL was grafted with PLGA by ring opening polymerization. Finally, the nanoparticles were formed by solvent displacement method. The aqueous pDNA solution was mixed with the acetone solution of the amine-modified PVAL-*g*-PLGA and the mixture was slowly injected to 0.1% aqueous Pluronic® solution for spontaneous nanoparticles formation.

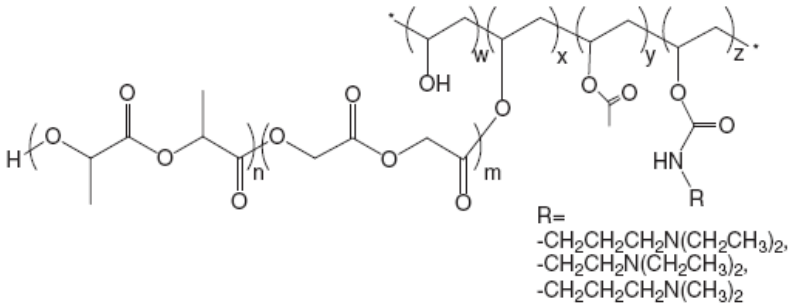

Figure 1.12. Structure of amine-modified poly(vinyl alcohol) (PVAL) backbones grafted with poly(lactic-co-glycolide) (PLGA).

The pDNA molecules were proposed to be encapsulated by the amine-modified backbone through electrostatic attraction and the pDNA can be released by PLGA degradation. The resultant DNA encapsulated nanoparticles have particle size about 200 nm and zeta potential of about +50 mV at particle nitrogen-to-pDNA phosphate (N/P) ratio of 2 and above. These results indicated that stable polyplexes have been formed.

1.3.4 Dendrimers

The word 'Dendrimers' originates from Greek words, in which, *dendra* means tree and *meros* stands for part. Dendrimers have a distinct architecture that several hyper-branched arms emanate from a central core to the surface functional groups in an ordered manner. They are usually synthesized by stepwise synthesis based on the divergent or convergent method. For divergent method, branch chains are grown from the multifunctional core. And for convergent method, the growth of branches starts from the end groups and terminates with the final attachment of a core. The controlled stepwise synthetic process forms a unique rigid, core–shell nanostructure with relatively low polydispersity. The terminal groups on the shell part also allow a wide range of modifications to perform different functions.[43] For examples, cationic dendrimers have been used as gene nanocarriers.

Certain kinds of the dendrimers, like poly(propylene imine) (PPI) dendrimers (Figure 1.13), exhibit proton sponge effect in a similar way as that of branched PEI to achieve intarcellular release of entrapped DNA molecules.[49] However, the PPI dendrimers also

have relatively high toxicity similar to the branched PEI. Tziveleka et al.[49] have developed a guanidinylated poly(propylene imine) dendrimers, which covert certain number of the amine groups to guanidinium groups in order to reduce cytoxicity and enhance transfection efficiency. The positively charged guanidinium groups are also capable of condensing DNA molecules via ionic interaction, the enhancing cellular endosytosis.

The synthetic method of guanidinylated poly(propylene imine) dendrimers with different degree of guanidinylations is illustrated in the lower part of Figure 1.13. Briefly, the PPI dendrimers of the forth generation with 32 primary amino end groups was reacted with different amount of propylene oxide to obtain different degree of hydroxylated dendrimers. After purification and dehydration, the remaining amine groups were guanidinylated with 1*H*-pyrazole-1-carboxamidine hydrochloride.

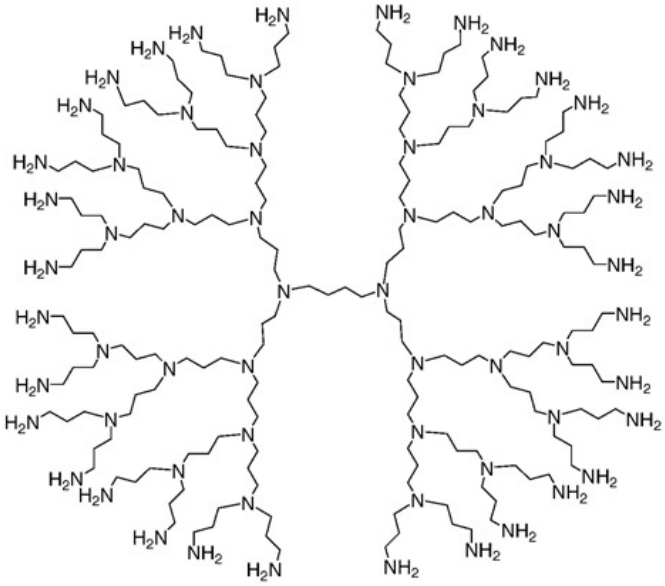

Poly(propylene imine) dendrimer

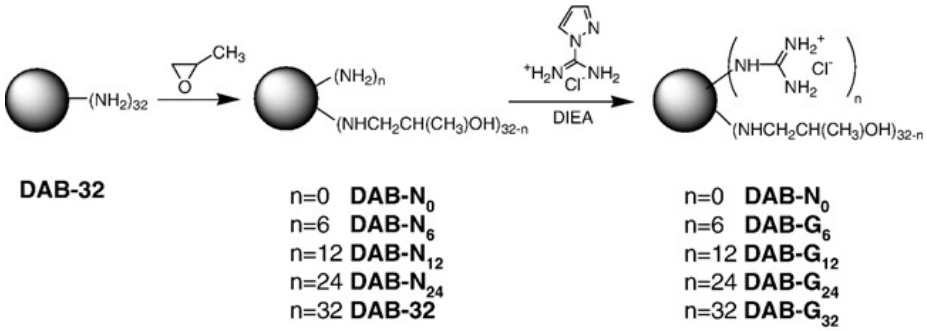

Figure 1.13. Chemical structure of poly(propylene imine) dendrimer (upper) and schematic illustration of the synthesis of the guanidinylated poly(propylene imine) dendrimers with different degree of guanidinylation.

Based on the results of agarose gel electrophoresis, the DNA condensing capacities increased with increasing degree of guanidinylation. The fully guanidinylated dendrimers can completely complex the pDNA at charge ratio (+/-) of 1.

The transfection efficiencies were increased by increasing degree of guanidinylation. The fully guanidinylated dendrimers gave the highest value, while the completely

hydroxylated moieties did not have any transfection. These results indicate that guanidinylation can effectively promote transfection. Among them, the derivative with 12 guanidinium groups exhibited the lowest toxicity, which is attributed to the decrease of the external primary amino groups coupled with the presence of hydroxylated moieties located at the dendrimeric surface.

1.3.5 Natural biopolymer based

Gene delivery using cationic natural biopolymers as gene nanocarriers has advantages of non-toxic, biocompatible and biodegradable. Thus, prolonged and sustained gene delivery can be achieved by encapsulating the therapeutic DNA molecules into the biopolymeric nanocarriers, in which degradation of the carriers cause slow release of DNA molecules. Besides, their economic prices make them become attractive candidates as gene delivery materials. Chitosan, collagen, gelatin and some proteins have been reported in *in vitro* and *in vivo* gene deliveries.

Gelatin based

Gelatin, a vitreous, brittle solid, is faintly yellow to white and nearly tasteless and odorless. It is widely used as gelling, thickening, water-binding, emulsifying, foaming and film forming agents in the food industry. [50] It is a natural, digestible water-soluble

product obtained from dissolution, disorganization, or degradation of the water-insoluble collagen fibres. The collagenolytic process involves alkali or acid treatment, followed by or accompanied with heating in the presence of water. Gelatin contains only 18 out of 20 essential amino acids (AA). The most abundant are glycine (almost 1 in 3 residues, arranged every third residue), proline and 4-hydroxyproline residues.[51] Gelatin also has low sulfur content and methionine is the only sulfur containing amino acid. Figure 1.14 shows a typical structure of gelatin.

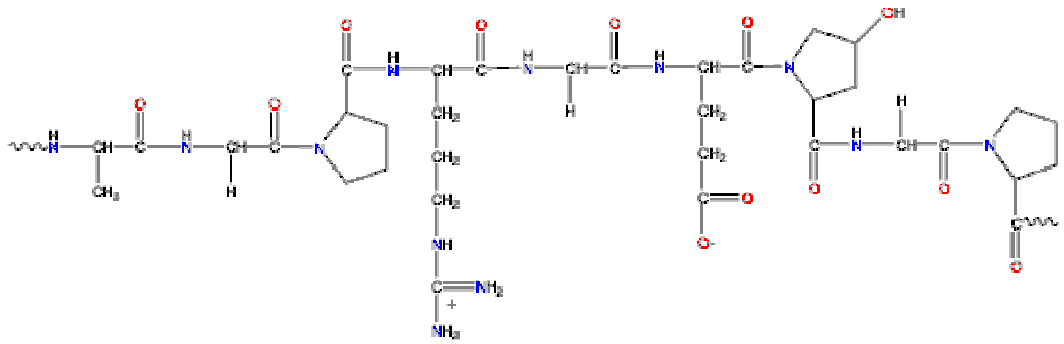

Figure 1.14. A segment of the polymeric chain of gelatin: -Ala-Gly-Pro-Arg-Gly-Glu-Hyp-Gly-Pro-.[51]

Based on the extraction conditions, gelatin is classified into two types. Type A (acid-precursor) gelatin has an isoelectric point (pI) of 7 – 9, while type B (alkali-precursor) gelatin is 4.6 – 5.2.[52] The amphoteric nature of gelatin is attributed to the presence of active amine groups (lysine and arginine residues) and carboxylic acid groups (aspartic acid and glutamic acid residues). Because of these functional groups, gelatin can be cationically or anionically modified to yield positively charged or negatively charged gelatin at physiological pH. In addition, as gelatin is biodegradable, controlled release of the gelatin encapsulated DNA molecules can be achieved by different extent of

crosslinking density of gelatin hydrogels.[53] Besides, as a gene carrier, gelatin can also be used as the scaffold for tissue engineering and tissue repair. [54-57]

Kaul and Amiji have reported the plasmid DNA encapsulation of PEGylated gelatin nanoparticles *in vitro* and *in vivo*. [58-60] PEGlyated gelatin were first synthesized through reaction between type B gelatin and PEG-epoxide. The plasmid DNA encapsulated nanoparticles were then prepared by ethanol precipitation method. The PEGylated-gelatin was dissolved in DI water, followed by the addition of pDNA. The complex was then treated with a EtOH/H_2O mixture slowly until the ethanol concentration reached 65%(v/v). The pDNA entrapped nanoparticles were formed and they were further crosslinked by glyoxal. As the pDNA was entrapped in the polymer matrix rather than forming electrostatical complex, the resultant nanoparticles had a relatively wide size distribution, ranging from 100 to 500 nm in diameter with slightly negative surface charge. Although the confocal microscopy images showed that the particles readily entered cells through non-specific endocytosis, the cellular uptake was not as efficient as that of the cationic charges nanoparticles. In addition, most of the entrapped pDNA was released from the nanoparticles within 8 hours through matrix diffusion and enzymatic degradation.

Other methods of cationic modifications of gelatin nanoparticles for pDNA transfections were demonstrated by Kushibiki *et al*,[61] Fukunaka *et al* [62] and Zwiorek *et al* [63] respectively. For Zwiorek's group, the cationized gelatin nanoparticles were prepared by a two-step desolvation process.[63] The first step was to remove the low molecular weight

of gelatin molecules. After that, the quaternary amine cholamine was covalently coupled onto the gelatin molecules with 1-ehtyl-3-(3-dimethylaminopropyl) carbodiimide hydrochloride salt (EDC) as the coupling agent. Figure 1.15 shows the synthetic method of this kind of cationized gelatin nanoaprticles. The zeta potential of the cationized nanoparticles changed from negative value to above +20 mV at physiological pH and can form complex with pDNA, but with low complexation ability. The gelatin-to-pDNA weight ratio above 100:1 was required to show significant gene transfection results. The most notable finding is that the nanoparticles showed almost no cytotoxicity when comparing with the PEI/pDNA nanoplex.

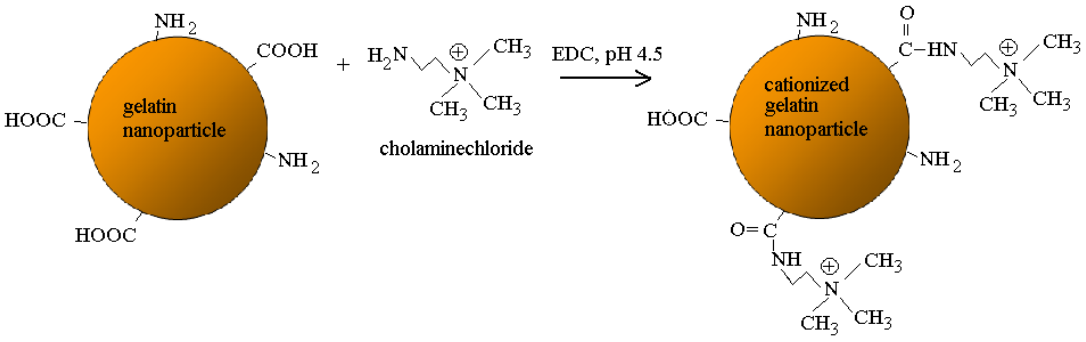

Figure 1.15. Schematic illustration of the synthesis of cationized gelatin nanoparticles proposed by Zwiorek *et al*.

Similarly, Fukunaka's group used ethylenediamine to increase the amine content of the gelatin hydrogel.[62] The cationized gelatin molecules were then crosslinked by glutaraldehyde to form hydrogels. Figure 1.16 displays the synthetic method. It was found that increasing the crosslinking density was able to retard the degradation rate of the hydogels. Therefore, it is more suitable for prolonged pDNA release. Kushibiki *et al*

followed the same procedures as Fukunaka for the preparation of cationized gelatin. The gelatin molecules were used to complex with TGF-βR siRNA expressing pDNA. Its *in vivo* local TGF-β receptor suppression effect was examined. Injection of plasmid DNA/cationized gelatin complex significantly decreased the level of TGF-*β*R and *α*-smooth muscle actin over-expression.[61]

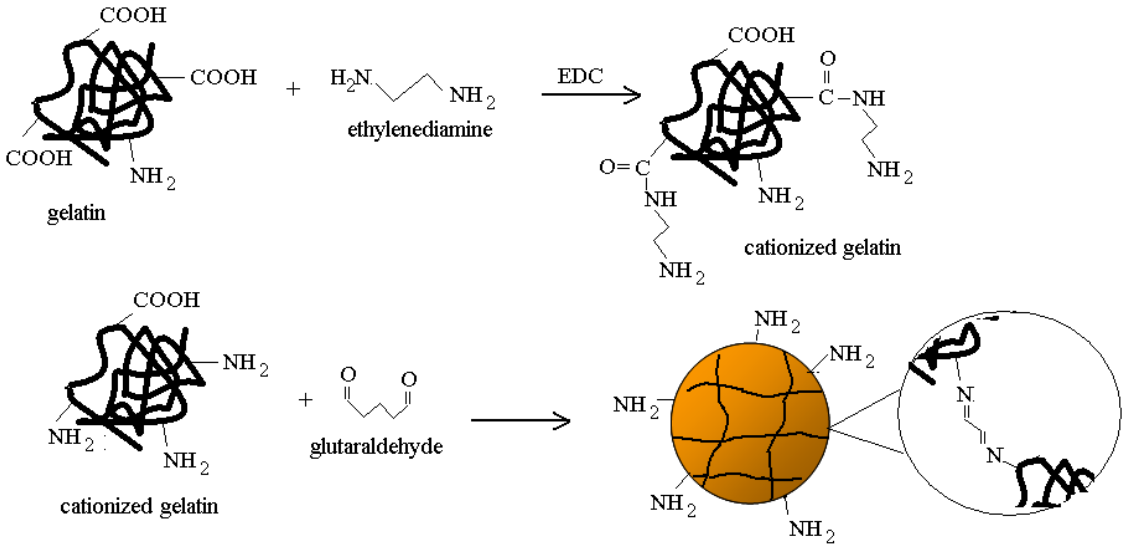

Figure 1.16. Schematic illustration of the synthesis of cationized gelatin hydrogels proposed by Fukunaka *et al*.

Chitosan based

Chitosan is obtained by deacetylation of chitin form crustacean shells. Figure 1.17 illustrates the typical chemical structure of chitsoan. It contains repeating units of *D*-glucosamine and *N*-acetyl-*D*-glucosamine units, linked via (1→4) glycosidic bonds and has a strong affinity for DNA complexation through electrostatic interaction to form stable nano-sized complex. As the pK_a value of the deacetylated subunit of chitosan is

about 6.5, it is protonated only in acidic and neutral pH environment.[64] Since chitosan has muco-adhensive property, it has been successfully applied to gene therapy via oral, intratracheal, gastro-intestinal and nasal routes.[65]

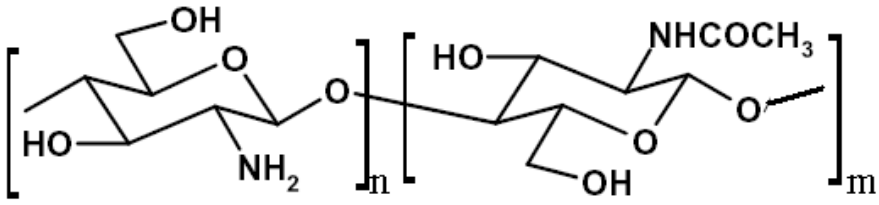

Figure 1.17. Chemical structure of chitosan. The higher the percentage of deacetylation, the higher the portion of m.

Zheng *et al* have investigated the *in vitro* and *in vivo* transfection efficiency of chitosan nanoparticles. Three types of chitosan nanoparticles, chitosan nanoparticles (MW 230 kDa, 90% deacetlyation), degraded chitosan nanoparticles (MW 44 kDa, 87% deacetlyation) and chitosan-trimethylated chitosan oligomer (TMCO) were used to encapsulate plasmid DNA for gene transfections.[66] The degraded chitosan was obtained by H_2O_2 treatment. TMCO was obtained by mixing with methyl-iodide in a basic solution of *N*-methylpyrrolidinone at 60 °C for 75 min. After ethanol precipitation and centrifugation, the product was undergone reductive methylation to obtain the final TMCO with 60% of degree of substitution and MW of 221 kDa. For pDNA complexation, the dissolved chitosan was mixed with pDNA under pH about 6.

It was observed that the TMCO-to-pDNA weight ratio of 2 showed complete pDNA condensation and the chitosan/pDNA complex encountered different degree of degradation after storing at 4^oC for 15 days. The TEM observation of the complexes

suggested that the pDNA molecules were warped inside the chitosan nanoparticles. The TMCO gave better transfection activity than the other two with minimal cytoxicity. *In vivo* study shows that gene expressions were concentrated in the gastric and upper intestinal mucosa.

Lee *et al* modified the chitosan nanoparticles by incorporating the polyanion poly-γ-glutamic aicd (γPGA) and combined with the low-pressure gene gun for transdermal DNA delivery. [67] The chitosan/γPGA/DNA nanoparticles were prepared by ionic gelation method. Upon adding chitosan solution into the solution mixture of γPGA and DNA, polyelectrolyte nanoparticles were formed by ionic interactions between the cationic chitosan and anionic γPGA and pDNA. The particles of charge ratio (amine groups of chitosan/carboxyl groups of γPGA/phosphate groups of pDNA) of 8:4:1 gave particle size of 17 nm with small size distribution and +21 mV of zeta potentials. Incorporation of γPGA made the morphology of the nanoparticles become spherical and homogenous. In addition, the particles are more compact in their internal structures and have a larger momentum to penetrate into the skin barrier, indicating that the particles to be a good substitute of gold nanoparticles in transdermal gene delivery with the advantage of biodegradable to prevent waste accumulation.

1.3.6 Nanoparticles

Certain kinds of chemically inert metals and semi-metals have been synthesized into nano-scaled nanoparticles. Quantum dots, gold nanoparticles and silica nanoparticles and

lipid-based nanoparticles are some of the examples. [75] Since they are inert, exhibit less cytotoxicity and can be excited and emit specific wavelength, they are often used in bio-imaging, such as protein labeling and tracking. The nanoparticles can also conjugate with some transfection agents to perform gene delivery. [75] Thus, the resultant modified nanoparticles can perform both gene delivery and intracellular trafficking. In addition, the nanoparticles are controllable in size and have narrow size distribution, which can perform passive targeting by enhanced permeability and retention (EPR) effect.

Fuller *et al* have demonstrated silica-PEI core-shell nanoparticles for both gene transfection and intracellular imaging.[68] The nanoparticles were synthesized by the modified Stöber process, by which, the PEI-coated C dots were prepared by dropwise addition of C dots to PEI solution. The PEI molecules were electrostatically coated on Si nanoparticle surface to form the core-shell nanoparticles with 60 nm of nominal diameter. In this way, branched PEI was constructed in the form of nanoparticle for gene transfection. It was found that aggregation occurred when the amount of PEI fed was too low and the optimized feed weight ratio of PEI:C dots was 1:1, which formed the stable particles with hydrodynamic diameters of 117 nm and surface charge of +31 mV. However, the percentage of PEI coated was very low that the nanoparticles contain only 5.5% of PEI by mass. So, the transfection efficiency of the particles was far lower than that of the PEI molecules.

But the nanoparticles had promising results in bioimaging because the PEI coatings greatly improve the cellular internalization and endosomal escape of the particles. The particles have higher quantum efficacy and brightness than dye-doped Si nanoparticles and have higher cell viability of COS-7 cells comparing with PEI molecules.[68]

1.4 Argininosuccinate synthetase targeting small inference ribonucleic acid (ASS-siRNA)

1.4.1 Mechanisms of siRNA in gene silencing

Proteins are synthesized in cells by a process, named gene expression. In brief, the protein encoded gene is identified and the corresponding messenger RNA (mRNA) is produced in the cell nuclei by transcription and RNA splicing. After that, the mRNA is exported to the cytoplasm and the nucleotide sequence of the mRNA is translated into the amino acid sequence of a protein via the genetic code. Gene silencing using siRNA is one of the way to down-regulate the level of a specific protein without affect other protein synthesis. By which, the genome of the specific protein is unaffected while the transcripted mRNA is knockdown by the siRNA. As a result, no protein can be translated and the protein level can be reduced in post-transcriptional level.

Gene silencing using double strand RNA is firstly discovered by Andrew Z. Fire and Craig. C. Mello in *C. elegans.*[19, 69] Among the three categories of RNAi, the double stranded siRNA gives high specificity in inhibiting the synthesis of the target protein and at a much lower dosage.[15] Fire *et al.* suggested that there could be a catalytic or amplification component in the interference process as only a few molecules of the injected siRNA were required per affected cell of *C. elegans*.[19] Although only the sense strand of the siRNA is responsible for the recognition of the target mRNA, the double-strand RNA (dsRNA) showed more effective interference effect than only applying either

the sense or anti-sense strand, suggesting that the single strands are probability degraded or rendered inaccessible in the absence of the opposite strand.[19] Figure 1.18 illustrates the mechanism of mRNA degradation by a siRNA. The siRNA is applied in double stranded form, composing of a sense strand and an anti-sense strand. In action, the double stand is unwound and either strand is incorporated with the RNA-induced silencing complex (RISC). The sequence of the siRNA strand is homologues to the target mRNA. It recognizes and binds to the target mRNA through sequence specific interaction to bring the RISC to the target mRNA. Finally, the target mNRA is degraded by the RISC. The siRNA can be obtained by three ways, degradation of the longer double stranded RNA (dsRNA) by an enzyme, Dicer, chemical synthesis and extraction from virus.

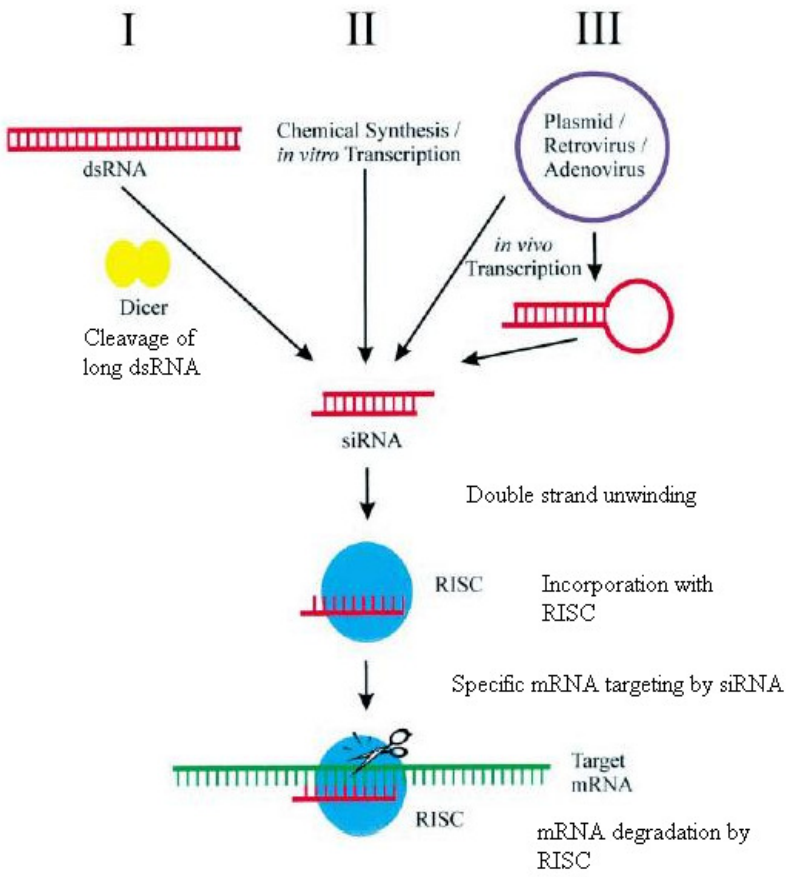

Figure 1.18. Schematic illustration of mechanism of mRNA degradation by siRNA.

1.4.2 Argininosuccinate synthetase (ASS)

Argininosuccinate synthetase (ASS, EC 6.3.4.5) is responsible for synthesizing the argininosuccinate, the immediate precursor of arginine, from aspartate and citrulline in the urea cycle.[70] The catalytic reaction is reversible and ATP-dependent. Figure 1.19 shows the reaction of ASS in the synthesis of argininosuccinate. ASS is the rate limiting enzyme in at least three kinds of synthesis, i.e., urea production, arginine production and nitric oxide (NO) production, which is displayed in Figure 1.20. Under-expression of ASS can causes citrullinemia in human and over-expression of ASS will lead to excessive NO production.

$$\mathrm{MgATP^{2-}} + \text{citrulline} + \text{aspartate} \Longleftrightarrow \text{argininosuccinate} + \mathrm{MgPP_i} + \mathrm{AMP}$$

Figure 1.19. Catalytic synthesis of argininosuccinate by argininosuccinate synthetase (ASS). [70]

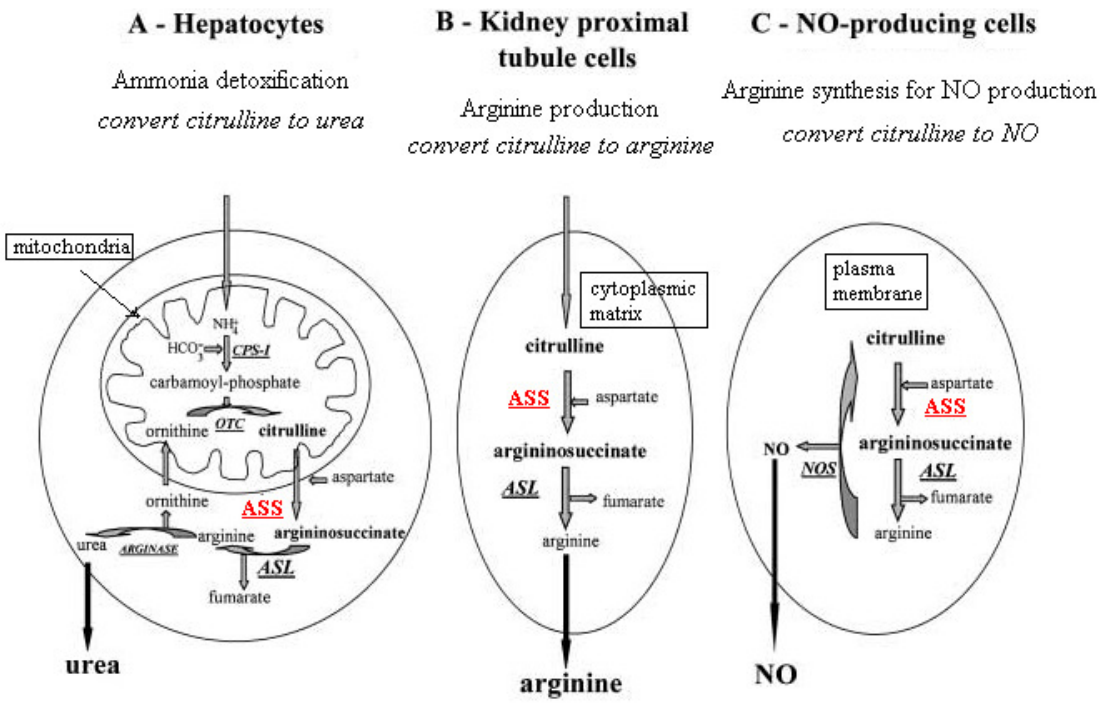

Figure 1.20. Schematic illustration of the functions of argininosuccinate synthetase (ASS) in three kind of synthesis: urea production in hepatocytes (A), arginine production in kidney proximal tubule cells (B) and nitric oxide production in NO-producing cells (C). Enzymes are: CPS-I, carbamoylph osphate synthetase-I (EC 6.3.4.16); OTC, ornithine transcarbamylase (EC 2.1.3.3); ASS, argininosuccinate synthetase (EC 6.3.4.5); ASL, argininosuccinate lyase (EC 4.3.2.1); NOS, nitric oxide synthase (EC 1.14.13.39). [70]

The expression levels of ASS vary in different kinds of cancer cell lines. Liver and kidney have the highest expression levels. Bowles *et al* evaluated that among the 47 human pancreatic adenocarcinoma cell lines, 87% of the specimens (41 cell lines) did not express ASS. Rest of the 13% (6 cell lines) expressed ASS at different levels, at which, L3.3 had the highest level of expression while MIA-PaCa-2 and PANC-1 had very low levels.[71]

1.4.3 Anti-tumor effect of arginine deiminase (ADI) in combination with ASS-siRNA

Arginine deiminase (ADI) is a microbial enzyme from *Mycoplasma*.[20, 71] It catalyzes the irreversible catabolism of protein-bound arginine to citrulline in the arginine dehydrolase (ADH) pathway and serves as an important source of energy in prokaryotic cells.[72] It is also reported that ADI can affects both antigenic switching and antibody-mediated cell death.[72]

Arginine is recognized to be an important nutrient for the growth of solid tumors. Thus, anti-cancer treatment strategy using ADI to quench the supply of arginine in ASS deficient cancer cell lines has been extensively investigated in recent years.[73, 74] The ASS deficient cancer cells cannot synthesize their own arginine while ADI depletes the intracellular arginine by reducing extracellular arginine level available for cellular uptake.[66] Bowles *et al* have investigated the effect of ADI in inhibition of cell growth of pancreatic cancer cells that have low ASS expression.[71] In their studies, the melanoma and hepatoma cancer cells were treated with PEGylated ADI (PEG-ADI). It was found that 87% of the cells lines lacked of ASS expression. Thus, the PEG-ADI is able to induce capase activation and apoptosis to those ASS deficient cells. In addition, *in vivo* studies revealed that tumor growth was inhibited by about 50% in mouse model. Kim *et al* also reported the *in vitro* antitumor effect of PEGylated ADI (ADI-PEG20) in prostate cancer cells.[71] They also found that the antitumor effect of ADI is directly correlated with ASS deficiency. ADI-PEG20 was able to reduce tumor activity, induce autophagy and

caspase-independent apoptosis in CWR22Rv1 cells which do not express ASS. ADI-PEG20 also partially induced cell death of PC3 cells which express reduced ASS. However, LNCaP cells, which highly express ASS, were resistance to ADI-PEG20.

ADI has achieved a successful clinical application in cancer treatment [76] and is now commercially available as drug pallets. [77] Although treatment of those ASS deficient cells can induce cell death, it is difficult to treat those cells with normal ASS levels. [64] This is because the inhibition of tumor growth is arginine depletion dependent. Tumor cells which express ASS can synthesize arginine from citrulline. The urea cycle enzyme ASS catalyzes the conversion of aspartate and citrulline to argininosuccinate, which is then converted to arginine by argininosuccinate lyase (ASL). [64, 70]

Therefore, in the treatment of those cancer cells which express ASS, such as liver and kidney cells, the ASS expression of those cells should be suppressed in order to achieve effective anticancer treatment using ADI. The siRNA technology may resolve the limitation of ADI in treating ASS positive cancer cells through specific ASS gene knockdown in post-transcriptional level. Since the ASS targeting siRNA can down-regulate the expression level of ASS by recognizing the ASS mRNA and causing ASS mRNA degradation, the cells will become ASS deficient and cannot synthesize enough amount of ASS for arginine synthesis. As a result, the growth of those tumor cells can be suppressed due to the insufficient supply of arginine.

Besides the cell growth inhibition activity, ADI also shows increased radiosensitivity of

MCF-7 cells, which have high level of ASS expression, in combination with ionic radiation (IR) to inhibit the cell growth. The factor of main cause of the growth inhibition is ammonia, another product of arginine degradation. [65, 66] ADI can also treats the iNOS – related neuronal diseases by regulating the arginine level.[67]

1.5 Conclusions

In this chapter, the background information of gene delivery has been introduced. Gene delivery is one of the strategies in treating hereditary diseases and cancers. The exogenous therapeutic genes are delivered to the infected cells to regulate the expression level of specific genes. However, as the genes are unstable in blood streams and the entry of the genes to target sites is infeasible due to the intracellular and intercellular barriers, the genes must be delivered using gene delivery systems, such as physical, viral and non-viral systems.

The designs of the non-viral gene delivery vectors, including liposomes, copolymer micelles, synthetic cationic polymers, dendrimers, natural biopolymers and nanoparticles with their synthetic methods and their gene transfer strategies have been discussed. In general, these gene delivery vectors have advantages of non-immunogenic, biocompatible and to be internalized by passive targeting. The nanocarriers can also be modified by targeting or external stimuli-responsive ligands to enhance cellular uptake. In addition, most of them are quite easy to synthesize and are feasible to be produced in a large scale for clinical uses. However, many of the nanocarrier systems encounter

destabilization in living bodies by the interference of blood components. Therefore, the breakthrough of the non-viral nanoparticle gene delivery vector systems requires further improvement of the stability *in vivo* in order to be successfully applied in gene therapies.

1.6 References

1. 1. Hughes, G. A (2007). Nanotechnologies for Diagnosis - Present and Future. In C. Kumar *Nanomaterials for Medical Diagnosis and Therapy* (pp. 1-50). LA: Wiley-VCH.
2. Idee, J. M *et al* (2007). Superparamagentic Nanoparticles of Iron Oxides for Magnetic Resonance Imaging applications. In C. Kumar *Nanomaterials for Medical Diagnosis and Therapy* (pp. 51-84). LA: Wiley-VCH.
3. Pedraz, J. L *et al* (2007). Solid Lipid and Polymeric nanoparticles for Drug delivery. In C. Kumar *Nanomaterials for Medical Diagnosis and Therapy* (pp. 471-508). LA: Wiley-VCH.
4. Liu, S *et al* (200). Lipoproteins as Pharmaceutical Carriers. In V. P. Torchilin, *Nanoparticulates as Drug Carriers* (pp. 173-186) London: Imperial College Press.
5. Polpanich, D *et al* (2008). Evolution in Malaria Disease Detection: From Parasite Visualization to Colloidal-Based Rapid Diagnosis. In A. Elaissari *Colloidal Nanoparticles in Biotechnology* (pp. 65-94) New Jersey: John Wiley & Sons, Inc.
6. Nabiev, I. *et al* (2008). Fluorescent Colloidal Particles as Detection Tools in Biotechnology Systems. In A. Elaissari *Colloidal Nanoparticles in Biotechnology* (pp. 133-168) New Jersey: John Wiley & Sons, Inc.

7. Jaffrezic-Renault, N. *et al* (2008). Biofunctionalized Magnetic Micro-Nanoparticles for Biosensing Technologies. In A. Elaissari *Colloidal Nanoparticles in Biotechnology* (pp. 169-198) New Jersey: John Wiley & Sons, Inc.

8. Nel, A. L *et al* (2008). Particles for Protein Analysis in Microfluidic Systems. In A. Elaissari *Colloidal Nanoparticles in Biotechnology* (pp. 275-298) New Jersey: John Wiley & Sons, Inc.

9. http://www.bret.org.uk/nec6a.htm

10. D. Robert Lu and Svein Øie, Chapter 5 of "**Cellular Drug Delivery: Principles and Practice**" Totowa, N.J.: Humana Press Inc., 2004, p. 81-94.

11. David V. Schaffer and Weichang Zhou, "Gene Therapy and Gene Delivery Systems as Future Human Therapeutics**"** *Adv Biochem Engin/Biotechnol 99* **(2005)** 1-5**.**

12. Steven A. Rosenberg, Paul Aebersold, Kenneth Cornetta, Attab Kasid, Richard A. Morgan, Robert Moen, Evelyn M. Karson, Michael T. Lotze, James C. Yang, Suzanne L. Topalian, Karia J. Merino, Kenneth Culver, A. Dusty Miller, R. Michael Blaese and W. French Anderson, "Genetransfer into humans – Immunotherapy of patients with advanced melanoma, using tumor-infiltrating lymphocytes modified by retroviral gene transduction", *New England Journal of Medicine 323* (9) (**1990**) 570-578.

13. Sayda M. Elbashir, Jens Harborth, Winfried Lendeckel , Abdullah Yalcin, Klaus Weber and Thomas Tuschl, "Duplexes of 21-nucleotide RNAs mediate RNA interference in cultured mammalian cells" *Nature 411* **(2001)** 494-498.

14. Theresa M. Allen and Pieter R. Cullis, "Drug delivery systems: Entering the mainstream", *Science 303* **(2004)** 1818-1822.

15. Daniela Reischl and Andreas Zimmer, "Drug delivery of siRNA therapeutics: potentials and limits of nanosystems" *Nanomedicine: Nanotechnology, Biology, and Medicines 5* **(2009)** 8-20.

16. Stahel RA, Zangemeister-Wittke U, "Antisense oligonucleotides for cancer therapy – an overview" *Lung Cancer 41* **(2003)** 81-88.

17. Jens Kurreck, "Antisense technologies, improvement through novel chemical modifications" *European Journal of Biochemistry 270* **(2003)** 1628-1644.

18. Doudna JA and Cech TR, "The chemical repertoire of natural ribozymes" *Nature 418* **(2002)** 222-228.

19. Andrew Z. Fire, "Gene silencing by double-stranded RNA" *Angewandte Chemie International Edition 46* **(2007)** 6966 –6984.

20. Paul Ning-Man Cheng, Tin-Lun Lam, Wai-Man Lam, Sam-Mui Tsui, Anthony Wai-Ming Cheng, Wai-Hung Lo, and Yun-Chung Leung, "Pegylated recombinant human arginase (rhArg-peg$_{5,000mw}$) inhibits the *In vitro* and *In vivo* proliferation of human hepatocellular carcinoma through arginine depletion" *Cancer Research 79 (1)* **(2007)** 309-317.

21. C. Bloquel, J.L. Bourges, E. Touchard, M. Berdugo, D. BenEzra, F. Behar-Cohen, "Non-viral ocular gene therapy: Potential ocular therapeutic avenues" *Advanced Drug delivery Review 58* (**2006**) 1224-1264.

22. C.H. Evans, E. Gouze, J.-N. Gouze, P.D. Robbins, S.C. Ghivizzani, "Gene therapeutic approaches—transfer in vivo", *Advanced Drug delivery Review 58* (**2006**) 243-258.

23. Shivaram Selvam, Padmaja B. Thomas, Sarah F. Hamm-Alvarez, Joel E. Schechter, Douglas Stevenson, Austin K. Mircheff and Melvin D. Trousdale, "Current status of gene delivery and gene therapy in lacrimal gland using viral vectors", *Advanced Drug delivery Review 58* (**2006**) 1243-1257.

24. Kentaro Kogure, Hidetaka Akita, Yuma Yamada and Hideyoshi Harashima, "Multifunctional envelope-type nano device (MEND) as a non-viral gene delivery system" *Advanced Drug delivery Review 60* (**2008**) 559-571.

25. Yosuke Obata, Daisuke Suzuki, and Shinji Takeoka, "Evaluation of cationic assemblies constructed with amino acid based lipids for plasmid DNA delivery", *Bioconjugate Chemistry*, In press.

26. Yuhong Xu and Francis C. Szoka, "Mechanism of DNA release from cationic liposome/DNA complexes used in cell transfection", *Biochemistry 35* **(1996)** 5616-5623.

27. Philip L. Felgner Philip L. Felgner, Thomas R. Gadek, Marilyn Holm, Richard Roman, Hardy W. Chan, Michael Wenz, Jeffrey P. Northrop, Gordon M. Ringold, and Mark Danielsen, **"**Lipofection: A highly efficient, lipid-mediated DNA-transfection procedure**",** *Proc. Natl. Acad. Sci. 84* (1987) 7413-7417.

28. Seok Min Kwon, Hae Yun Nam, Taehwan Nam, Kyeongsoon Park, Seulki Lee, Kwangmeyung Kim, Ick Chan Kwon, Jun Kim, Dongmin Kang, Jae Hyung Park and Seo Young Jeong, "*In vivo* time-dependent gene expression of cationic lipid-

based emulsion as a stable and biocompatible non-viral gene carrier", *Journal of Controlled Release. 128* (**2008)** 89-97.

29. Toshifumi Hara", Feng Liub, Dexi Liub, Leaf Huang, " Emulsion formulations as a vector for gene delivery in vitro and in vivo", *Advanced Drug delivery Review 24* (**1997**) 265-271.

30. Yoshinori Kakizawa and Kazunori Kataoka, "Block copolymer micelles for delivery of gene and related compounds", *Advanced Drug delivery Review 54* **(2002)** 203-222

31. Jung Wan Hong, Jae Hyung Park, Kang Moo Huh, Hesson Chung, Ick Chan Kwon and Seo Young Jeong, "PEGylated polyethylenimine for in vivo local gene delivery based on lipiodolized emulsion system", *Journal of Controlled Release 99* **(2004)** 167-176.

32. Ankit Agarwal, Robert C. Unferb, Surya K. Mallapragada, "Dual-role self-assembling nanoplexes for efficient gene transfection and sustained gene delivery", *Biomaterials 29* **(2008)** 607-617.

33. Fu-Jian Xu, Hongzhe Li, Jun Li, Zhongxing Zhang, En-Tang Kang, Koon-Gee , "Pentablock copolymers of poly(ethylene glycol), poly((2-dimethyl amino) ethyl methacrylate) and poly(2-hydroxyethyl methacrylate) from consecutive atom transfer radical polymerizations for non-viral gene delivery", *Biomaterials* **(2008)** 1-11 (In press).

34. David Oupicky, Kenneth A. Howard, Cÿ estmı´r Konˇa´k, Philip R. Dash, Karel Ulbrich, and Leonard W. Seymour, "Steric stabilization of poly-L-Lysine/DNA

complexes by the covalent attachment of semitelechelic poly[*N*-(2-Hydroxypropyl)methacrylamide]", *Bioconjugate Chemistry 11* **(2000)** 492-501.

35. Dandan Huang, Nikolay Korolev, Khee Dong Eom, James P. Tam and Lars Nordenskiöld, "Design and Biophysical Characterization of Novel Polycationic ε-Peptides for DNA Compaction and Delivery", *Biomacromolecules,* In press.

36. Mei Ou, Xu-Li Wang, Rongzuo Xu, Chien-Wen Chang, David A. Bull and Sung Wan Kim, "Novel biodegradable poly(disulfide amine)s for gene delivery with high efficiency and low cytotoxicity" *Bioconjugate Chemistry,* In press.

37. Daniel W. Pack, David Putnam and Robert Langer, "Design of imidazole-containing endosomolytic biopolymers for gene delivery", *Biotech. and Bioengin 67*(2) **(2000)** 217-223.

38. Rongqin Huang, Weilun Ke, Yang Liu, Chen Jiang and Yuanying Pei, "The use of lactoferrin as a ligand for targeting the polyamidoamine-based gene delivery system to the brain" *Biomaterials 29* **(2008)** 238–246.

39. Dai Yamanouchi, Jun Wu, Andrew N. Lazar, K. Craig Kent, Chih-Chang Chu, Bo Liu, "Biodegradable arginine-based poly(ester-amide)s as non-viral gene delivery reagents" *Biomaterials* **(2008)** 1–9, In press.

40. Junmin Zhu, Angie Tang, Lai Pang Law, Min Feng, Kin Man Ho, Daniel K. L. Lee, Frank W. Harris and Pei Li, "Amphiphilic core-shell nanoparticles with poly(ethylenimine) shells as potential gene delivery carriers", *Bioconjugate Chemistry16* **(2005)** 139-146.

41. Junghun Suh, Hyun-jong Paik and Byung Jeun Hwang, “Ionization of poly(ethylenimine) and poly(allylamine) at various pH’s” *Bioorganic Chemistry 22* **(1994)** 318-327.

42. Antoine Kichler, Christian Leborgne, Emmanuel Coeytaux and Olivier Danos, “Polyethylenimine-mediated gene delivery: a mechanistic study”, *J. Gene Med. 3* **(2001)** 135–144.

43. Ji Hoon Jeong, Sung Wan Kim and Tae Gwan Park, “Molecular design of functional polymers for gene therapy”, *Prog. Polym. Sci. 32* **(2007)** 1239-1274.

44. W.T. Godbey , Kenneth K. Wu and Antonios G. Mikos, “Poly(ethylenimine) and its role in gene delivery”, *Journal of Controlled Release 60* (1999) 149-160.

45. Christine G. Oster, Matthias Wittmar, Udo Bakowsky and Thomas Kissel, “DNA nano-carriers from biodegradable cationic branched polyesters are formed by a modified solvent displacement method”, *Journal of Controlled Release 111* (**2006)** 371-381.

46. Sun-Woong Kang, Hee-Won Lim, Sang-Woo Seo, Oju Jeon, Minhyung Lee and Byung-Soo Kim, “Nanosphere-mediated delivery of vascular endothelial growth factor gene for therapeutic angiogenesis in mouse ischemic limbs”, *Biomaterials.29* (**2008)** 1109-1117.

47. Liang Jia, Jeffrey R. Kovacs, Ying Zheng, Hongmei Shen, Ellen S. Gawalt and Wilson S. Meng, “Expansion of Foxp3-expressing regulatory T cells in vitro by dendritic cells modified with polymeric particles carrying a plasmid encoding interleukin-10” *Biomaterials.29* (**2008)** 1250-1261.

48. Sudhir P Kasturi, Karishma Sachaphibulkij and Krishnendu Roy, "Covalent conjugation of polyethyleneimine on biodegradable microparticles for delivery of plasmid DNA vaccines", *Biomaterials 26* (**2005**) 6375-6385.

49. Leto-Aikaterini Tziveleka, Anna-Maria G. Psarra, Dimitris Tsiourvas, Constantinos M. Paleos, "Synthesis and characterization of guanidinylated poly(propylene imine) dendrimers as gene transfection agents" *Journal of Controlled Release 117* (**2007**) 137–146.

50. http://www.gmap-gelatin.com/about_gelatin.html

51. http://www.lsbu.ac.uk/water/hygel.html

52. J.M. Krochta, E.A. Baldwin and M. Nisperos-Carriedo, (1994) "*Edible Coatings and Films to Improve Food Quality*", Lancaster: Technomic Pub. Co. Inc, p 229-230.

53. Simon Young, Mark Wong, yasuhiko Tabata and Antonios G. Mikos, "Gelatin as a delivery vehicle for the controlled release of bioactive molecules", *Journal of Controlled Release 109* (**2005**) 256-274.

54. Jiyoung M. Dang and Kam W. Leong, "Natural polymers for gene delivery and tissue engineering" *Advanced Drug Delivery Review 58* (**2006**) 487-499.

55. Laura De Laporte and Lonnie D. Shea, "Matrices and scaffolds for DNA delivery in tissue engineering", *Advanced Drug Delivery Review 59* (**2007**) 292-307.

56. K. Gelse and H. Schneider, "Ex vivo gene therapy approaches to cartilage repair", *Advanced Drug Delivery Review 58* (**2006**) 259-284.

57. Dennis P. Link, Juliette van den Dolder, Jeroen J. van den Beucken, Joop G. Wolke, Antonios G. Mikos and John A. Jansen, "Bone response and mechanical

strength of rabbit femoral defects filled with injectable CaP cements containing TGF-β1 loaded gelatin microparticles", *Biomaterials 29* **(2008)** 675-682.

58. Goldie Kaul and Mansoor Amiji, "Cellular Interactions and In Vitro DNA Transfection Studies with Poly(ethylene glycol)-Modified Gelatin Nanoparticles", *Journal of Pharmaceutical Science 94*(1) **(2005)** 184-198.

59. Goldie Kaul and Mansoor Amiji, "Tumor-targeted gene delivery using poly(ethylene glycol)-modified gelatin nanoparticles: *in vitro* and *in vivo* studies", *Pharmaceutical Research 22(6)* **(2005)** 951-961.

60. Goldie Kaul and Mansoor Amiji, "Long-circulating poly(ethylene glycol)-modified gelatin nanoparticles for intracellular delivery", *Pharmaceutical Research 19(7)* **(2002)**1061-1067.

61. Toshihiro Kushibiki, Natsuki Nagata-Nakajima, Manabu Sugai, Akira Shimizu and Yasuhiko Tabata, "Delivery of plasmid DNA expressing small interference RNA for TGF-β type II receptor by cationized gelatin to prevent interstitial renal fibrosis", *Journal of Controlled Release 105* **(2005)** 318-331.

62. Yasunori Fukunaka, Kazunori Iwanaga, Kazuhiro Morimoto, Masawo Kakemi and Yasuhiko Tabata, "Controlled release of plasmid DNA from cationized gelatin hydrogels based on hydrogel degradation", *Journal of Controlled Release 80* **(2002)** 333-343.

63. Klaus Zwiorek, Julia Kloeckner and Conrad Coester, "Gelatin nanoparticles as a new and simple gene delivery system", *J. Pharm Pharmaceut. Sci 7*(4) **(2004)** 22-28.

64. Ji Hoon Jeong, Sung Wan Kim and Tae Gwan Park, "Molecular design of functional polymers for gene therapy", *Prog. Polym. Sci. 32* **(2007)** 1239-1274.

65. Jiyoung M. Dang and Kam W. Leong, "Natural polymers for gene delivery and tissue engineering" *Adv. Drug Delivery Rev. 58* **(2006)** 487-499.

66. Fang Zheng, Xiao-Wen Shi, Gui-Fang Yang, Ling-Ling Gong, Hong-Yin Yuan, Ye-Jian Cui, Yan Wang, Yu-Min Du, Yan Li, "Chitosan nanoparticle as gene therapy vector via gastrointestinal mucosa administration: Results of an in vitro and in vivo study", *Life Sciences 80* **(2007)** 388–396.

67. Po-Wei Lee, Shu-Fen Peng, Chun-Jen Su, Fwu-Long Mi, Hsin-Lung Chen, Ming-Cheng Wei, Hao-Jan Lin, Hsing-Wen Sung, "The use of biodegradable polymeric nanoparticles in combination with a low-pressure gene gun for transdermal DNA delivery", *Biomaterials 29* **(2008)** 742–751.

68. Jason E. Fuller, Gregory T. Zugates, Lino S. Ferreira, Hooisweng S. Ow, Nicholas N. Nguyen, Ulrich B. Wiesner and Robert S. Langer, "Intracellular delivery of core-shell fluorescent silica nanoparticles", *Biomaterials 29* **(2008)** 1526-1532.

69. Andrew Z. Fire, "Gene silencing by double-stranded RNA" *Angewandte Chemie International Edition 46* **(2007)** 6966 –6984.

70. Annie Husson, Carole Brasse-Lagnel, Alain Fairand, Sylvie Renouf and Alain Lavoinne, "Argininosuccinate synthetase from the urea cycle to the citrulline–NO cycle" *European Journal of Biochemistry 270* **(2003)** 1887-1899.

71. Randie H. Kim, Jodi M. Coates, Tawnya L. Bowles, Gregory P. McNerney, Julie Sutcliffe, Jae U. Jung, Regina Gandour-Edwards, Frank Y.S. Chuang, Richard J. Bold, and Hsing-Jien Kung, "Arginine deiminase as a novel therapy for prostate

cancer induces autophagy and caspase-independent apoptosis" *Cancer Research 69 (2)* **(2009)** 700-708.

72. Maria Carolina Touz, Andrea Silvana Rópolo, Maria Romina Rivero, Cecilia Veronica Vranych, John Thomas Conrad, Staffan Gunnar Svard3 and Theodore Elliott Nash, "Arginine deiminase has multiple regulatory roles in the biology of *Giardia lamblia" Journal of Cell Science 121(17)* **(2008)** 2930-2938.

73. H Gong, F Zölzer, G von Recklinghausen, W Havers and L Schweigerer, "Arginine deiminase inhibits proliferation of human leukemia cells more potently than asparaginase by inducing cell cycle arrest and apoptosis" *Leukemia 14* **(2000)** 826-829.

74. Beloussow K, Wang L, Wu J, Ann D and Shen WC, "Arginine deiminase as an innovative anti-breast cancer agent", *Cancer Letters 183 (2)* **(2002)** 155-162.

75. Meredith A. Mintzer and Eric E. Simanek, "Nonviral vectors for gene delivery" *Chemical Reviews 109* **(2009)** 259 – 302.

76. Francesco Izzo, Paolo Marra, Gerardo Beneduce, Giuseppe Castello, Paolo Vallone, Vincenzo De Rosa, Franco Cremona, C. Mark Ensor, Frederick W. Holtsberg, John S. Bomalaski, Mike A. Clark, Chaan Ng, Steven A. Curley, **"**Pegylated Arginine Deiminase Treatment of Patients With Unresectable Hepatocellular Carcinoma: Results From Phase I/II Studies" *Journal of Clinical Oncology 22(10)* **(2004)** 1815-1822.

77. http://tw.commerce.com.tw/modules.php?modules=products&action=detail&ID=E0063452&no=81219

78. Marie Morille, Catherine Passirani, Arnaud Vonarbourg, Anne Clavreul, Jean-Pierre Benoit, "Progress in developing cationic vectors for non-viral systemic gene therapy against cancer" *Biomaterials* **(2008)** 1-20 In press.

79. Nobuhiro Nishiyama a,c, Kazunori Kataoka, "Current state, achievements, and future prospects of polymeric micelles as nanocarriers for drug and gene delivery", *Pharmacology & Therapeutics 112* **(2006)** 630–648.

2. Objective

2.1 Gene delivery using biodegradable PEI-based core-shell nanoparticles

Gene delivery using branched polyethylenimine (PEI) as the non-viral carrier has been studied extensively. Branched PEI is regarded as one of the most effective non-viral gene carrier because it contains very high density of amine groups which can be protonated at the physiological pH to condense exogenous therapeutic genes effectively. Moreover, it also contains high amount of secondary and tertiary amine groups which are pH responsive and contribute to endosomal escape. When the complex of PEI/DNA is internalized into the cells by endocytosis, the complex is trapped inside an endsomal vesicle. The pH value of the environment drops to about 5.5 which cause protonation of the secondary and tertiary amine groups. The PEI/DNA complex swells and expends, named as the sponge effect, causing disruption of the vesicle. As a result, the condensed DNA can be escaped and released to the cytoplasm.

However, the usage of PEI is limited by its cytotoxicity. In addition, the resultant complexes of PEI and DNA have a broad size distribution and poor stability. Usually, aggregation appears after several hours of complexation. One of the solutions to address these limitations is to covalently link the PEI polymers onto the surface of preformed nanoparticles. Thus, the resultant nanoparticles possess the following features:

1) Controllable size and surface charge with minimal aggregation.

2) Improving particle uniformity and stability.

3) High surface area to volume ratio of the nanoparticle allows for high loading amounts of DNA molecules.

4) Enabling passive targeting by enhanced permeability and retention (EPR) effect.

The objective of this research is to develop a novel kind of core-shell nanoparticles with biodegradable gelatin cores and PEI shells as gene carriers. The gelatin cores provide supports for the nanoparticles while the PEI shells condense the DNA molecules. Gelatin is biodegradable and biocompatible in nature. It has low antigenicity and coagulation activity towards platelets. Therefore, it is safe to use in human bodies. Besides, waste accumulation in blood circulation and intracellular space can be reduced. The polycation PEI processes high positive charge density due to its rich amine content. Thus, it enables effective condensation of negative charged DNA molecules with minimal dosage of nanoparticles. The condensed DNA molecules are protected by the particles through reducing the surface area of the DNA exposed to the environment, thus protecting the DNA molecules from degradation by the digestive enzymes (such as DNase). The excessive positive charge of the DNA/nanoparticles complex also facilitates effective cellular internalization of the complex via adsorptive endocytosis. The proton sponge effect of branched PEI in the endosome also assists endosomal escape of the nanoparticles for subsequent gene expression.

This research is an extensive of previous study of our groups that involves the use of

amphiphilic poly(methyl methacrylate)/polyethylenimine (PMMA/PEI) core-shell nanoparticles in gene delivery. [1-2] This thesis is composed of three major parts regarding to the synthesis and characterizations of the gelatin/PEI nanoparticles and their application in gene delivery:

1. Synthesis and characterizations of gelatin/PEI nanoparticles with core-shell nanostructure

Synthetic strategy to prepare gelatin/PEI core-shell nanoparticles has been developed. Nanoparticles with various PEI contents were prepared by varying reaction pH and PEI concentration. The physiochemical properties of the resultant nanoparticles such as particle sizes, surface charges, morphology, core-shell nanostructures and biodegradability were characterized.

2. Complexation studies of the gelatin/PEI nanoparticles with plasmid DNA (pDNA) and small interfering RNA (siRNA)

Selected gelatin/PEI nanoparticles were used to complex with the pDNA and siRNA. The efficiency for complete DNA condensation (nitrogen-to-phosphate (N/P) ratio, DNA integrity retention ability and DNA protection effect of the nanoparticles were determined

3. *In vitro* studies of siRNA delivery

The siRNA is condensed by the gelatin/PEI nanoparticles and delivered to HeLa cells. The gene silencing effect of the complexed siRNA was studied. The internalization efficiency of the siRNA/nanoparticle complexes and intracellular distribution of the

siRNA and nanoparticles were also analyzed. Finally the cytotoxicity of the nanoparticles and the antitumor effect using a combination of siRNA delivery and arginine deiminase (ADI) treatment were also investigated.

2.2 Uniqueness of gelatin/PEI nanoparticles

Although gelatin is biodegradable, some literatures pointed out that the degradation rate of gelatin nanoparticles is too fast that most of the nanoparticles are rapidly cleared within several hours in blood circulations that make drug or gene delivery not effective. Surface modification of gelatin nanoparticles using the PEI molecules can retard the degradation rate of gelatin, thus extending its life-time in blood circulation. In addition, the positive surface charge provided by PEI shell can considerably improve the stability of the nanoparticles in aqueous solution and promote re-dispersion after lyophilization.

The following is the novel aspect of this work:

1) The synthesis conducts mainly in aqueous medium and does not contain toxic solvent. The coupling agent *N*-Ethyl-*N*′-(3-dimethylaminopropyl)carbodiimide hydrochloride (EDC·HCl) is less harmful than those available hetero-bifunctional crosslinkers.[3]
2) Microgel particles consisting of gelatin cores and PEI shells can be fabricated via an ethanol treatment process. The PEI molecules are covalently grafted onto the surface of gelatin nanoparticles. The covalent linkage is stable, thus the PEI molecules will not dissociated upon environmental changes, such as temperature, pH and ionic

strength.

3) The covalently linked nanoparticles are stable in aqueous environment.

4) The PEI-based nanoparticles are more regular in shape and homogenous with narrow size distribution and reproducible surface charges.

2.3 References

1. Junmin Zhu, Angie Tang, Lai Pang Law, Min Feng, Kin Man Ho, Daniel K. L. Lee, Frank W. Harris and Pei Li, *Bioconjugate Chemistry 16(1)* **(2005)** 139-146.
2. Pei Li, Junmin Zhu, Panya Sunintaboon, and Frank W. Harris, *Langmuir 18* **(2002)** 8641-8646
3. Kuijpers, Alma J.; Engbers, Gerard H. M.; Krijgsveld, Jeroen; Zaat, Sebastian A. J.; Dankert, Jacob; Feijen, Jan.," Cross-linking and characterization of gelatin matrices for biomedical applications" *Journal of Biomaterials Science -- Polymer Edition 11(3)* **(2000)** 225-243.

3 Synthesis, Purification and Characterization of gelatin/polyethylenimine (gelatin/PEI) nanoparticles

3.1 Materials

Type-B gelatin which has pI 4.9, as determined by zeta-potential (see Section 4.3.2.and mean weight average molecular weight (Mw) of 100,000(as reported in literature) was purchased from Acros. Branched polyethylenimine (average molecular weight of 25 kDa) and glyoxal (40 wt% in H_2O), and potassium phosphate (dibasic, trihydrate) were purchased from Aldrich. *N*-Ethyl-*N*′-(3-dimethylaminopropyl)carbodiimide hydrochloride (EDC·HCl) was obtained from BioChemika. Absolute ethanol was purchased from International Laboratory. were 2,4,6-Trinitrobenzenesulfonic acid solution (TNBS, 5% in H_2O(w/v)), phosphotungstic acid (PTA), sodium dodecyl sulfate (SDS), protease (from bacillus sp, ≥ 8 U/g), analytical grade of hydrochloric acid solution and sodium chloride were all purchased from Sigma. Low range protein marker was obtained from Bio-Rad. Carbon coated copper grids (400 meshes) were used. All aqueous solutions and buffers were prepared using DI water which has been purified by Milli-Q integral.

3.2 Methods

3.2.1 Synthesis and purification of gelatin/ polyethylenimine (gelatin/PEI) nanoparticles

Synthesis of gelatin microgels

Gelatin powder (0.6 g, contain about 17% moisture, proven by thermogravimetric analysis (TGA) in Aappendix A) was dissolved in a 50 mL of water under a magnetic stirring, giving a pale yellow clear solution. The solution was continuously stirred for different times (5, 6 or 7 h) at 70℃. A crude product of gelatin microgels was formed, while appearance of the solution remained almost the same. The concentration of the microgels in solution (solid contents) was determined to be approximately 1.0 w/w% through freeze drying 10 mL of microgel solution, giving a white solid.

Synthesis of gelatin/PEI nanoparticles

Various amount of branched polyethylenimine (PEI) (0.470 g, 0.235 g, 0.118 g and 0.047g) was dissolved in a 25 mL water under a magnetic stirring for 15 min. The pH of the solution was adjusted to 5 and 3.8, respectively, using a hydrochloric acid solution (HCl, 2 M). *N*-Ethyl-*N*′-(3-dimethylaminopropyl)carbodiimide hydrochloride (EDC·HCl) (0.083 g) was added and completely dissolved in the PEI solution. The

mixture was heated to 40℃ in a water-jacket flask, followed by addition of the gelatin microgel solution (25 mL, 1.0 wt %). (The mole ratio of EDC to –COOH group of gelatin = 1.5:1; while the mole ratio of $–NH_2$ group of PEI to –COOH group of gelatin was 8.8:1, 4.4:1, 2.2:1 and 0.88:1, respectively. A detailed calculation of the amounts of gelatin, PEI and EDC added is shown in Appendixes B and C. The mixture was stirred at 350 rpm for 24 h at 40℃ to allow grafting of PEI onto the gelatin microgels.

Purification of gelatin/PEI nanoparticles

The gelatin/PEI nanoparticles were purified by an ultrafiltration (MWCO of filter membrane = 50 kDa) against Milli-Q water until the conductivity of the water used could not be further reduced. The nanoparticles was further purified by a dialysis (MWCO of dialysis tubing = 50 kDa) until the conductivity of the water was similar to that of the fresh Milli-Q water used. This purification processes remove all unreacted PEI and coupling agent. The purified nanoparticles were then freeze dried for storage at room temperature. Solid contents of the purified gelatin/PEI nanoparticles weew determined by freeze drying a portion of the nanoparticle solution (5 mL) and measuring the weight of the dry solid. Scheme 3.1 illustrates the synthesis and purification processes.

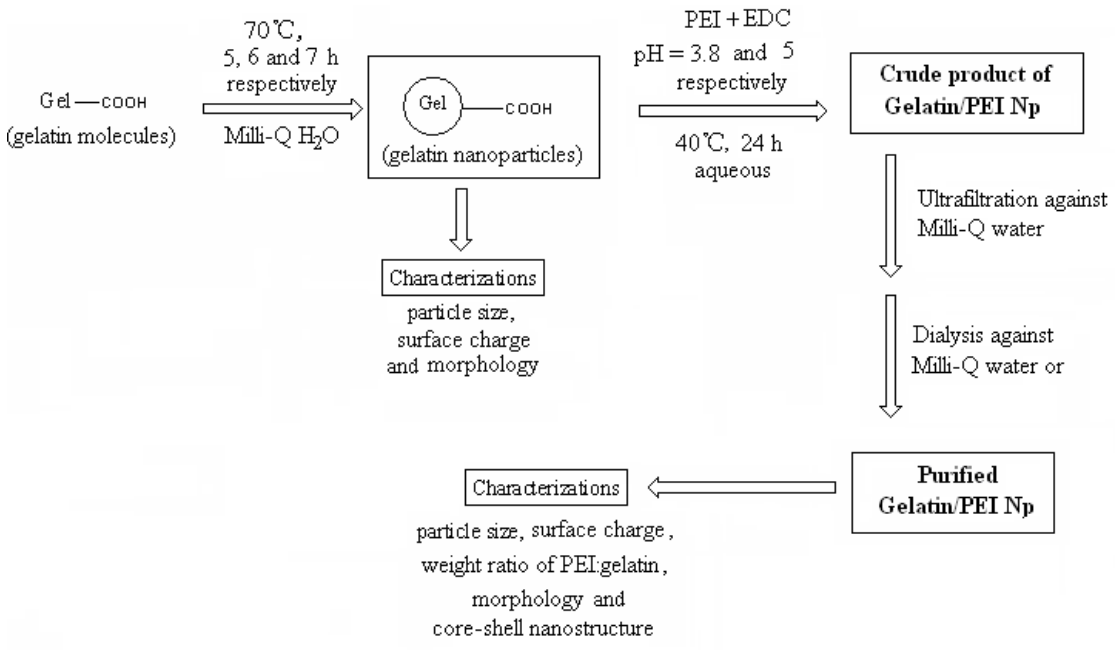

Scheme 3.1. Schematic diagram of synthesis, purification and characterizations of gelatin/PEI nanoparticles.

Ethanol treatment of gelatin/PEI nanoparticles

Freeze dried purified gelatin/PEI nanoparticles (20 mg) were redispersed in a 5 mL of ethanol or a mixture of ethanol/water (100%, 90% or 80% v/v ethanol) respectively. The mixture was then placed inside an ultrasonic bath for 45 min. The precipitates (if any) were removed by centrifugation (8000 rpm for 10 min). The amounts of precipitates were determined by gravimetric method. The supernatants were dried under vacuum. The resultant pale yellow or white solid was redispersed in the same concentration of ethanol solution again and dried under vacuum in the same way. This ethanol treatment cycle was repeated twice. The final solids were redispersed in a Milli-Q water to give a turbid dispersion. The ethanol treated nanoparticles were

stored in either liquid or solid form by freezing in liquid nitrogen for lyophilization.

Crosslinking of gelatin/PEI nanoparticles

After dispersing the gelatin/PEI nanoparticles in 80% ethanol, different amount of glyoxal (weight = 4% to 12% of total weight of PEI) was added and the mixture was stirred at room temperature for 30 min to allow crosslinking of amine groups of PEI. After that, the mixture was dried under vacuum environment and the resulting nanoparticles were redispersed in Milli-Q water.

3.2.2 Characterization of gelatin microgels and gelatin/PEI nanoparticles

3.2.2.1 Particle size distribution measurement

Hydrodynamic diameters ($Z_{average}$ or Z_{ave}) and size distributions of the resulting gelatin microgels, purified gelatin/PEI nanoparticles and the nanoparticles obtained after ethanol treatments were analyzed .using a ZetaSizer 3000HSA. All samples were diluted to appropriate concentrations with DI water and ultrasonically treated for 20 min prior to the measurement.

3.2.2.2 Surface charge measurements

Surface charges (zeta potentials) of the resulting gelatin microgels and gelatin/PEI nanoparticles were determined using a ZetaSizer 3000HSA. All samples were diluted to 300 ppm in 1 mM NaCl solution and pH values were adjusted to 3, 5, 7, 9, 11 and 13, respectively. The samples were then treated in an ultrasonic both for 20 min prior to measurement.

3.2.2.3 Actual weight ratio of gelatin to PEI of the gelatin/PEI nanoparticles determined by UV/VIS spectrophotometry

Weight ratios of gelatin to PEI of the purified gelatin/PEI nanoparticles were determined by a UV/VIS spectrophotometry according to the literature method [5-6] This method is based on the reaction between 2,4,6-trinitrobenzenesulfonic acid (TNBS, refer to figure 3.1 for the chemical structure) with primary amine groups to from yellowish orange compound as shown in Figure 3.2. Thus the PEI contents on the nanoparticles can be acutely determined.

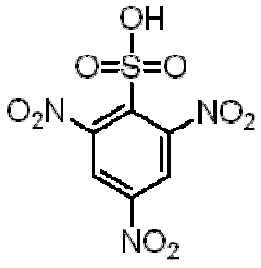

Figure 3.1. Chemical structure of 2,4,6-trinitrobenzenesulfonic acid (TNBS)

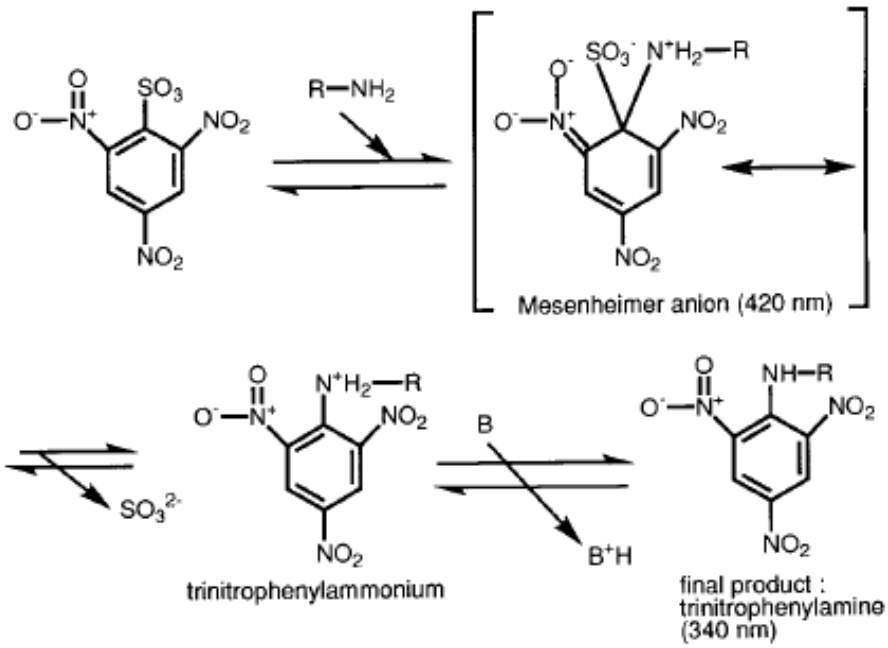

Figure 3.2. Mechanism of trinitrophenylation reaction between TNBS and primary group [5]

Figure 3.3 shows the UV-VIS absorption spectrum of the branched PEI (25 kD). There are two absorption peaks at 420 nm and about 350 nm which are corresponding to the intermediate and final product of the reaction between PEI and TNBS. As the apex at 420 nm is smoother and has a higher intensity, it was used for characterization of the PEI.

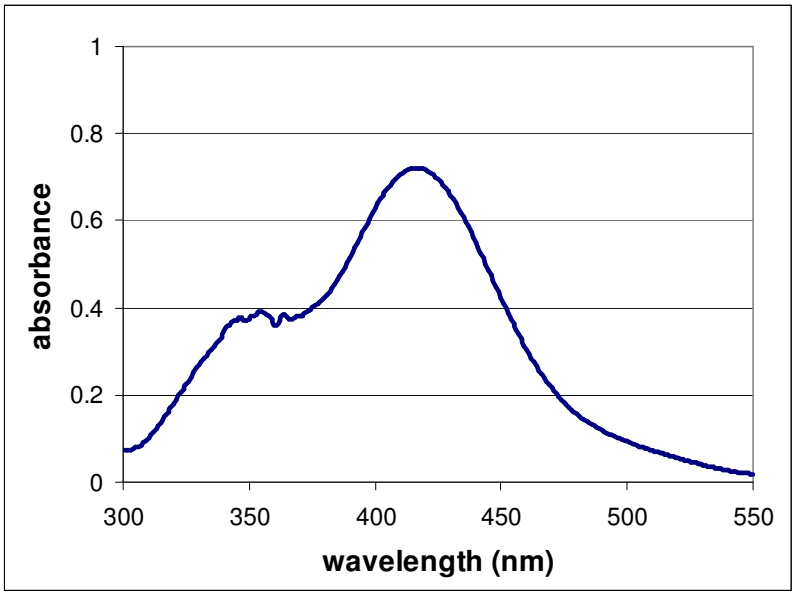

Figure 3.3. Absorption spectrum of branched PEI (25 kD) + TNBS. (Conditions: 7.2 x 10^{-7} M (or 18 ppm) PEI + 7.3 X 10^{-4} M TNBS in 50 mM K_2HPO_4 buffer (pH 7.7). The mixture was incubated for 2 h at room temperature in dark.

A calibration curve of the PEI was firstly constructed by dissolving a set of standard PEI solutions (concentration from 7 to 37 ppm) in K_2HPO_4 buffer solution (50 mM, pH 7.7). 50 μL of TNBS solution (2 mL, 0.03 M) was then added to each of the standard PEI solutions. The mixtures were incubated for 2 h at room temperature in dark for color development. The reagent blank consisting of 50 μL TNBS in 2 mL of the buffer (50 mM K_2HPO_4, pH 7.7) was treated the same way as that of the PEI standards. After 2 h incubation, the absorbance at λ 420 nm was measured by a HITACHI U-2800 spectrophotometer. A calibration curve of absorbance against PEI concentrations was constructed as illustrated in Figure 3.4.

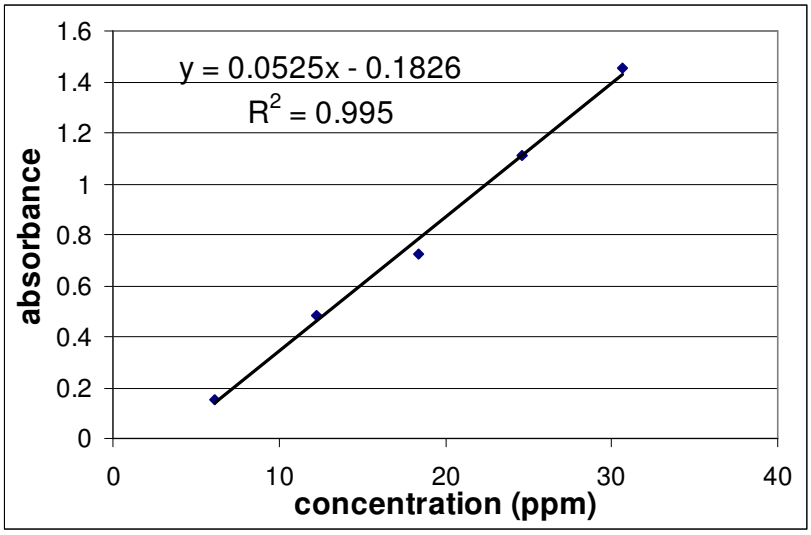

Figure 3.4. Calibration curve of absorbance at 420 nm (λ_{420}) against PEI concentration (ppm). Conditions: 7 - 30 ppm PEI + 7.3 X 10^{-4} M TNBS in 50 mM K_2HPO_4 buffer (pH 7.7). The mixture was incubated for 2 h at room temperature in dark.

For analyzing the amount of PEI grafted onto the nanoparticles, the purified nanoparticle dispersions were diluted in 50 mM K_2HPO_4 buffer of pH 7.7 with appropriate concentrations. The diluted samples (2 mL) were mixed with the same amount of TNBS (0.03 M, 50 µL) and treated under the same conditions as the PEI standards.

3.2.2.4 Particle morphologies observed by the scanning electron microscopy (SEM)

Particle morphologies of the resulting gelatin microgels and gelatin/PEI nanoparticles were observed with a scanning electron microscopy (JEOL JSM-6335F Field Emission Scanning Electron Microscope). All samples were diluted to 100 - 500 ppm

in DI water or ethanol, followed by ultrasonic treatments for 20 min. Then 10 μL of the samples were placed on glass slices and allowed them to be dried in air. After that the dried specimens were coated under vacuum with a thin layer of gold to a depth of 5 Å.

3.2.2.5 Core-shell nanostructures observed by the transmission electron microscopy (TEM)

The purified gelatin/PEI nanoparticles (before and after ethanol treatments) were analyzed for their core-shell nanostructures using transmission electron microscope (JEOL-100CXII) at an accelerating voltage of 100 kV. All samples were diluted to 500 ppm in DI water or ethanol and then treated in the ultrasonic both for 20 min. 10 μL of the sample was added to a carbon coated copper grids. After drying, it was stained with 0.5 wt% of PTA solution for 60 sec.

3.2.2.6 Biodegradability of gelatin microgels and gelatin/PEI nanoparticles

The biodegradability of gelatin microgels and gelatin/PEI nanoparticles were determined using protease as the digesting enzyme. The degrees of degradation were determined by a sodium dodecyl sulfate polyacrylamide gel electrophoresis (SDS-PAGE). A detailed procedure is as follows: 12.5 μg of the gelatin molecules, gelatin microgels and gelatin/PEI nanoparticles were diluted in an enzyme buffer (50

mM K_2HPO_4 Buffer, pH 7.5) to obtain 8 µL mixtures. After that, 2 µL of protease solution, which had activity of 1.1 x 10^{-4} U, was added to each of the mixture. The mixture was then incubated at 37 ^{o}C in a water bath for 10 min to allow protein digest. The mixtures were then placed into 90 ^{o}C water bath for 5 min to deactivate the enzyme. 10 µL of 2X reducing sample buffer containing 2% of SDS was added and the mixture was boiled for 3 min for protein unfolding, followed by ice cooling for 3 min. After the process of protein unfolding, the mixture was loaded to an acrylamine gel [4% stacking gel (pH 6.8) and 12% running gel (pH 8.8)] for electrophoresis. The samples were run with low range protein marker with running time and applied voltage of 1 h and 220 V, respectively. After electrophoresis, the gel was stained for 30 min in a comassie blue solution, followed by destaining overnight in methanol-water-acetic acid solution.

3.3 Results and Discussions

3.3.1 Synthesis and characterization of gelatin microgels

The gelatin/PEI core-shell nanoparticles are synthesized through a three-step process: In the first step, gelatin microgels is generated by stirring the gelatin solution at 70 ^{o}C for 5, 6 and 7 h, respectively. The size distribution, surface charge and morphology of the resultant microgels were determined.

Synthesis of the gelatin microgels

For the tertiary structure of gelatin, the spiral winds and folds itself to a right-hand spiral (triple helix). This results in a rod-shaped molecule, the so-called proto fibril.[2] Becasue gelatin is a partially crystalline polymer, it has both glass-rubber transition temperature (T_g) and thermal unfolding temperature (T_m).[3] At temperature above its T_m, Gelatin can undergo thermal denaturation and cause disruption of hydrogen bonding among the protein chains, resulting in unfolding of the protein. D'Cruz suggested that T_m is larger than T_g and they have a linear relationship. Thus the gelatin in the rubbery state has the necessary mobility for hydrogen bond disruption that leads to protein unfolding.[3] Therefore, T_m is also defined as helix-coil transition temperature in the literature.

In this expermient, the gelatin aqueous solution was stirred at 70^{o}C for 5 to 7 hrs to form gelatin microgels through thermal denaturation. During this process, the gelatin molecules undergo this helix-coil transition and change their shape from rod-like to globular structure.

Size distributions

The average hydrodynamic diameter (Z_{ave}) and polydispersity index (PDI) of gelatin microgels prepared at different reaction times were measured and their results are summarized in Table 3.1. The average hydrodynamic diameter of the gelatin microgels prepared at different stirring time (5 h, 6 h and 7 h) gave very similar particle size and size ditribution. They were about 90 nm in diameter with broad size distribution as the polydispersity index is approaching to 1, which indicates that the gelatin microgels have very wide distribution of size in aqueous medium. Since gelatin is the degraded product of collagen with wide molecular weight distribution, the PDI of gelatin microgels was relatively large. As the size distribution of the microgels are very large, it is not suitable or gene delivery and need further modification (in the following sections) to reduce the size distribution.

Table 3.1. Table of average hydrodynamic diameter (Z_{ave}) and polydispersity index (PDI) of gelatin microgels with different reaction times.

Reaction time	Z_{ave} [1]	PDI [2]
5 h	89.0 ± 13.5	0.998
6 h	88.6 ± 16.6	0.998
7 h	90.6 ± 16.9	1.000

[1] The values were the average of 5 measurements.

[2] PDI, ranging from 0 to 1, implies the degree of size distribution in aqueous medium. The higher the value, the wider is the size distribution. The general acceptable value is 0.7 (provided by the manufacturer).

Surface charges

The surface charges of the gelatin molecules and gelatin microgels (obtained after 7 h of reaction time) as a function of pH with ZetaSizer in 1 mM NaCl solution. Figure 3.5 shows that neutral surface charge of gelatin molecules is at about pH 4.9, which is corresponding to the isoelectric point (pI) of the type B gelatin molecule. The gelatin microgels which formed after thermal treatment of the type B gelatin have the pI of 5.4. Thus the transformation of molecular gelatin to its microgels has minor effect on the acidic and alkaline functional groups (such as COOH and NH_2 groups). This may be due to the fact that thermal denaturation mainly involves the disruption of hydrogen bondings of protein unfolding, but not changing the functional groups.

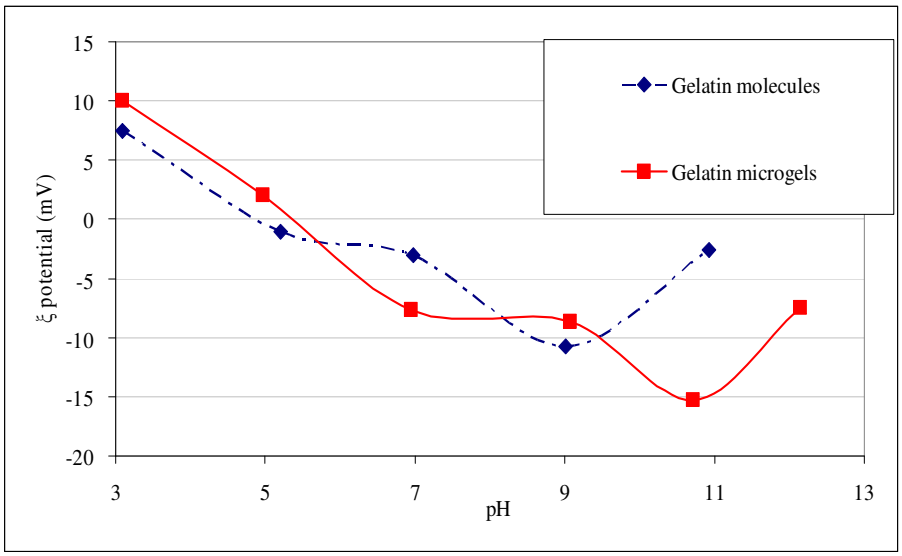

Figure 3.5. *Zeta*-potentials of gelatin molecules (◆) and gelatin nanoparticles (■) as a function of pH from 3 to 13 in 1 mM NaCl solution.

Particle morphology

Table 3.2 summarizes the SEM images of gelatin microgels after reacting for 5 to 7 h. It was observed that after reacting for 5 h, majority of the gelatin microgels obtained were in spherical shape with diameters ranging from 70 to 240 nm. However, some of the microgels were still in rod shape, indicating that the complete helix-coil transition had not yet achieved. When reacting the gelatin molecules for 6 hours, even though a few rod-shaped particles with much bigger sizes were still observed, there was an increasing number of spherical particles ranging from 50 to 100 nm Prolonging the reaction time to 7 hours gave all spherical microgels with bi-model distribution.

Table 3.2. SEM micrographs of gelatin microgels prepared at 70 ^{0}C for various reaction times.

Reaction time	**5 h**	**6 h**	**7 h**
SEM micrographs	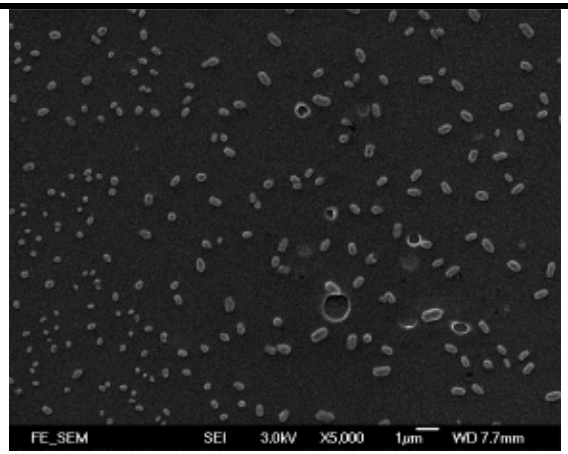	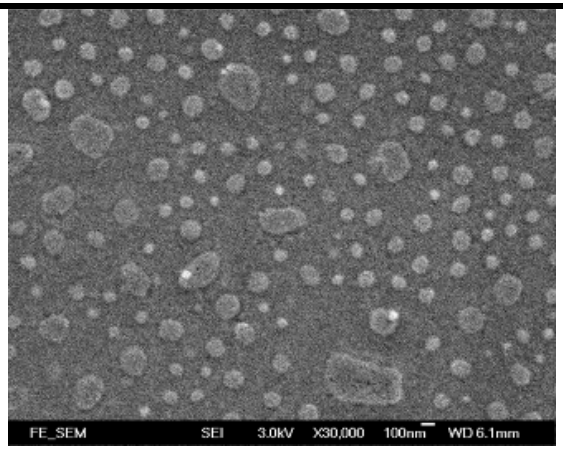	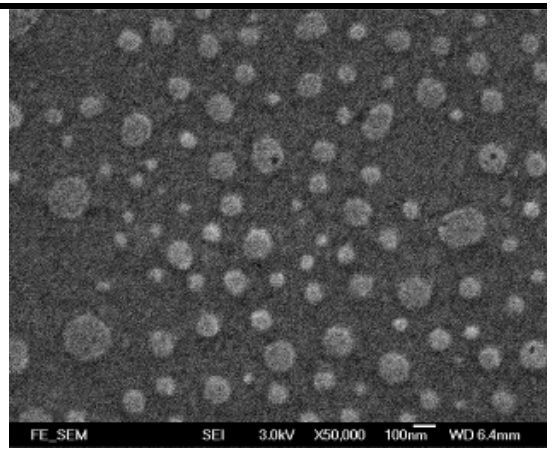
	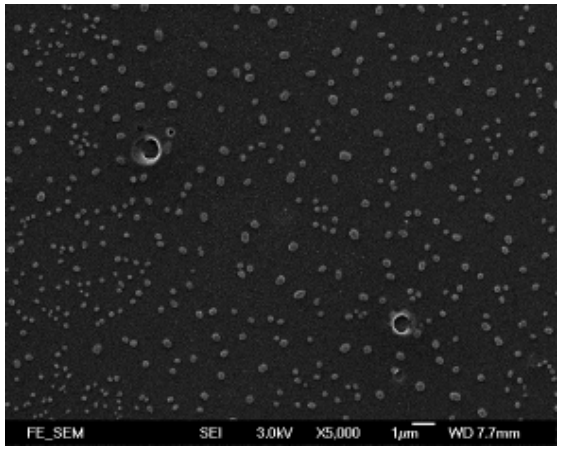	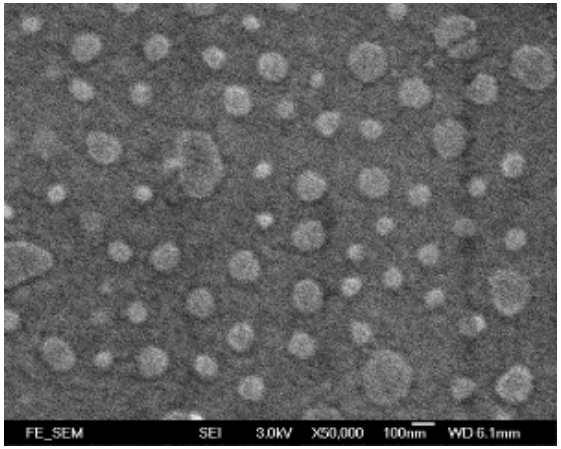	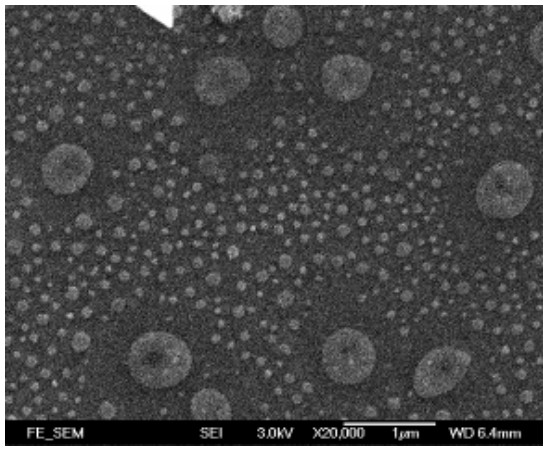

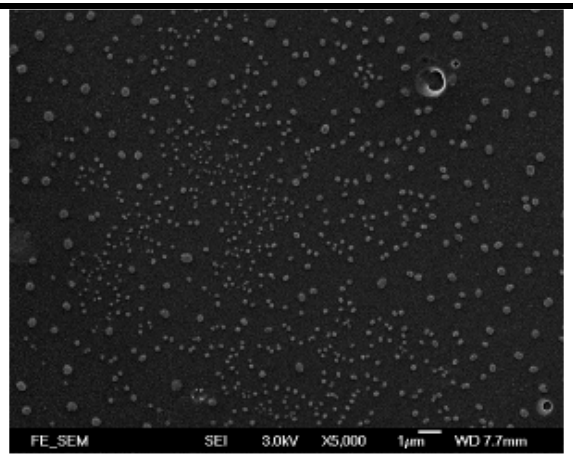

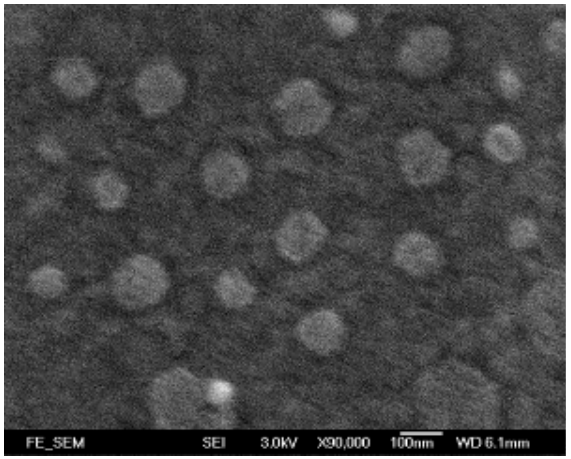

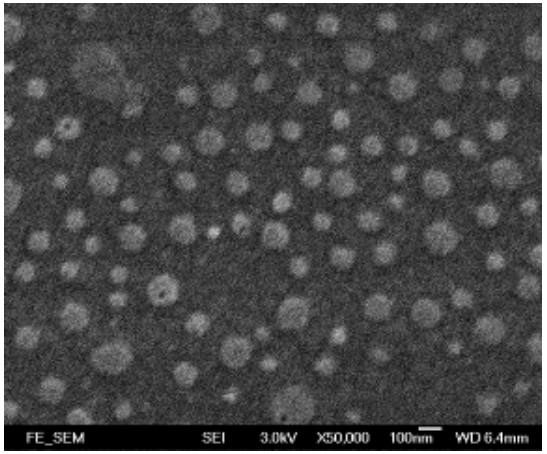

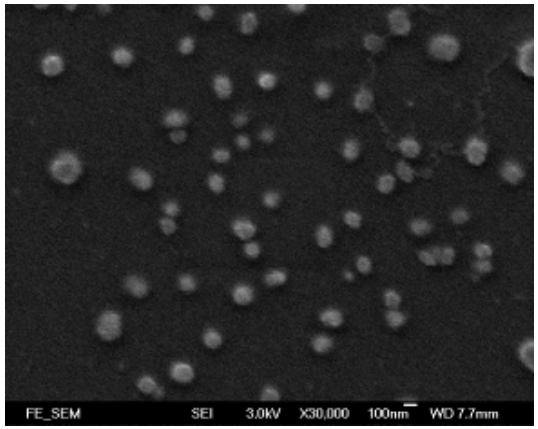

Shape of the microgels	Some rod-like shape, some spherical	Spherical	Spherical
Measured size	70 – 240 nm, mean 148 nm	50 – 100 nm, 300 – 600 nm	50 – 100 nm, 300 – 600 nm

3.3.2 Synthesis of gelatin/PEI nanoparticles

After synthesizing the gelatin microgels via stirring the gelatin solution at 70^{o}C for 7 h, varies concentrations of PEI were mixed with the gelatin microgels in the presence of a coupling agent, EDC. Thus PEI molecules were grafted onto the pre-formed gelatin microgels surface. The resulting gelatin/PEI nanoparticles were then purified by the ultrafiltration followed by the dialysis. For the gelatin/PEI nanoparticle dispersions prepared at both pH 3.8 and 5, the final dispersions were pale yellow clear solutions.

Since the isoelectric point (pI) of gelatin microgels is at about pH 5.4 (see Section 3.3.1) while the zero of charge pH of PEI is at about pH 12. It is necessary to carry out the coupling reaction at pH below the isoelectric point of the gelatin. Otherwise, the cationic PEI molecules may absorb onto the negative gelatin microgels through electrostatic interaction. Therefore, the coupling reactions were carried out at either pH 5 or 3.8. At these two pH medium, the gelatin microgels carry either nearly neutral surface charges or positively charge. As a result, the PEI molecules could be attached onto the gelatin microgel surface via covalent linkage. Scheme 3.2 shows the reaction mechanism. The carboxylic group of gelatin is firstly activated by EDC to form an O-acylisourea group. The amino group of PEI molecule then undergoes a nucleophilic attack to the carbonyl group, forming an amide linkage through releasing a urea derivative.[4]

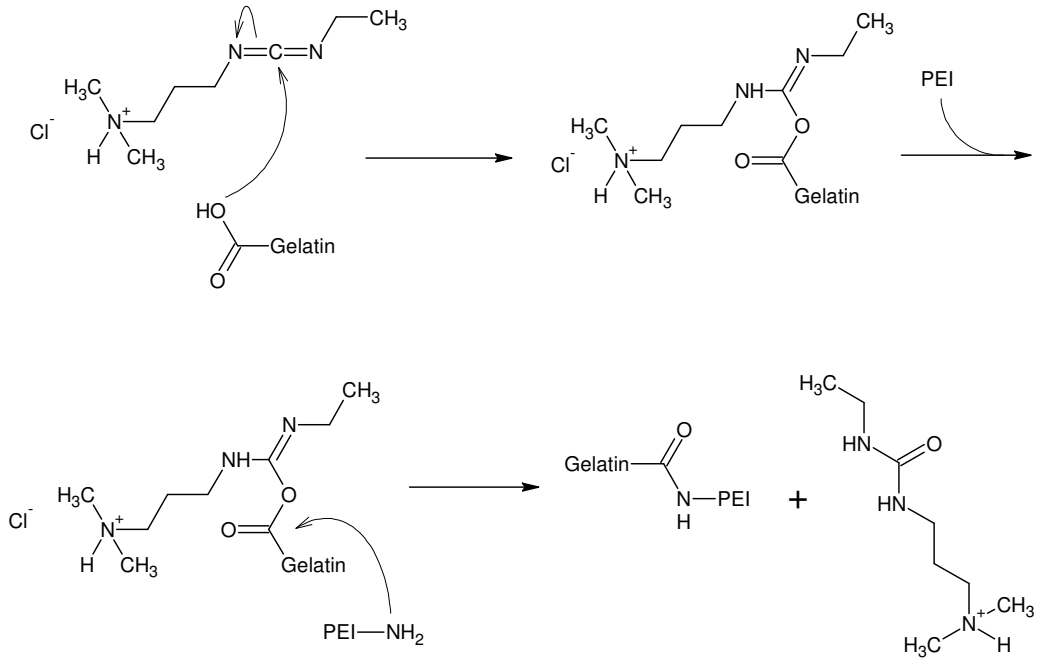

Scheme 3.2. Reaction mechanism of the coupling reaction between the carboxylic group of gelatin and amine group of PEI using *N*-Ethyl-*N*′-(3-dimethylaminopropyl)carbodiimide hydrochloride (EDC·HCl) as coupling reagent.

3.3.3 Core-shell formation induced by ethanol treatment

After purification, surface charges of the gelatin/PEI nanoparticles prepared above were determined at different pH values (see Section 3.3.5). It was noted that their zeta potentials values were all below +10 mV. This result was very unusual because PEI molecules usually possess very high surface charges (>+30 mV). One possible explanation for this phenomenon may be that both PEI and gelatin are water soluble. Once PEI molecules are grafted onto the gelatin particles, they may interpenetrate to each other instead of localizing on the particle surface. As a result, PEI is distributed within the microgels matrix instead of concentrating on the particle surface.

In order to concentrate the PEI molecules on the particle surfaces to create a core-shell nanostructure, the gelatin/PEI nanoparticles were treated with different percentages of ethanol (80-100%, v/v) to induce phase separation. Since gelatin is insoluble in ethanol, it shrinks inwardly to form a compacted core driven by the minimization of surface energy. In contrast, PEI molecules extend outwardly in the ethanol medium because they have high solubility in ethanol. Thus, this treatment process transforms the gelatin/PEI nanoparticles from the interpenetrated nanostructure into the well-defined core-shell nanostructure where gelatin molecules act as the core, and PEI molecules form as the thick shell. This morphological change could be reflected from the appearance of the dispersion because the original clear, pale yellow dispersion changed to turbid after the ethanol treatment. The turbidity is caused by the light scattering of the compacted gelatin cores. To gain more insights into this phase separation phenomenon, the effects of ethanol treatments on particle size, surface charge and particle morphology were systematically studied by measuring the particle size, zeta potential, and observing particle morphology and nanostructure with scanning electron microscopy (SEM) and transmission electron microscopy (TEM) images.

3.3.4 Effect of reaction pH and charging ratio on PEI grafting contents

In order to determine the PEI content of the gelatin/PEI nanoparticles by UV/VIS spectrophotometry, a series of PEI standard solution was prepared and a fixed amount of 2,4,6-trinitrobenzenesulfonic acid (TNBS) solution was added. The absorption peak at 420 nm was measured and a calibration graph was constructed as shown in Figure 3.4 in Section 3.2.2.3. The PEI contents of the gelatin/PEI nanoparticles

dispersions were calculated based on Equation 3.1.

$$\lambda_{420nm} = 0.0525c - 0.1826 \quad (3.1)$$

where λ_{420nm} is the absorption at 420 nm and c is the PEI concentration in ppm.

Calculations of the weight ratio of PEI to gelatin of the gelatin/PEI nanoparticles are shown in Appendix E. Table 3.3 summarizes the PEI contents of the gelatin/PEI nanoparticles synthesized under different reaction pH and charging ratio of PEI to gelatin. For both reactions at pH 3.8 and 5, the PEI contents of the resultant gelatin/PEI nanoparticles increased with the increasing PEI fed ratios. This is because if the PEI concentration is lower, there is higher chance for the gelatin microgels to couple with the amine groups of the same PEI molecules. However, there was no precipitation for the nanoparticles with lower PEI content may be because both gelatin and PEI are also water soluble. Oppositely, when the PEI concentration is higher, there is higher chance for the gelatin microgels to couple with the amine groups of different PEI chains, resulting in higher numbers of PEI chains to be grafted onto the same gelatin microgel.

Table 3.3. Formation of gelatin/PEI nanoparticles with different charging weight ratio of PEI to gelatin and different reaction pHs

Sample ID	161107	090108	240108	290108	191207	170309	300409
Reaction pH	3.8				5		
Mole ratio of $-NH_2$ of PEI to –COOH of gelatin added	8.8:1	4.4:1	2.2:1	0.88:1	8.8:1	4.4:1	0.88:1
Charging weight ratio of PEI:gelatin	1.87:1	0.94:1	0.47:1	0.20:1	1.87:1	0.94:1	0.20:1
PEI content of the nanoparticles	**64%**	**43%**	**38%**	**36%**	**49%**	**47%**	**26%**
Actual weight ratio of PEI to gelatin of the nanoparticles	1.78:1	0.75:1	0.61:1	0.56:1	0.96:1	0.89:1	0.35:1

At pH 3.8, the gelatin microgels have a net positive charge surface. The protonated primary groups (NH_3^+) and carboxylic acid groups (COOH) are in dominant forms:

$$NH_2 \rightleftharpoons NH_3^+$$

$$COOH \rightleftharpoons COO^-$$

The shifting of COO^- to COOH causes increase in the COOH concentration, while the shifting of NH_2 to NH_3^+ causes decrease in NH_2 concentration. Since the COOH group concentration of the gelatin microgels is higher at pH 3.8, higher number of PEI molecules can be grafted onto them. In addition, when the NH_2 concentration of the gelatin microgels is lowered at pH 3.8, the chance of intramolecular coupling reaction is lower. As a result, the PEI content of the gelatin/PEI nanoparticles reacted at pH 3.8 is higher than at pH 5 under the same charge ratio of PEI.

The actual PEI contents of the gelatin/PEI nanoparticles were determined by allowing the PEI/gelatin nanoparticles to react with 2,4,6-trinitrobenzenesulfonic acid (TNBS) according to the mechanism descried in Figure 3.1. The sulfonic acid groups of TNBS react with the primary amine groups to give a yellowish orange trinitrophenylation reaction mixture with intensity proportional to the concentration of the primary amine groups.[4] Snyder *et al* [5] modified the procedure using a more acidic buffer (pH 7.7 instead of pH 9.3) as the reaction medium and a longer incubation time (2 h instead of 30 min) because of the large molecular weight of PEI and gelatin/PEI nanoparticles and relatively slower rate of reaction in more acidic medium.[6] It was observed that the PEI containing samples precipitated after incubating with TNBS in pH 9.3. The precipitation might be due to lack of electrostatic stabilization by PEI at a higher pH. On the other hand, more acidic medium has slower reaction rate and needs longer incubation time. Under near neutral pH (7.7), the rate of trinitrophenylation with

gelatin is very slow, thus the amino groups of the gelatin almost don't contribute to the color intensity at 420 nm after 2 h of incubation time (Figure 3.6). Therefore, the absorbance at 420 nm is attributed from the amino groups of PEI only.

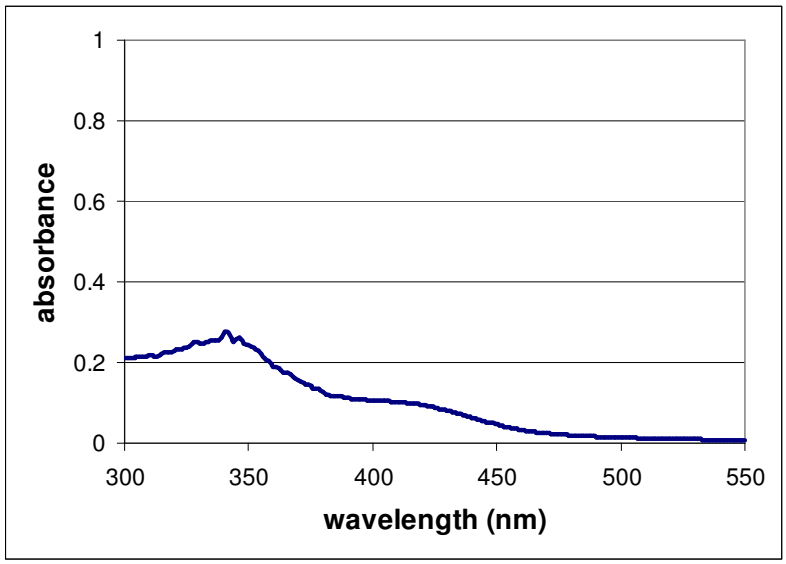

Figure 3.6. Absorption spectrum of gelatin nanoparticles + TNBS. Conditions: 4200 ppm gelatin Np + 7.3 X 10^{-4} M TNBS in 50 mM K_2HPO_4 buffer (pH 7.7). Incubated for 2 h at room temperature in dark.

3.3.5 Effect of ethanol treatment on particle sizes and size distributions

Effect of ethanol treatment on particle size and size distribution

Hydrodynamic diameters (Z_{ave}) and polydispersity indexes (PDI) of the purified gelatin/PEI nanoparticles (at different reaction pH and fed PEI-to-gelatin ratio) before and after treating with 80% of ethanol solution were measured. The results are summarized in Table 3.4.

In general, the higher the PEI content of the PEI/gelatin nanoparticles, the larger is the particle size. For all the gelatin/PEI nanoparticles before ethanol treatment, their polydispersity indexes were 1, which means that the nanoparticles had broad size distribution. . The poor uniformity of the microgels may be attributed to the broad size distribution of the original gelatin microgels. Their particle size distribution had not improved with the attachment of PEI molecules.

After treating the gelatin/PEI nanoparticles with ethanol solution, the polydispersity index (PDI) values of all samples were considerably reduced from 1.000 to 0.355~0.566. Such significant improvement of their size distributions may be attributed to the fact that the PEI shell is able to improve particle stability through strong electrostatic and steric stabilizations. As a result, the core-shell nanoparticles have much better stability in water with minimum particle aggregation. On the other hand, the influence of ethanol treatment on the particle size seemed to be more complicated because there were two opposite effects exerting on the particle: 1) The insoluble gelatin molecules tended to aggregate together and formed tightly-packed cores driven by the minimization of surface free energy. As a result, the particles size should decrease. 2) In contrast, the PEI chains localized on the particle surface could extend into ethanol, thus forming highly extended shell which might increase the particle size. Because the final particle size is strongly depended on the overall of these two opposite effects, the particle size results as shown in Table 3.4 are actually quite fluctuated. Thus it is difficult to draw a clear trend.

Table 3.4. The hydrodynamic diameter (Z_{ave}) and polydispersity index (PDI) of gelatin/PEI nanoparticles prepared using various reaction conditions[1]

		No ethanol treatment		After ethanol treatment (80%)	
Reaction condition[1]	PEI content	Z_{ave} (nm)	PDI	Z_{ave} (nm)	PDI
pH 5; 8.8:1	49%	269.3 ± 24.4	1.000	312.8 ± 4.3	0.358
pH 5; 4.4:1	47%	142.2 ± 32.8	1.000	282.6 ± 5.2	0.566
pH 3.8; 8.8:1	64%	477.7 ± 36.1	1.000	309.6 ± 1.8	0.407
pH 3.8; 4.4:1	43%	407.3 ± 8.8	1.000	253.8 ± 5.3	0.523
pH 3.8; 2.2:1	38%	351.1 ± 43.6	1.000	320.5 ± 5.0	0.355
pH 3.8; 0.88:1	36%	195.3 ± 29.3	0.986	206.0 ± 1.9	0.560

[1] Variation of reaction pH and fed mole ratio of $-NH_2$ of PEI to –COOH of gelatin, without ethanol treatment and after treating with 80% ethanol solution. The values of hydrodynamic diameter and PDI are based on the mean values of five measurements.

Effect of ethanol concentration on particle size and size distribution of gelatin/PEI nanoparticles

Hydrodynamic diameters (Z_{ave}) and polydispersity indexes (PDI) of the purified gelatin/PEI nanooparticles (with PEI contents of 64% and 49%), which were treated with different concentrations of ethanol solution (80% and 100% v/v), were measured and the results are summarized in Table 3.5 When the nanoparticles were treated with

higher concentration of ethanol solution, particle sizes of the resultant nanoparticles became smaller and the polydispersity was lower. It is because when the nanoparticles were dispersing in higher ethanol concentration, the gelatin had higher degree of shrinkage and formed more compacted core.

Table 3.5. Effect of ethanol concentration on the hydrodynamic diameter (Z_{ave}) and polydispersity index (PDI) of gelatin/PEI nanoparticles[1]

PEI content of nanoparticles	64%		49%	
Ethanol solution concentration	Z_{ave} (nm)	PDI	Z_{ave} (nm)	PDI
80%	367.2 ± 5.5	0.411	308.4 ± 5.9	0.757
100%	319.0 ± 4.6	0.367	196.1±5.1	0.424

[1] The hydrodynamic diameter and PDI values were an average of five measurements.

3.3.6 Effect of ethanol treatment on surface charges

The effect of ethanol treatment on particle surface charges was studied through measuring the *zeta*-potential (ξ potential) of the gelatin/PEI nanoparticles (with PEI contents of 49%) before and after treatment with different concentrations of ethanol solution (80%, 90% and 100% v/v). The sample was diluted to about 300 ppm in 1 mM NaCl solution and the pH of the nanoparticle dispersion was adjusted to the range from 3 to 13.

Based on Figure 3.5 in Section 3.3.1, gelatin microgels have near neutral surface charge at about pH 5.4. Upon modifying the gelatin microgels with PEI, the neutral surface charges of gelatin/PEI nanoparticles shifted to about pH 12.2, which is similar to those of the PEI/PMMA nanoparticles (pH 11.6). These results indicated that PEI molecules were present on the nanoparticle surface. However, the overall surface charges of gelatin/PEI nanoparticles were relatively small (<10 mV). This confirms the hypothesis in Section 3.3.3 that the gelatin cores and PEI chains are interpenetrated with each other under aqueous environment as both gelatin and PEI are water soluble. After treating with ethanol solution, gelatin/PEI nanoparticles with a well defined core-shell structure is formed as described in Section 3.3.3. The core-shell nanostructure could be confirmed by the significant increase of surface charges to +38 mV at pH 7. The surface charges could be as high as +60 mV at pH 7 when treating the gelatin/PEI nanoparticles with 100% of ethanol solution. Figure 3.7 also shows the trends of surface charge changes as a function of pH for nanoparticles treated with 90% and 80% of ethanol solution. Their trands are similar and the *zeta*-potential values are about +40mV at pH 7. Moreover, the surface charges of the nanoparticles increase with decreasing pH as more and more primary, secondary and tertiary amine groups of PEI are protonated.

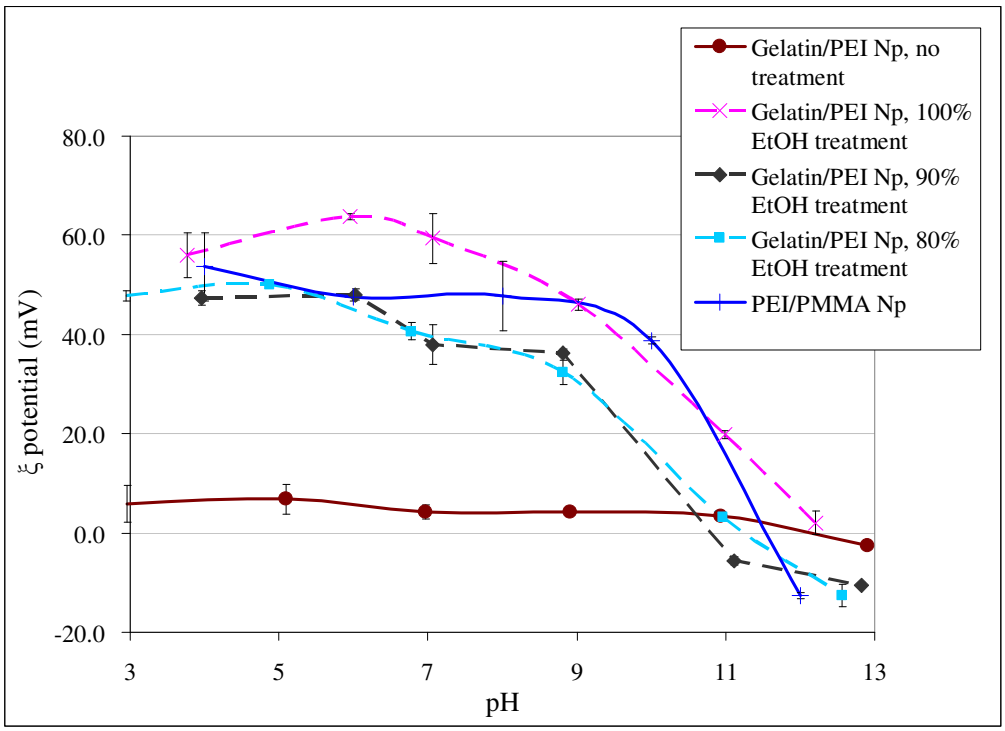

Figure 3.7. Effect of ethanol concentration on the zeta potential values of the resultant gelatin/PEI nanoparticles: (●) without ethanol treatment; (--x--) gelatin/PEI nanoparticles treated with 100% ethanol; (--♦--) treated 90% ethanol; ,(--■--) treated 80% ethanol; (+) PMMA/PEI core-shell nanoparticles. The zeta potential, ζ values were mean values of five measurements.

Although the nanoparticles which were treated with 100% of ethanol solution could give the highest surface charge value with the smallest particle size, the nanoparticles were actually not very stable in ethanol. For example, only 36 % of the particles could be stably dispersed in 100% ethanol. The stability of the nanoparticles could be improved when those gelatin/PEI microgels were treated with a mixture of ethanol and water. For example, 78 % of gelatin/PEI nanoparticles were stable when treated with 90% (v/v) ethanol, while those gelatin/PEI nanoparticles treated with 80% (v/v) ethanol/water solution were completely stable. Thus, 80% ethanol treatment of the gelatin/PEI microgels was chosen as the optimal ethanol treatment condition.

3.3.7 Effect of PEI contents on surface charges

The effect of PEI contents of the gelatin/PEI nanoparticles on particle surface charges was studied. Firstly, gelatin/PEI nanoparticles with different PEI contents (64%, 43% and 36%) were prepared, followed by treating these microgels with 80% ethanol solution for three times. The surface charges of the resultant nanoparticles as a function of pH between 3 and 13 were plotted as shown in Figure 3.8. The reported values were the mean values of five measurements.

In general, increasing PEI contents of the nanoparticles increases surface charges of the nanoparticles. It was also observed that the zero of charge pH of the resultant nanoparticles decrease with decreasing the PEI contents. The zero of charge pH of nanoparticles with PEI contents of 64%, 43% and 36% were about 11.6, 11.2 and 9.4 respectively. This phenomenon may be attributed to the rearrangement of PEI chains after re-dispersing in water. Although the core-shell nanostructure of the nanoparticles is formed after dispersing in ethanol solution, the nanoparticles are required to be dispersed in water after vacuum dry in order to perform gene delivery. After dispersing in aqueous medium, water molecules can re-enter into the gelatin cores, resulting in the core swelling. Thus, it is possible that some PEI chains could penetrate into the cores. This phenomenon is more obvious with those nanoparticles having lower PEI contents. If the PEI contents of the nanoparticles are higher, there are still much PEI chains at the nanoparticle surface even though some PEI chains may have penetrated into the gelatin cores. But this change will considerably affect the surface charges of those nanoparticles with lower PEI contents if some PEI chains

are penetrated into the gelatin cores. Therefore, higher PEI contents are more suitable to ensure the presence of PEI shells for condensation of biological molecules.

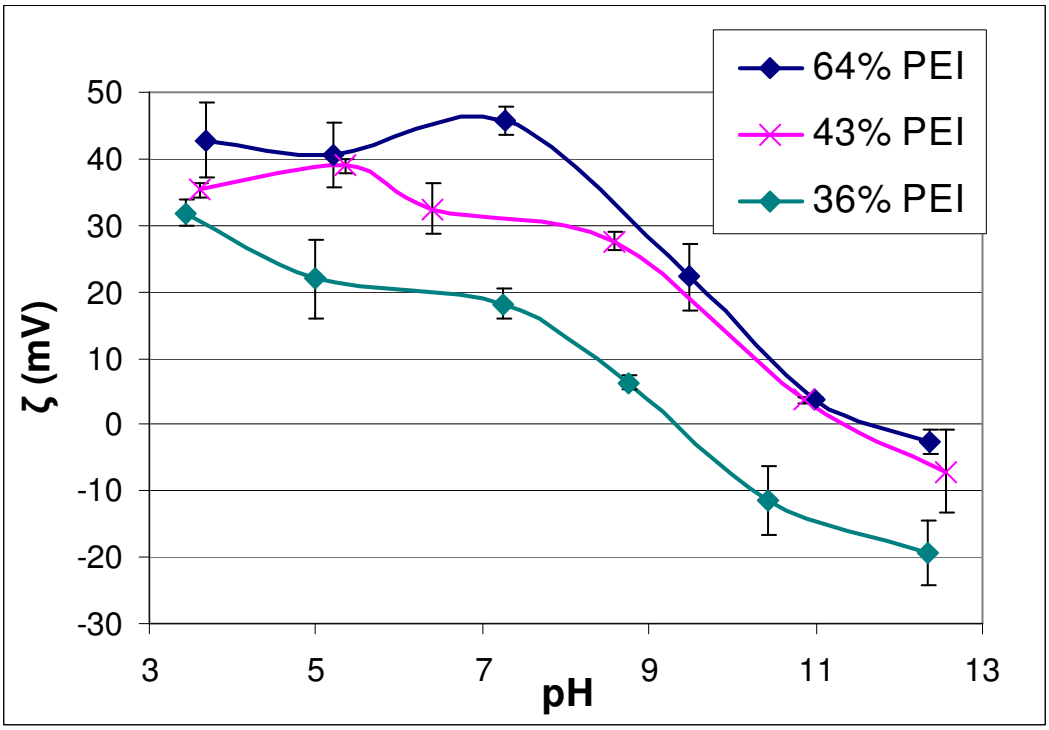

Figure 3.8. Zeta potentials of gelatin/PEI nanoparticles with PEI contents of 64% (◆), 43% (x), and 36% (♦) as a function of pH from 3 to 13 in 1 mM NaCl solution. All nanoparticles were treated with 80% of ethanol solution for three times before measurement.

3.3.8 Effect of PEI crosslinking on the particle sizes and surface charges

In the previous part (Section 3.3.6), it is shown that after treating with 80%-100% of ethanol, the surface charges of the gelatin/PEI nanoparticles were increased in at least several folds. However, the particle sizes of the most of the nanoparticles were

relatively large (>200 nm). Theoretically, the particle size should be between 100 nm to 200 nm in order to have passive targeting effect on penetrating tumor blood vessels instead of normal blood vessels. In addition, the increase of particle size raises the difficulty of endocytosis. In order to further reduce the particle size of the ethanol treated (80%) gelatin/PEI nanoparticle, the PEI shell was crosslinked with glyoxal according to the reaction shown in Scheme 3.3.

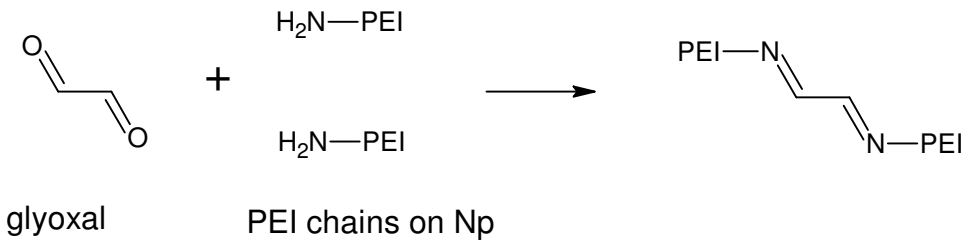

Scheme 3.3. Crosslinking reaction of PEI using glyoxal as crosslinking agent.

In fact, the aim of PEI crosslinking is not only to reduce particle size, but also to fix the core-shell structure. This is because after ethanol treatment, the particles were redispersed into water medium. As both PEI and gelatin are soluble in water, interpenetration of the two polymers can occur, resulting in the reduction of ξ potentials of the particles after storage for several weeks.

For this study, the gelatin/PEI nanoparticles containing 64.1% of PEI was used. The nanoparticles were crosslinked by different amount of glyoxal in 80% of ethanol. The effect of different degree of crosslinking on the particle size and surface charges are shown in Figure 3.9.

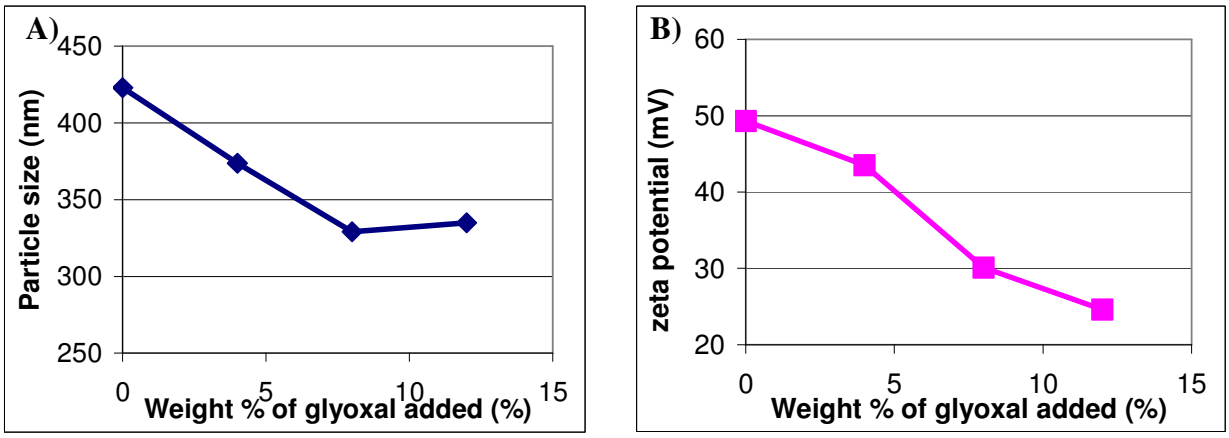

Figure 3.9. A) Particle sizes of crosslinked gelatin/PEI nanoparticles containing 64% of (Concentration of Np in H_2O = 0.1~0.4%); B) Zeta potential of crosslinked gelatin/PEI nanoparticles as a function of degree of crosslinking (400 ppm nanoparticles in 1 mM NaCl at pH 7.2-7.6)

When the amount of glyoxal increased from 0 to 12 weight % of the PEI, the particle sizes were reduced from 423.9 nm to 334.8 nm. However, due to the consumption of the surface amine groups, the surface charges were also decreased from +49.4 mV to +24.6 mV. The size of the nanoparticles after crosslinking were still larger than the desired diameter for intracellular internalization and some of the primary amine groups of PEI have been scarified during the crosslinking reaction. However, the crosslinking was unable to convert the gelatin/PEI nanoparticles with desirable properties. Thus, the gelatin/PEI nanoparticles used for gene delivery were only treated with 80% ethanol solution for three times to create gelatin/PEI nanoparticles with core-shell nanostructure and good dispersible property in water.

Crosslinking using glyoxal consumes some of the primary amine groups of PEI. Since DNA condensation requires primary amine groups of PEI, reduction of amine groups reduce the condensation ability of nanoparticles. Therefore, higher amount of

nanoparticles are needed for condensation.

3.3.9 Effect of ethanol treatments on surface morphologies of gelatin/PEI nanoparticles

The surface morphology of the gelatin/PEI nanoparticles was studied by scanning electron microscopy (SEM). Table 3.6 shows SEM images of untreated and ethanol treated (65% and 90%) gelatin/PEI nanoparticles containing 32% of PEI content. For the untreated nanoparticles with a lower PEI content (32%), the nanoparticles were hard to observe. A continuous film was observed on the glass slide. Based on the micrographs, the shape of the nanoparticles is spherical with diameter about 660 nm, but they are irregular in shape. As there are only a few nanoparticles could be observed in the SEM, the diameter value may not be representative. For the nanoparticles treated with 65% ethanol solution, the shape of the particles was more spherical with diameter about 110 - 280 nm and the mean size was166 nm. Finally for the nanoparticles treated with 90% ethanol solution, the shape of the particles is the most spherical among these three samples and the diameters were in the range between 125 to 260 nm with mean size of 181 nm. The SEM images were in agreement with the results of particle size and size distribution measurement. That is, the sizes of the gelatin/PEI nanoparticles are reduced after ethanol treatment. This is due to the shrinkage of the gelatin cores and formation of more “solid” nanoparticles.

Table 3.6. Scanning electron microscopy (SEM) images of gelatin/PEI nanoparticles (PEI content 32%) without and after treating with 65% or 90% ethanol solution.

Sample	Untreated	65% ethanol treatment	90% ethanol treatment
SEM micrographs	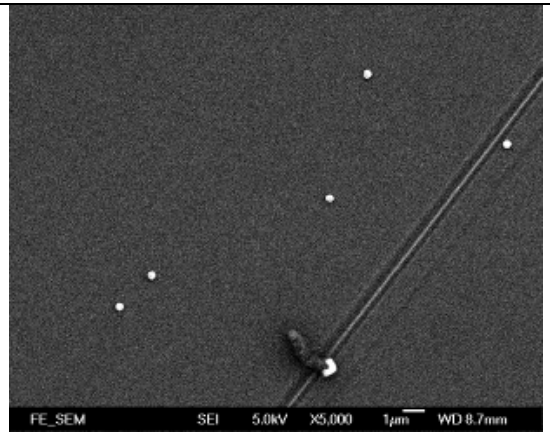 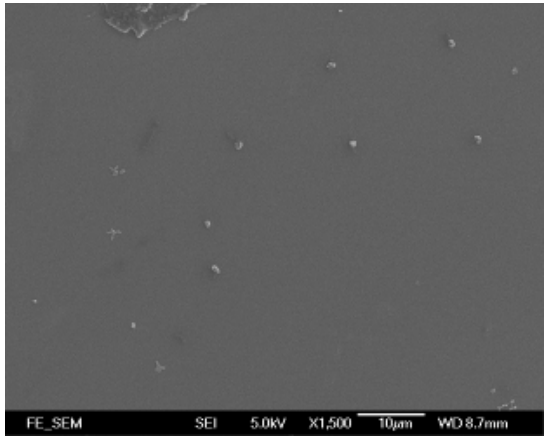	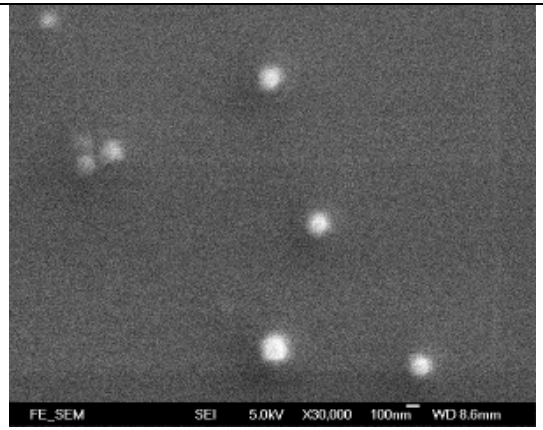 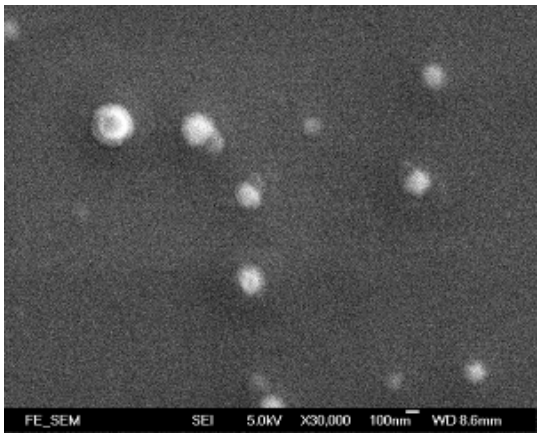	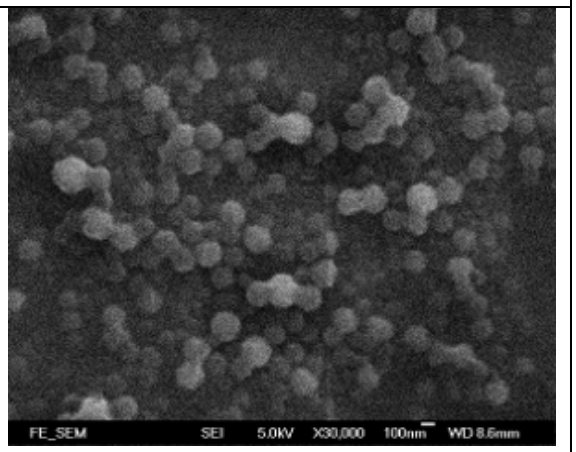 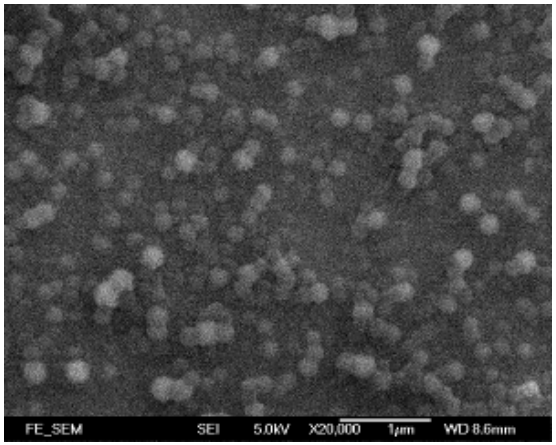

	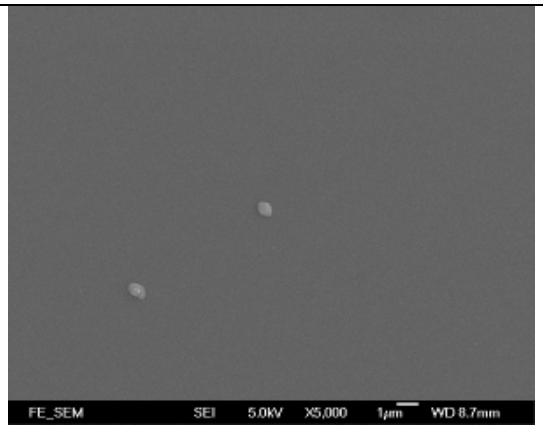 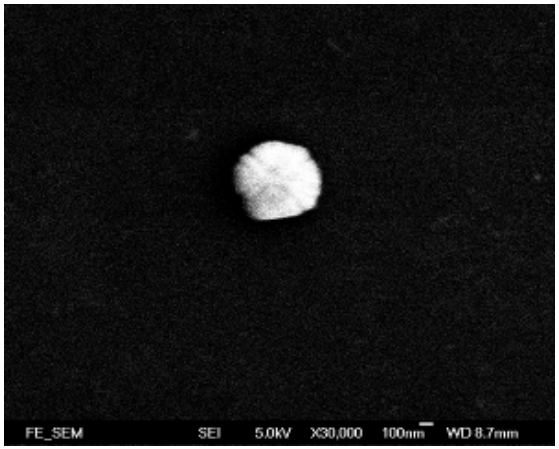	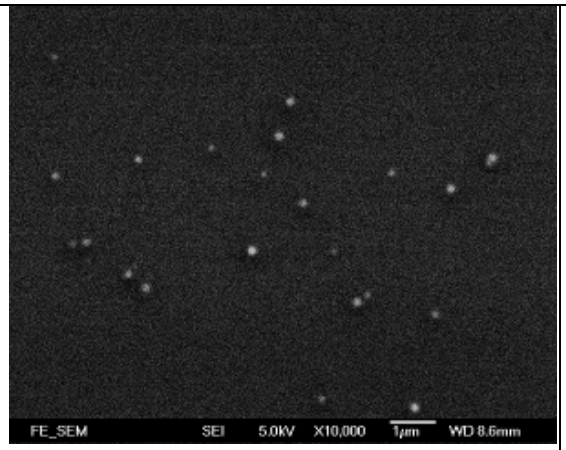 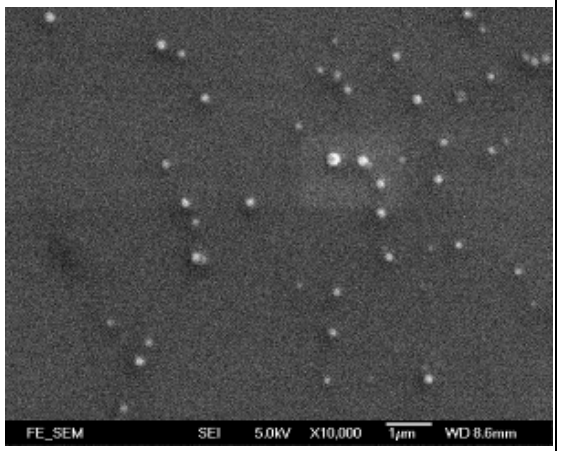	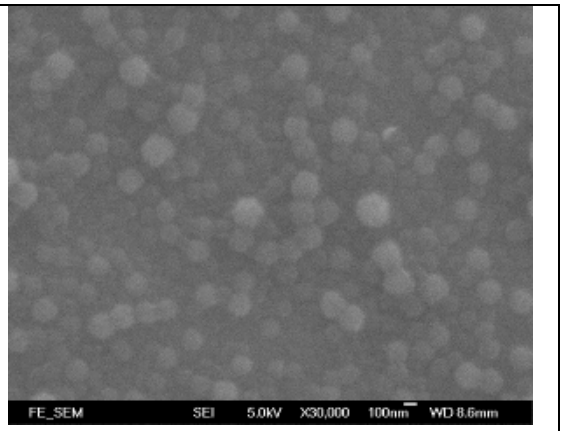 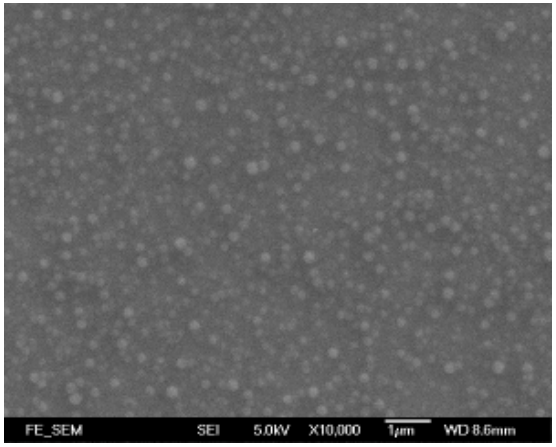
Measured size	Mean 660 nm	About 110 – 280 nm, Mean 166 nm	About 125 – 260 nm, Mean 181 nm
Observations	Particles are hard to observe. The shape of the nanoparticles is irregular	More particles can be observed. The shape of the nanoparticles are more uniform than untreated samples	A large quantity of particles can be obtained. The nanoparticles are the most uniform and spherical.

Table 3.7 shows SEM images of the gelatin/PEI nanoparticles containing higher PEI content (49%). Morphologies of the nanoparticles with and without ethanol treatment were examined. From the SEM images of the untreated nanoparticles, it was noted that the number of observable nanoparticles was higher than those nanoparticles containing 32% of PEI content. The shape of the particle is spherical with diameters between 73 and 128 nm. However, the boundaries of the nanoparticles could not be observed clearly. This indicates that the nanoparticles were not "solid" enough. Some film formation was observed under SEM.

For the same nanoparticles being treated with 80% ethanol, more particles were obtained with diameters in the range of about 169 to 380 nm. When the same nanoparticles were treated with 90% ethanol, much clear morphology and higher intensity of nanoparticles were observed and the shape of the particles is more regular. The mean diameter was of 301 nm with diameters ranging from 220 to 380 nm. These results confirm that the higher the ethanol concentration, the better is the nanoparticle properties with respect to their particle concentration, size, and shape.

Table 3.7. SEM images of gelatin/PEI nanoparticles (PEI content 49%) without and after treating with 80% or 90% ethanol solution.

Sample	Untreated	80% ethanol treatment	90% ethanol treatment
SEM micrographs	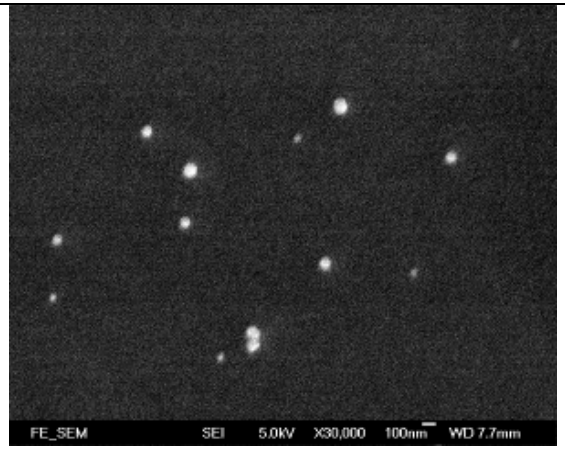 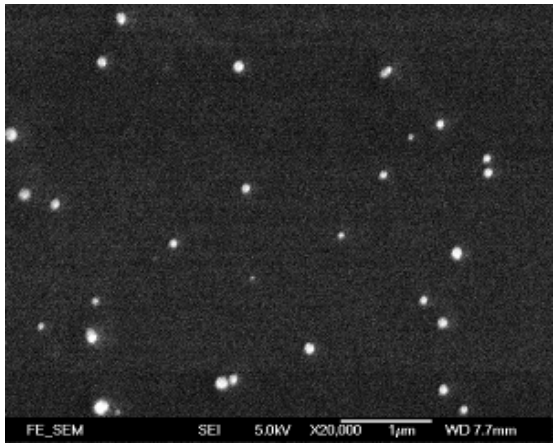	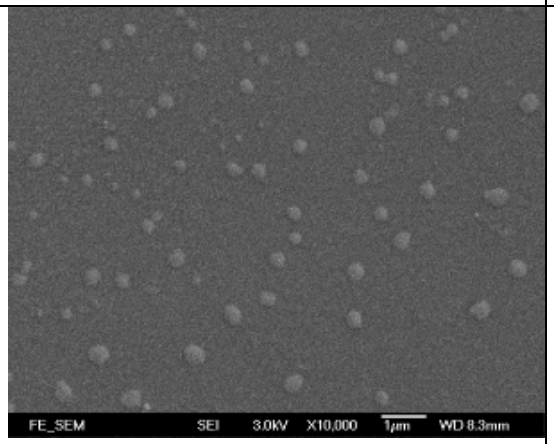 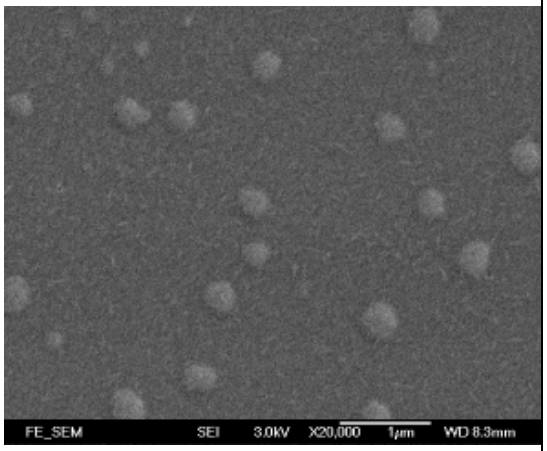	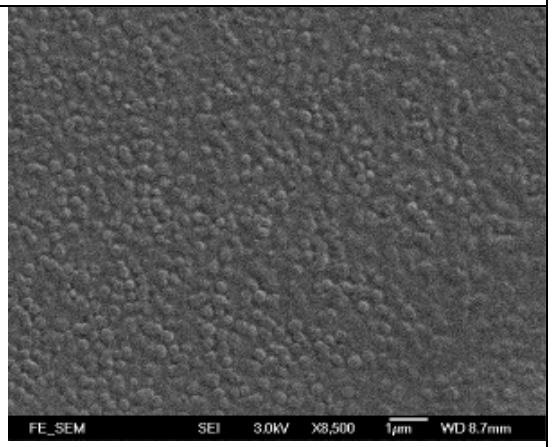 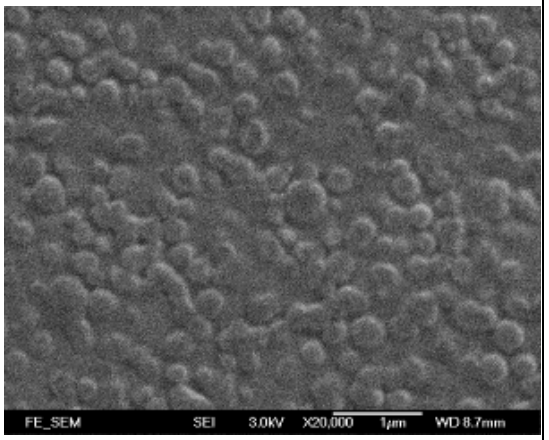

	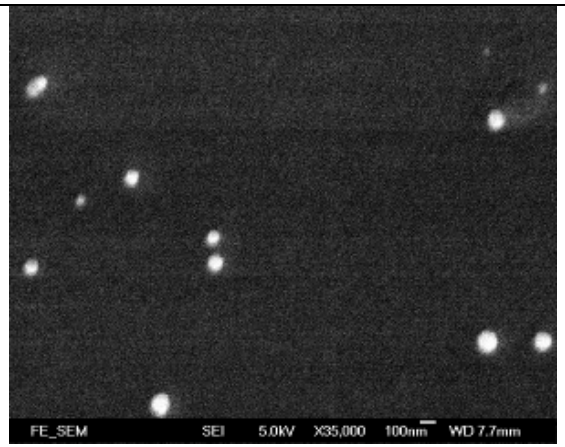 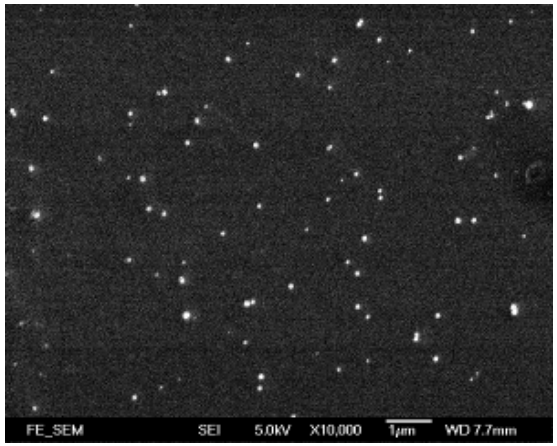	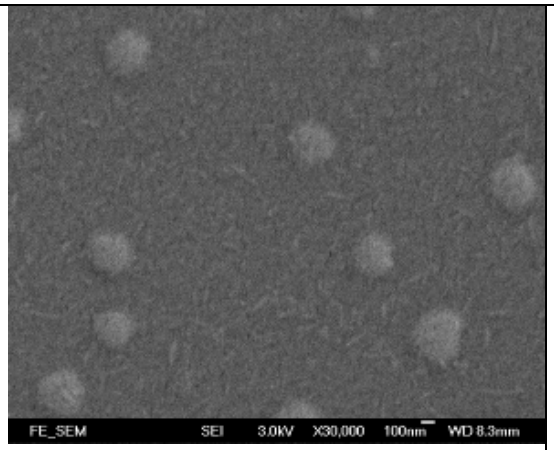	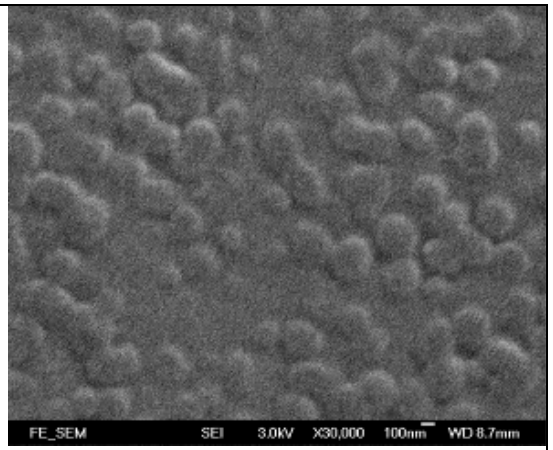 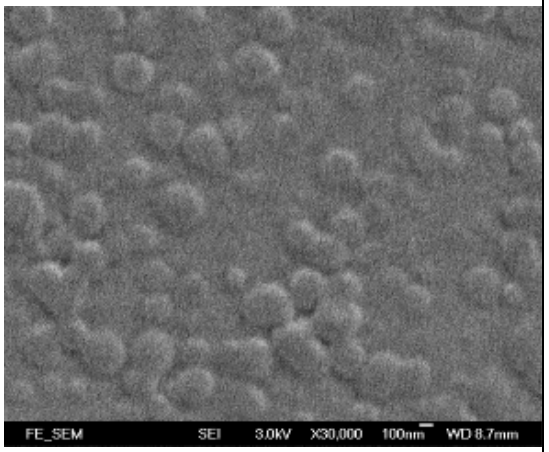
Measured size	73 - 128 nm with mean size of 98 nm	169 – 380 nm with mean size of 288 nm	220 – 380 nm with mean size of 301 nm
Observations	The shape of nanoparticles are quite uniform, but the nanoparticles boundaries are unclear	The shape of nanoparticles are uniform and the nanoparticles boundaries are clear, but nanoparticle density is not high	The shape of nanoparticles are uniform, the nanoparticles boundaries are clear, and nanoparticle density is high

3.3.10 Morphology of the gelatin/PEI nanoparticles with various PEI contents

Table 3.8 summaries SEM images of the gelatin/PEI nanoparticles containing various PEI contents (ranging from 32% to 64%). The nanoparticles were treated with 80% or 90% of ethanol solution.

For the nanoparticles having 64% of PEI content, the diameters are ranged from about 125 nm to 325 nm with the mean diameter of 209 nm. Moderate density of nanoparticles is observed. The nanoparticles are spherical but have quite large variation in size distribution. For the nanoparticles having 49% of PEI content, the diameters are ranged from about 220 to 380 nm with the mean diameter of 301 nm. High density of nanoparticles is observed and the nanoparticles are quite uniform in size. For the nanoparticles having 43% of PEI content, the diameters are ranged from about 189 to 300 nm with the mean diameter of 222 nm. Although moderate density of nanoparticles is observed, the nanoparticles are quite spherical and uniform in shape. For the nanoparticles having 32% of PEI content, the diameters are ranged from 125 to 260 nm with the mean diameter of about 181 nm. Highest density of nanoparticles is observed. The nanoparticles are also the most uniform and spherical.

Table 3.8. SEM images of gelatin/PEI nanoparticles with various PEI content (64%, 49%, 43% and 32%) after treating with 80% or 90% of ethanol solution.

PEI content of nanoparticles	64%	49%	43%	32%
% of ethanol treatment	90%	90%	80%	90%
SEM micrographs	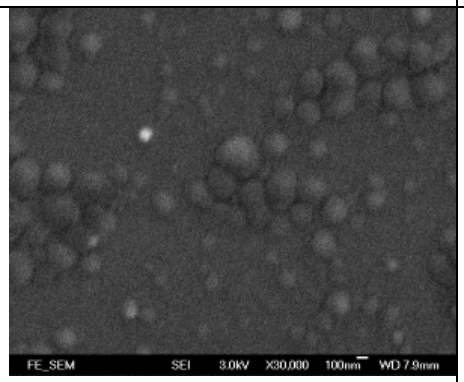 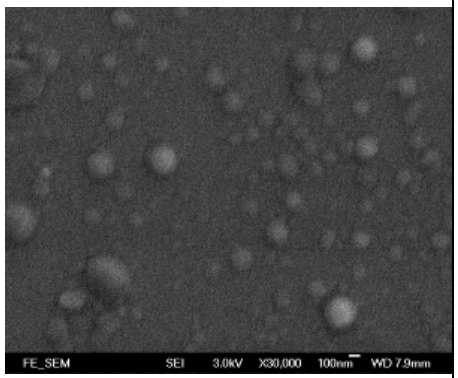	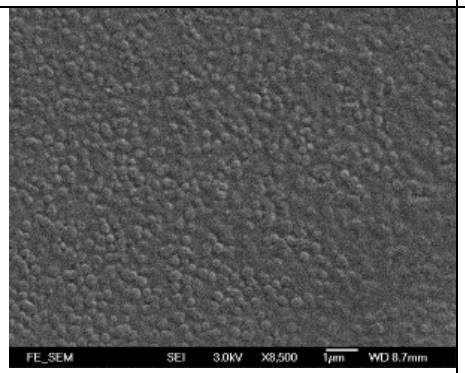 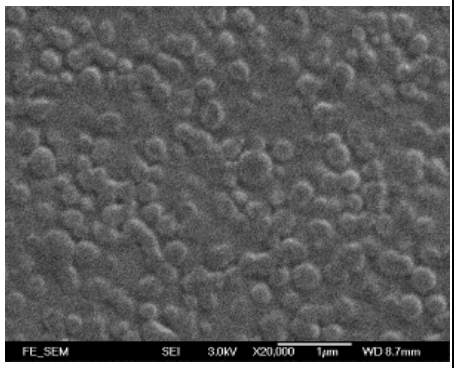	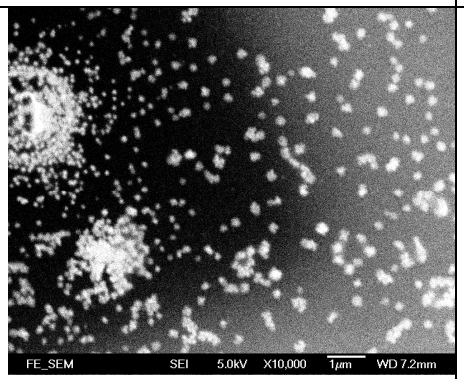 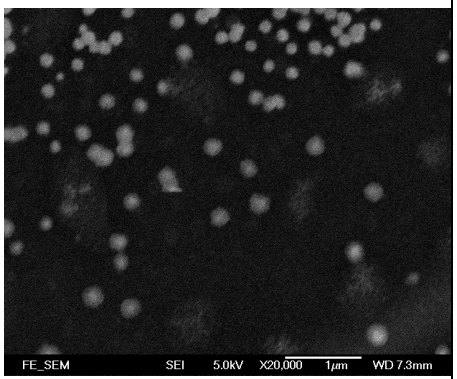	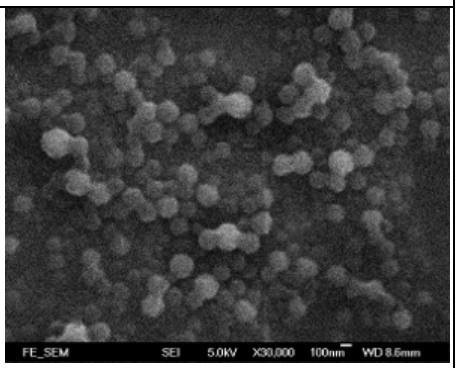 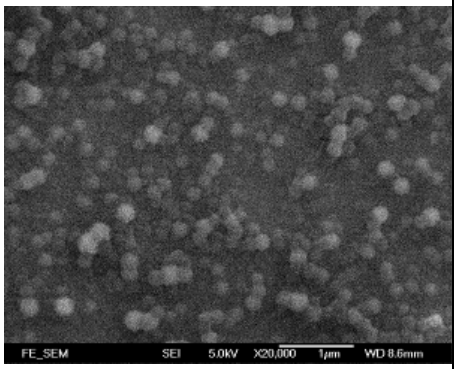

	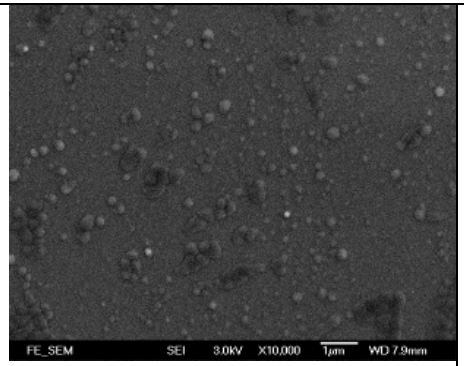 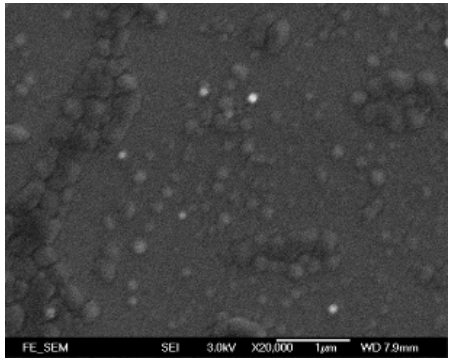	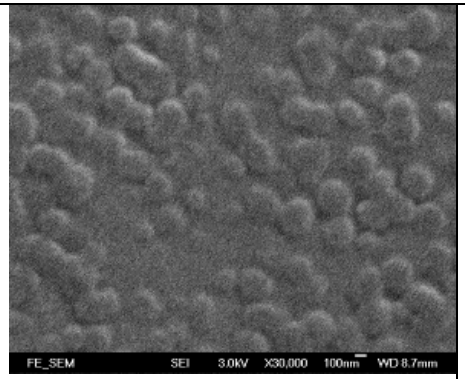 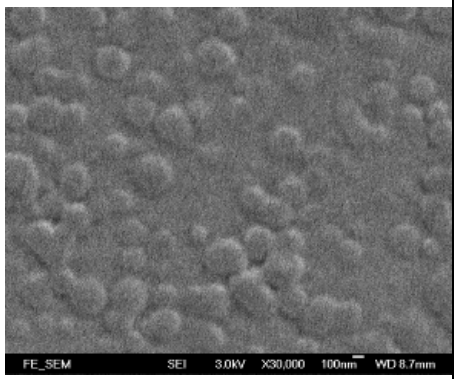	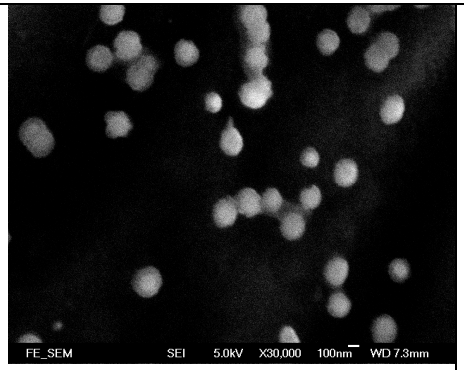 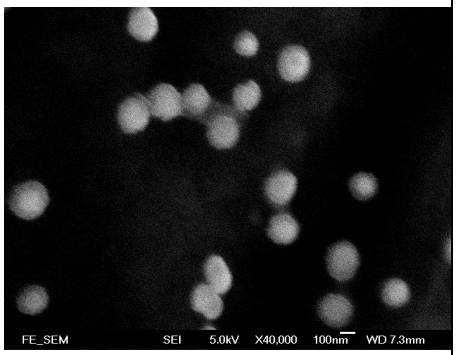	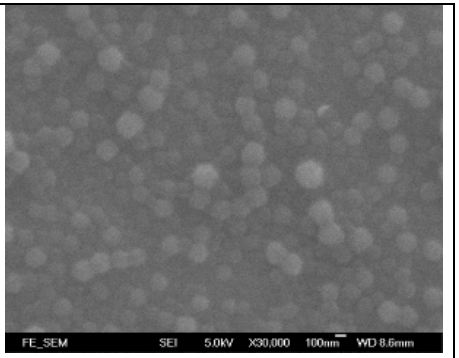 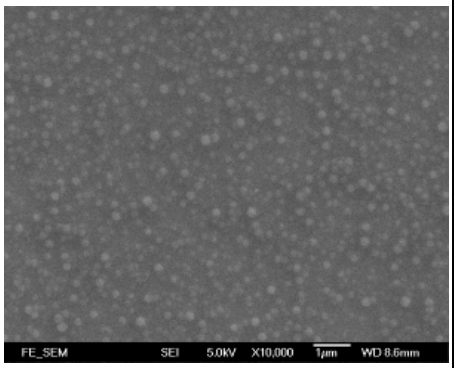
Measured size	125 – 325 nm, mean 209 nm	220 – 380 nm, mean 301 nm	189 – 300 nm, mean 222 nm	125 – 260 nm, mean 181 nm
Observations	Moderate density of nanoparticles, nanoparticles are spherical but have quite large variation of size distribution	High density of nanoparticles and the nanoparticles are quite uniform in size	Moderate density of nanoparticles but the nanoparticles are quite uniform in shape	Highest density of nanoparticles, the nanoparticles are the most uniform and are highly spherical

3.3.11 Effect of ethanol treatment on the core-shell nanostructures of the gelatin/PEI nanoparticles

As discussed previously, the ethanol treatment can trigger the formation of core-shell nanostructure of the gelatin/PEI nanoparticles. This phenomenon could be verified by examining the nanoparticles with staining technique and observing their resulting morphology with transmission electron microscopy. The gelatin/PEI nanoparticles were air dried on a carbon-coated copper grid. The nanoparticles were then stained in 0.5% (w/v) of phosphotungstic acid (PTA) solution. The PTA can stain the positively charged PEI molecules selectively. The increase of electron density of the PTA staining will give a darker color to the PEI. Table 3.9 illustrates the TEM images of the gelatin/PEI nanoparticles with 49% PEI content. The nanoparticles were either untreated or treated with 90% of ethanol solution.

For the nanoparticles without ethanol treatment, the nanoparticles are spherical in shape with two size distributions about 10 – 20 nm and about 50 – 100 nm in diameter. The smaller particles may contribute from the PTA staining agent. In this case, the core-shell structure cannot be observed since the whole nanoaprticles appear to be dark. As mentioned before, both gelatin and PEI are water soluble and can be interpenetrated with each other. Therefore, the core-structure is not well defined. After treating the gelatin/PEI microgels with 80% ethanol solution, the nanoparticles change their morphology to form spherical nanoparticles with a well defined core-shell structure where the inner core is gelatin (lighter) and the outer shell is PEI (darker).

Table 3.9. Transmission electron microscopy (TEM) images of gelatin/PEI nanoparticles (PEI content 49%) without and after treating with 80% ethanol solution.

	Without Ethanol treatment	Treated with 80% ethanol
TEM micrographs	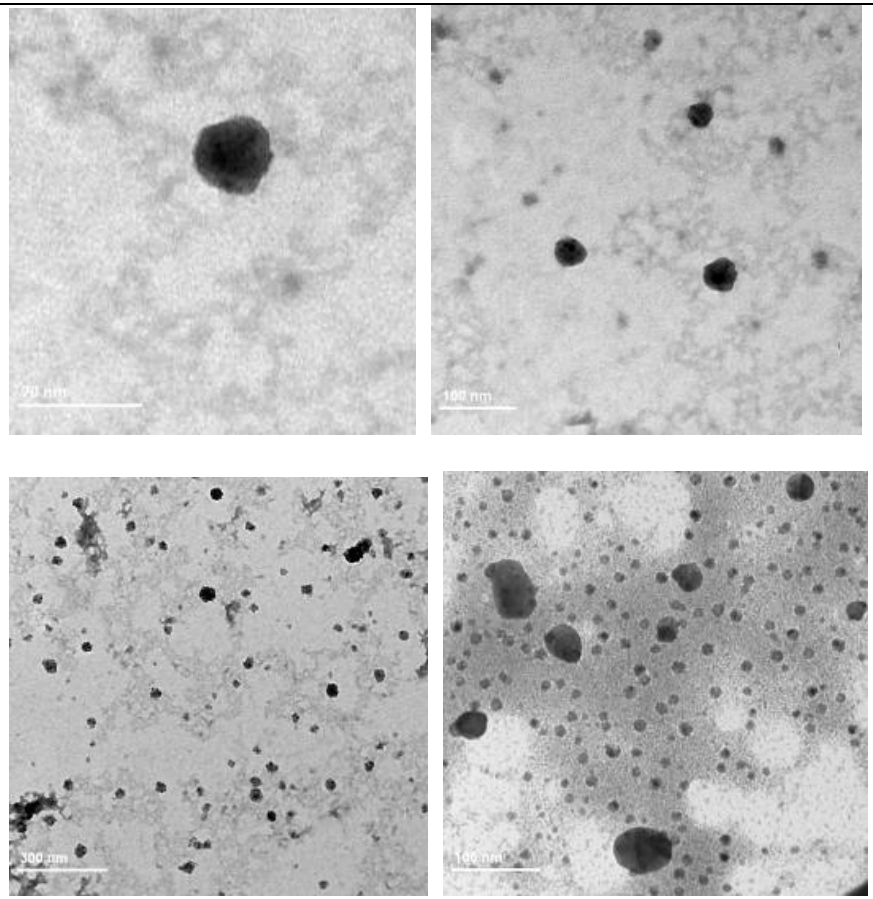	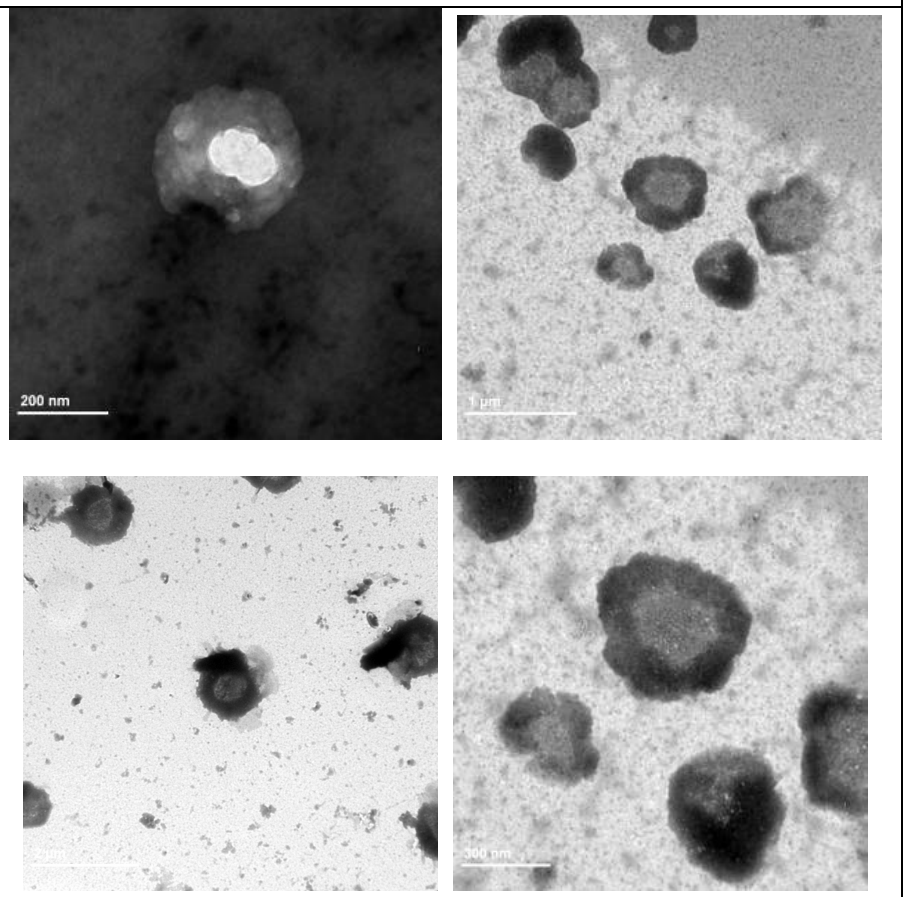
Observations	Most of the nanoparticles are dark in color with no observable core-shell nanostructure	Core-shell nanostructure is observed. The core is gelatin (lighter) and the shell is PEI (darker)

3.3.12 Core-shell nanostructure of gelatin/PEI nanoparticles with various PEI contents

Table 3.10 summarizes the TEM images of the gelatin/PEI nanoparticles with various PEI contents, ranging from 35% to 64%. All of the nanoparticles were treated with 80% of ethanol solution. After air drying on copper grids, the nanoparticles were stained with PTA solution. Except the nanoparticles containing 64% PEI, all of the ethanol treated nanoparticles show well-defined core-shell nanostructure with darker PEI shells and lighter gelatin cores. In addition, the nanoparticles were evenly distributed with little aggregation. In the case of nanoparticles containing 64% of PEI content, the nanoparticles appear like vesicles rather than core-shell structure. The particles sizes are also quite large, about 1- 2 μm in diameter. In the case of nanoparticles containing 43% of PEI content, the nanoparticles are highly spherical and the PEI shells are the thickest. The measured size is about 100 – 200 nm. For the nanoparticles containing 38% of PEI content, the nanoparticles are less spherical and the shells are thinner. The measured sizes are quite small ranging from 60 – 150 nm. Lastly, for the nanoparticles with 35% PEI content, the number of observable nanoparticle is low. But the nanoaparticles are highly spherical and with thinner shells. The measured size is about 100 nm.

Table 3.10. TEM images of gelatin/PEI nanoparticles with different PEI contents. All nanoparticles were treated with 80% ethanol solution.

PEI content	64%	43%	38%	35%
TEM micrographs	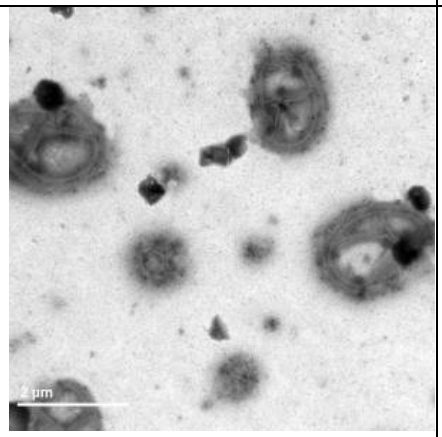 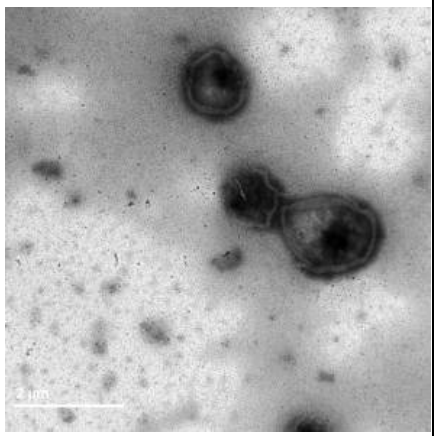	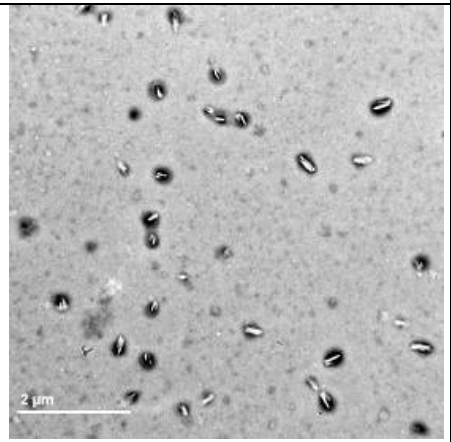 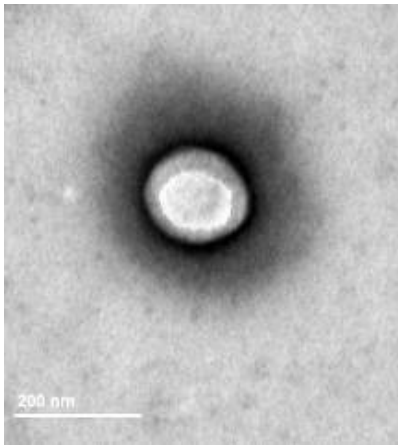	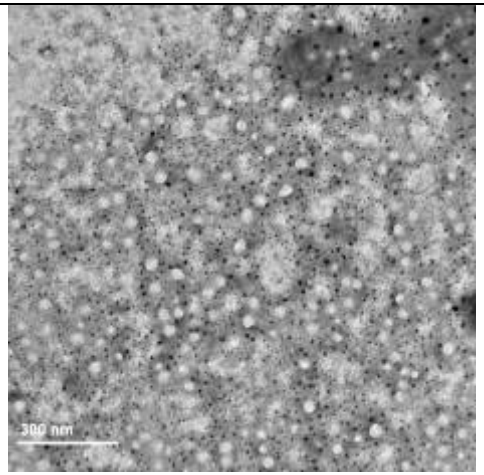 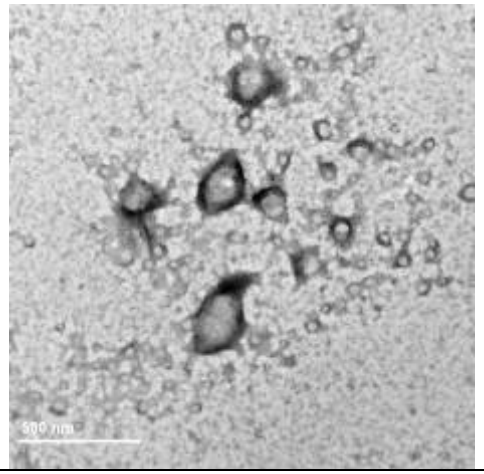	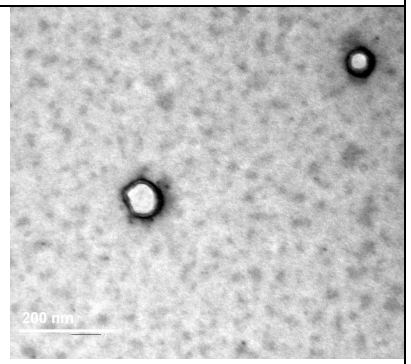 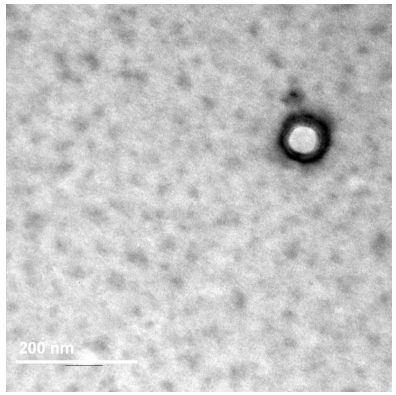

	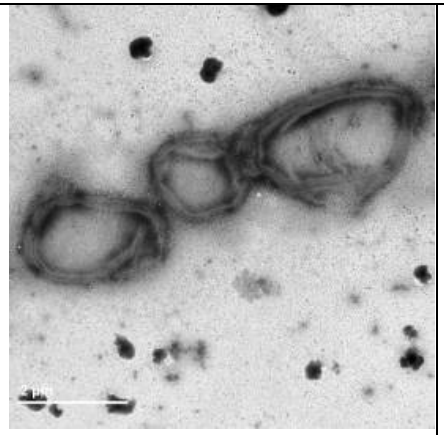	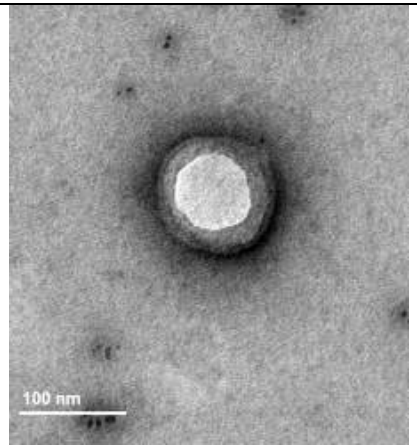 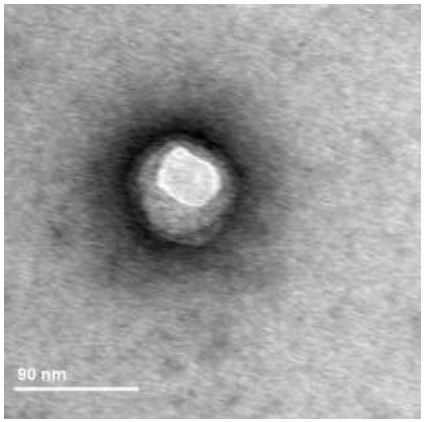	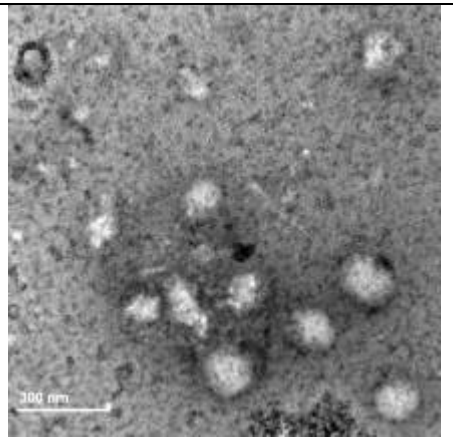 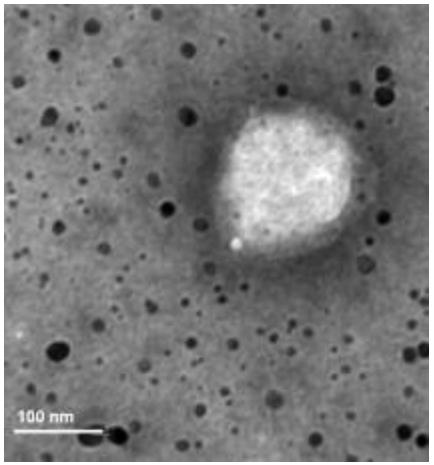	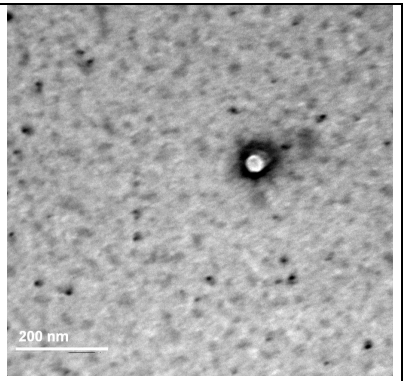
Observations	Large vesicles instead of nanoparticles, size about 1 – 2 μm	Clear core-shell nanostructure with dark PEI shells, the shells are the thickest, size about 100 – 200 nm	Clear core-shell nanostructure with dark PEI shells, size about 60 – 150 nm	Clear core-shell nanostructure with dark PEI shells, but low nanoparticle density, size about 100 nm

3.3.13 Biodegradability of gelatin/PEI nanoparticles

The biodegradability of the gelatin microgels and gelatin/PEI nanoparticles were determined using protease as the digestive enzyme. In this study, the gelatin in molecular form, gelatin microgels and gelatin/PEI nanoparticles were all treated with fixed amount of protease at pH 7.5 and 37^{o}C (optimal conditions for enzyme digestion). After thermal deactivation to quench the enzymatic digestions, the degrees of digestions of the samples were analyzed by SDS-PAGE and the untreated samples were also analyzed for comparison.

Figure 3.10 reveals the degree of degradation of various samples. For molecular gelatin, a smear is observed, indicating that the gelatin has a quite broad molecular weight distribution. The gelatin microgels have a similar smear pattern to those of the molecular gelatin. This result suggests that there is little change in molecular weight after thermal denaturation of gelatin. Since the gelatin microgels are not hard solid particles, it can be unfolded by SDS. After treating the molecular gelatin and gelatin microgels with protease, no band is observed, suggesting that both of them have been degraded completely.

In the case of gelatin/PEI nanoparticles, there are two distinct bands appeared at the well and at the top of the separating gel, indicating that after grafting with PEI, more "solid" nanoparticles were formed and the nanoparticles cannot not be unfolded by SDS. The large size of the nanoparticles greatly reduces the mobility in electrophoresis. After treating with protease, similar two bands at the well and at the top of the separating gel are still observed, but with lower band intensities than those

of the untreated nanoparticles. These results suggest that part of the nanoparticles have been degraded by the protease while rest was intact. Therefore, it can be concluded that both of the gelatin microgels and gelatin/PEI nanoparticles are biodegradable. However, the nanoparticles are less susceptible for protease degradation than the naked gelatin microgels because the gelatin cores are protected by the PEI shells.

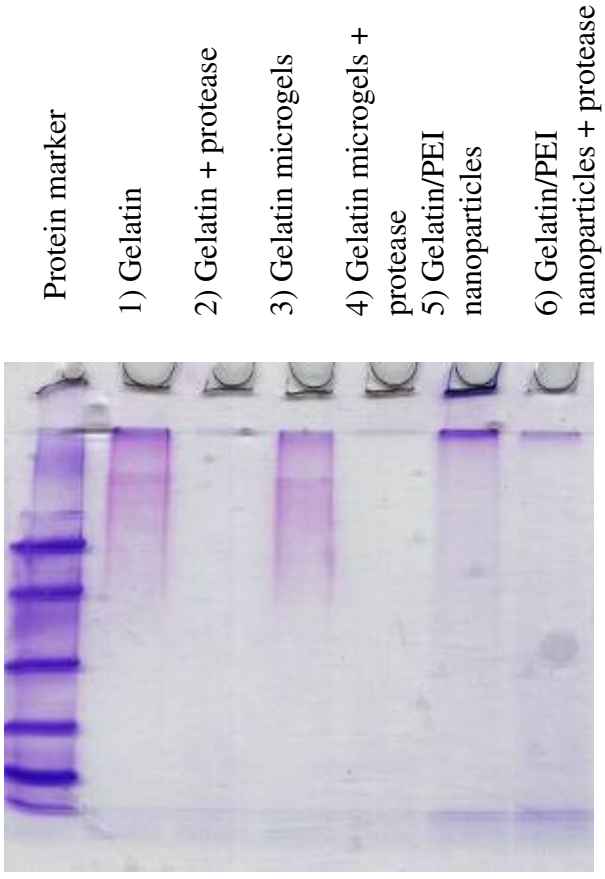

Figure 3.10. SDS-PADE study of the gelatin biodegradability based on electrophoretic mobility: (1) gelatin in molecular form, (2) molecular gelatin with protease, (3) gelatin microgels, (4) gelatin microgels with protease (5) gelatin/PEI nanoparticles and (6) gelatin/PEI nanoparticles with protease. Low range protein marker was used.

3.4 Conclusions

The gelatin/PEI core-shell nanoparticles have been synthesized successfully. Firstly, the gelatin microgels are formed by thermal denaturation through stirring molecular gelatin in water at 70^{o}C for 7 hours. After that, the branched polyethylenimine (PEI) polymers were covalently attached onto the gelatin microgels through coupling reaction using *N*-Ethyl-*N*′-(3-dimethylaminopropyl)carbodiimide hydrochloride (EDC·HCl). The resultant nanoparticles with PEI contents ranging from 26% to 64% were obtained by varying the reaction pH and amount of PEI charged.

However, as both the gelatin and PEI are hydrophilic in nature, the PEI molecules could interpenetrate inside the gelatin matrix. Thus the gelatin/PEI nanoparticles had low surface charges (< +10 mV) which were not suitable for gene condensation. Therefore, the nanoparticles were treated with different concentrations of ethanol solution to create core-shell nanoparticles driven by gelatin and PEI solubility difference in ethanol. Thus, nanoparticles with well-defined gelatin cores and PEI shells could be generated, resulting in a significant increase of surface charges. The core-shell nanostructure of the ethanol treated nanoparticles has been verified by transmission electron microscopy (TEM). In addition, the spherical morphology and narrow size distribution of the treated nanoparticles are also confirmed by scanning electron microscopy (SEM).

After treating with ethanol solutions, the hydrodynamic diameters and surface charges of gelatin/PEI nanoparticles were analyzed. For the same kind of nanoparticles, the higher the concentrations of the ethanol used, the higher are the overall surface

charges, and the smaller sizes are the nanoparticles. When the concentration of ethanol solution was increased from 80% to 100%, the surface charges at pH 7 increased from + 40 mV to + 60 mV, and the hydrodynamic diameters decreased from 367 nm to 196 nm. Considering the particle re-dispersity, morphology and size, it was found that 80% ethanol solution was most suitable. In addition, overall surface charges of the nanoparticles increased with increasing PEI contents. With the PEI contents of the nanoparticles increased from 36% to 64%, the zeta potentials of the nanoparticles increased from + 18 mV to + 46 mV.

The biodegradability of the gelatin microgels and gelatin/PEI nanoparticles were studied by sodium dodecyl sulfate polyacrylamide gel electrophoresis (SDS-PAGE). It suggested that both of the microgels and nanoparticles can be degraded by protease and the PEI shells can retard the degradation rate of the nanoparticles comparing with the gelatin microgels. So, the gelatin/PEI nanoparticles can have a longer circulation time in the blood stream.

Finally, the gelatin/PEI nanoparticles with PEI contents of 26% and 49% were chosen to carry out the gene complexation studies in the following section. The nanoparticles were treated with 80% ethanol solution for three treatment cycles. The hydrodynamic diameters of the resultant nanoparticles were between 200 and 300 nm and the surface charges were about +18 to + 46 mV, depending on the PEI contents.

3.5 References

1. J. M. Krochta, E. A. Baldwin, M. Nisperos-Carriedo, *Edible Coatings and Films to Improve Food Quality*, Technomic Pub. Co. Inc, Lancaster, **1994**.
2. http://www.gmap-gelatin.com/about_gelatin.html
3. M. D'Cruz, L. N. Bell, *Journal of Food Science* **2005**, 5.
4. Kuijpers, Alma J.; Engbers, Gerard H. M.; Krijgsveld, Jeroen; Zaat, Sebastian A. J.; Dankert, Jacob; Feijen, Jan.," Cross-linking and characterization of gelatin matrices for biomedical applications" *Journal of Biomaterials Science -- Polymer Edition 11(3)* **(2000)** 225-243**.**
5. Philippe Cayot and Ge´rard Tainturier, "The quantification of protein amino groups by the trinitrobenzenesulfonic acid method: a reexamination" *Analytical Biochemistry 249* **(1997)** 184-200.
6. Stephen L. Snyder and Philip Z. Sobocinski, "An improved 2,4,6-trinitrobenzenesulfonic acid method for the determination of amines", Analytical Biochemistry 64 (1975) 284-288.
7. J. E. EASTOE, "The amino acid composition of mammalian collagen and gelatin", *Bioch* 61 **(1955)** 589-600.
8. W.T. Godbey , Kenneth K. Wu and Antonios G. Mikos, "Poly(ethylenimine) and its role in gene delivery", *J. of Contr. Rel. 60* (1999) 149-160. (ref 11, amine groups of PEI)

3.6 Appendix

A. *Thermogravimetric anaylsis (TGA) of gelatin powder*

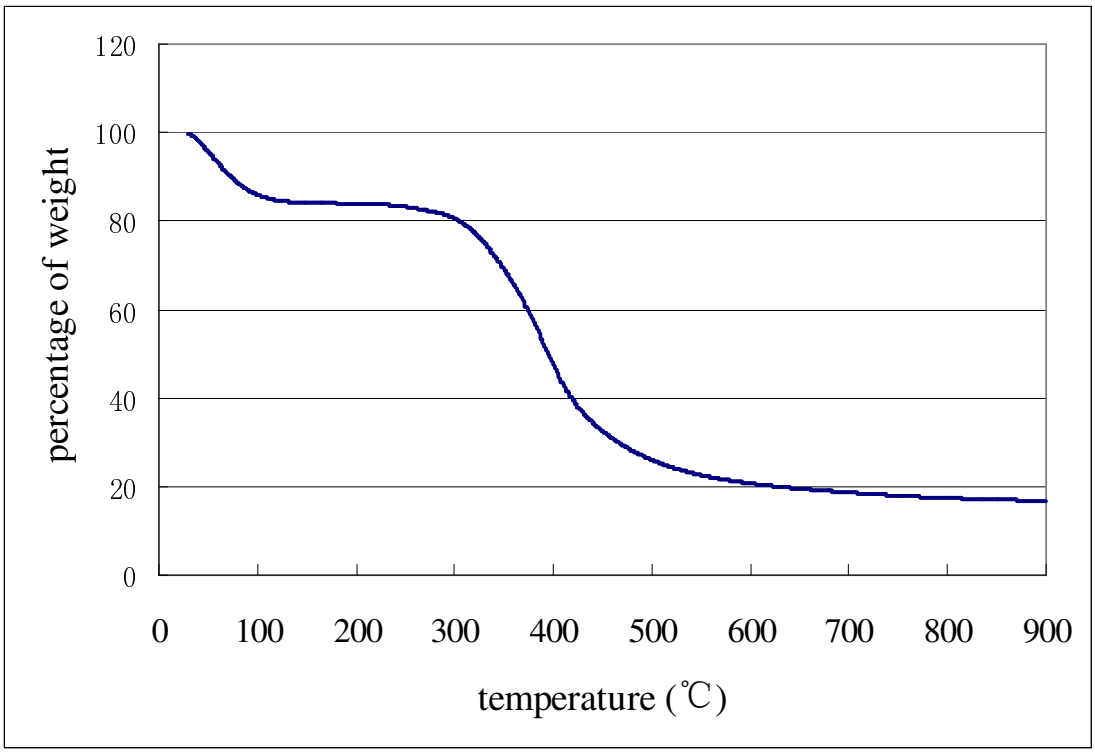

Figure 3.11. TGA thermograph of gelatin powder.

The percentage of weight of gelatin powder drops from 100% to about 83% at 100 ^{o}C, indicating that the gelatin powder contains about 17% of moisture.

B. *Calculation of the mole numbers of carboxylic group of gelatin and EDC*

Weight of gelatin (W) = 25 mL x 1.0% = 0.25 g

The aspartic acid and glutamic acid residues of gelatin contain carboxylic groups (COOH)

Amino acid residue	Aspartic acid	Glutamic acid
Molecular structure	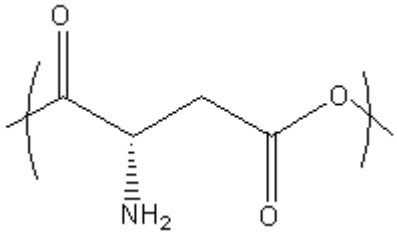	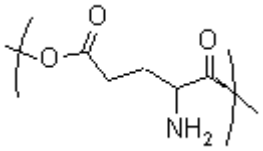
Molecular weight (g/mol)	115.10	129.13

The weight % of aspartic acid residue in a single gelatin chain is about 5.68%.[7]

The number of mole of –COOH group from aspartic acid = W x 5.68% / $Mw_{(asp)}$

= 0.25 x 5.68% / 115.10

= 1.23 x 10^{-4} mol

The weight % of glutamic acid residue in a single gelatin chain is about 9.58%.[7]

The number of mole of –COOH group from glutamic acid = W x 9.58% / $Mw_{(glu)}$

= 0.25 x 9.58% / 129.13

= 1.85 x 10^{-4} mol

The total mole number of –COOH group of gelatin = 1.23 x 10^{-4} + 1.85 x 10^{-4}

= 3.08 x 10^{-4} mol

The mole ratio of EDC to –COOH of gelatin is 1.4:1

The mole number of EDC = 3.08 x 10^{-4} x 1.4 = 4.31 x 10^{-4} mol

The weight of EDC added = 4.31 x 10^{-4} mol x $MW_{(EDC)}$

= 4.31 x 10^{-4} x 191.7

= 0.0826 g

C. *Calculation of the mole numbers of carboxylic group of gelatin and amine group of PEI*

The total mole number of –COOH group of gelatin = 3.10×10^{-4} mol

The mole ratio of $–NH_2$ of PEI to –COOH of gelatin = 8.8 : 1

The mole number of primary amine group of PEI = $3.10 \times 10^{-4} \times 8.8$

$= 2.73 \times 10^{-3}$ mol

Calculation of the molecular weight of the repeating unit of branched PEI:

Amine	Primary (1^o)	Secondary (2^o)	Tertiary (3^o)
Molecular structure	($-CH_2-CH_2-NH_2$)	($-CH_2-CH_2-NH-$)	($-CH_2-CH_2-N-$)
Molecular weight	44.1	43.1	42.1
Mole ratio in branched PEI [8]	1	2	1

The weight percentage of primary amine group ($–NH_2$) of a PEI chain is:

44.1 / (44.1 + 43.1x2 + 42.1) x 100% = 25.6%

The weight of PEI added = $mole_{-NH2} \times Mw_{(-NH2)} / 25.6\%$

$= 2.73 \times 10^{-3} \times 44.1 / 25.6\%$

= 0.470 g

D. *Calculation of absorption coefficient different between gelatin and PEI based on Figures 3.3 and 3.6*

Substance	PEI	Gelatin
Concentration (ppm)	18	4200
Λ_{420}	0.72	0.09
Absorption coefficient (λ_{420} ppm^{-1})	4.0×10^{-2}	2.1×10^{-5}

The absorption coefficient of PEI is about 1900 times large than that of the gelatin

E. Calculation of the PEI contents of the gelatin/PEI nanoparticles

λ_{420nm} of diluted gelatin/PEI nanoparticles dispersion: 0.76981

$\lambda_{420nm} = 0.0525c - 0.1826$

PEI concentration of the nanoparticles dispersion: 18.14 ppm

Times of dilution: 70

Original PEI concentration of the nanoparticle dispersion = 18.14 x 70 = 1270 ppm

Solid content of the nanoparticles dispersion: 2460 ppm

Gelatin concentration of the nanoparticles dispersion = 2460 – 1270 = 1190 ppm

PEI content of the nanoparticles = 1270 / 2460 x 100% = 51.6 %

Table 3.11. Weight ratio of PEI to gelatin in the gelatin/PEI nanoparticles under different reaction conditions (different reaction pH and added weight ratio of PEI:gelatin)

Sample	161107	090108	280409	290108	191207	170309	300409
Reaction pH	3.8	3.8	3.8	3.8	5	5	5
Mole ratio of $-NH_2$ of PEI to –COOH of gelatin added	8.8:1	4.4:1	2.2:1	0.88:1	8.8:1	4.4:1	0.88:1
PEI added (g)	0.4643	0.2359	0.1178	0.0470	0.4672	0.2369	0.0491
Gelatin added (g)	0.25	0.25	0.25	0.25	0.25	0.25	0.25
solid content of purified Np (% w/v)	0.827%	0.664%	0.528%	0.561%	0.915%	0.340%	0.386%
PEI grafted (determined by TNBS) (ppm)	5302	2861	1981	1958	4477	1591	999
gelatin content of purified Np (ppm)	2968	3799	3299	3652	4673	1809	2861
weight ratio of PEI:gelatin added	1.86:1	0.94:1	0.47:1	0.19:1	1.87:1	0.95:1	0.20:1
weight ratio of PEI:gelatin of Np	1.79:1	0.75:1	0.60:1	0.54:1	0.96:1	0.88:1	0.35:1
Weight % of PEI of Np	64.3%	43.1%	37.5%	34.9%	48.9%	46.8%	25.9%

4 Complexation studies of gelatin/PEI nanoparticles with plasmid deoxyribonucleic acid (pDNA) and small interfering ribonucleic acid (siRNA)

4.1 Materials

Agarose, ethdium bromide and ampicillin were purchased from Invitrogen (San Diego, CA). Poly(L-aspartic acid) (mol wt 5,000 – 15,000), DNase I and RNase A were purchased from Sigma (St. Louis, MO). DNA ladder (100 bp and 1 kbp), loading dye and pGL-3-control plasmid encoding the luciferase reporter gene were obtained from Promega (Madison, WI). The Wizard® *Plus* SV Minipreps DNA Purification System was purchased from Promega and was used for the purification of amplified plasmid DNA. ASS1-siRNA (stealth select RNAi: HSS181354) was purchased from Invitrogen. The sense strand of the siRNA was 5´-AGCAGCUGAGCUCAAACCGGACCUG-3´ while the antisense strand was 5´-CAGGUCCGGUUUGAGCUCAGCUGCU-3´. All other reagents were of analytical grade.

4.2 Methods

4.2.1 Mini-perparation of plasmid DNA (pDNA) and determination of pDNA concentration

The pGL-3-control plasmid was amplified in transformed JM109 *E. Coli* cells in 5 mL of LB agar broth supplemented with 50 μg/mL of ampicillin. The mixture was shaken at 37 ^{o}C and 225 rpm overnight (12 – 16 h). The amplified pDNA was purified using the rapid plasmid miniprep purification system (protocol provided by Promega).[1]

The cells containing pGL-3-control plasmid DNA grown overnight were harvested by centrifuging the 5 mL of the cell culture at 13,000 rpm for 3 min. After discarding the supernatant, the cells pallet was re-suspended in 250 μL of cell resuspension solution. Then 250 μL of cell lysis solution and 10 μL of alkaline protease solution were added. For each addition, the mixture was mixed by inverting the microcentrifuge tube for 4 times. The mixture was incubated for 5 min at room temperature for cell lysis. After that, 350 μL of cell neutralization solution was added and mixed by inverting the mixture for 4 times. Precipitates appeared and were separated from the solution by centrifugation at 13,000 rpm for 10 min. Then the supernatant was transferred to a clean spin column with a collection tube and was centrifuged at 13,000 rpm for 1 min. After discarding the solution, the plasmid DNA in the spin column was washed by 750 μL of wash solution (ethanol was added) and centrifuged at the same speed for 1 min followed by adding

another 250 μL of the wash solution and centrifugation for 2 min. Then, the pDNA was collected by transferring the spin column to a clean microcentrifuge tube and adding 100 μL of the DNase free water into the spin column. After 1 min of incubation, the pDNA solution was collected by centrifugation at 13,000 rpm for 2 min. The pDNA solution was stored in a -20^{o}C refrigerator and was thawed before use.

The concentration and purity of the pDNA were measured by UV absorption by a GeneQunat DNA/RNA calculator. The concentration was measured by the pDNA's absorption at 260 nm (λ_{260}) and the purity was calculated by the ratio of absorbance at 260 nm to the absorbance at 280 nm ($A_{260/280}$).

4.2.2 Complexations of pDNA and siRNA with gelatin/PEI nanoparticles

After purifications and treatment with 80% ethanol solution, the gelatin/PEI nanoparticles with various PEI contents (49%, 43%, 30% and 26% of PEI contents) were used for complex formation with the pDNA and siRNA.

For pDNA and siRNA condensation, 0.3μg of the pDNA or siRNA was allowed to mix with different amounts of gelatin/PEI nanoparticles with the PEI nitrogen-to-pDNA (or siRNA) phosphate (N/P) ratios ranging from 0.5 to 9. The calculations of pDNA, siRNA and nanoparticles added are shown in Appendix A. After mixing an appropriate volume of pDNA, nanooparticles and Milli-Q H_2O, the mixtures with the total volume of 15 μL were allow to incubate for 30 min at room temperature for complexations. After that, 3

μL of the loading dye was added to each of the samples. The formation of pDNA/nanoparticle complex was analyzed by agarose gel electrophoresis (AGE) with 0.8% agarose gel using 1 kbp DNA ladder as the marker; whereas the formation of siRNA/nanoparticle complex was analyzed by AGE with 2.0% agarose gel using 100 bp DNA ladder as the marker.

4.2.3 Release of pDNA and siRNA from gelatin/PEI nanoparticles

After forming complexes with pDNA or siRNA, the ability of the gelatin/PEI nanoparticles (49%, 43% and 38% of PEI contents) to release condensed pDNA or siRNA was determined. After mixing the pDNA and nanoparticles with an N/P ratio of 2 and 5 or mixing the siRNA and nanoparticle with an N/P ratio of 5, the mixtures were incubated for 30 min for complex formation. After that, different amounts of poly(L-aspartic acid) (pAsp) (pAsp carboxylic group-to-pDNA phosphate (COO^-:P) ratio from 50:1 to 1000:1) were added to the complex. The calculations of the amount of pAsp added are shown in Appendix B. After incubation for 2 h or overnight, the results of pNDA release were analyzed by AGE using 0.8% gel, while the results of siRNA release were analyzed by AGE using 2.0% gel.

4.2.4 Protection of pDNA and siRNA against enzymatic degradation

After forming complexes with pDNA or siRNA, the ability of the gelatin/PEI nanoparticles to protect the condensed pDNA or siRNA against enzymatic degradation was determined. The native and condensed pDNAs were added with different amounts of DNase I while the native and condensed siRNAs were added with different amount of RNase A. The degrees of degradation of the condensed pDNA and siRNA were compared with the native ones.

For pDNA digestion, a series of mixture each containing 0.3μg of pDNA and nanoparticles with an N/P ratio of 5 were incubated for 30 min at room temperature for complex formation. After that, 10X enzyme buffer (1 μL, 60 mM $MgCl_2$ and 400 mM Tris-HCl, pH 7.5 at 25^{o}C) and DNase I solutions of different activities were added to the series of the complex or native pDNA; and milli-Q H_2O was added to make up the total volume to 10 μL. The mixtures were incubated at 37^{o}C for 10 min for DNA digestions. Immediately after 10 min, 50 mM of EDTA solution was added for enzyme chelation and the mixtures were incubated for 5 min to denature the DNase. Then, pAsp (COO^-:P of 100:1) was added for pDNA release. After incubation for 2 h, the degrees of pNDA digestion were analyzed by AGE using 0.8% of agarose gel.

For siRNA digestion, a series of mixture each containing 0.3μg of siRNA and nanoparticles with an N/P ratio of 5 were incubated for 30 min at room temperature for complex formation. After that, 2X PBS (5 uL, pH 7.4) and RNase A solutions of different

amounts were added to the series of the complex or native siRNA; and Milli-Q H_2O was added to make up the total volume to 10 uL. The mixtures were incubated at 37^{o}C for 10 min for siRNA digestions. Immediately after 10 min, the samples were incubated at 85^{o}C for 5 min for RNase A inactivation. Then, pAsp (COO^-:P of 50:1) was added for siRNA disassembly. After incubation for 2 h, the degrees of siRNA degradation were analyzed by AGE using 2.0% of agarose gel.

4.3 Results and discussions

Being gene delivery carriers, the gelatin/PEI core-shell nanoparticles are able to condense the plasmid DNA or siRNA onto its surface using the cationic branched PEI shells. The amounts of gelatin/PEI nanoparticles required to completely condense the plasmid DNA and siRNA are determined and quantified as the PEI nitrogen-to-DNA phosphate (N/P) ratio. In addition, the nanoparticles should be able to protect the condensed DNA molecules against enzymatic degradation and release its condensed DNA molecules. In the following section, the condensation, protection and release properties of the nanoparticles will be discussed.

4.3.1 Complexations of pDNA with gelatin/PEI nanoparticles

Figures 4.1 to 4.2 show the results of pDNA/nanoparticle complex formation using nanoparticles of different PEI contents (49%, 43%, 38% and 26% of PEI contents

respectively) analyzed by agarose gel electrophoresis (AGE). The physical properties of the gelatin/PEI nanoparticles used are summarized in Table 4.1.

Table 4.1. Properties of gelatin/PEI nanoparticles of different PEI contents, including reaction pH, added ratios of PEI to gelatin, hydrodynamic diameters (Z_{ave}) and surface charges.

PEI content	**Reaction pH**	**Added mole ratio of $-NH_2$ of PEI to –COOH of gelatin**	**Z_{ave} (nm)**	**PDI**	**Zeta potential (mV);(measured pH)**
49%	5	8.8:1	309.6 ±1.8	0.407	+45.8 (± 5.1); (pH 7.11)
43%	3.8	4.4:1	253.8±5.3	0.523	+32.5 (± 3.8); (pH 6.41)
38%	3.8	2.2:1	320.5±5.0	0.355	+28.4 (± 2.4); (pH 7.55)
26%	5	0.88:1	206.0 ± 1.9	0.560	+18.1 (± 2.3); (pH 7.24)

In preparation of the pDNA/nanoparticle complexes with different N/P ratios, different volumes of the nanoparticle dispersions were mixed with the pDNA solution, which contained 0.3 μg pDNA. For the details of calculations and volume added, please refer to Appendix A. After incubating for 30 min at room temperature, the electrophoretic mobility of the pDNA in the mixture was analyzed by gel electrophoresis (AGE).

Figure 4.1 shows the effect of pDNA/nanoparticle formation using nanoparticles with 49% PEI contents. Lane 1 contains free pDNA. The three bands present in the middle level of the gel were nicked, linear and supercoiled pDNA, ranging from top to bottom. Lanes 2 to 7 contain pDNA and gelatin/PEI nanoparticles. The bands present in the wells (on the top level) indicated formations of pDNA/nanoparticles complex. The absence of bands at the middle level at lanes 5-8 indicated that there is no free pDNA. It can be presumed that all of the pDNAs were condensed by the nanoparticles using an N/P ratio of 2 (NP/pDNA ratio (w/w) = 0.5341) or above.

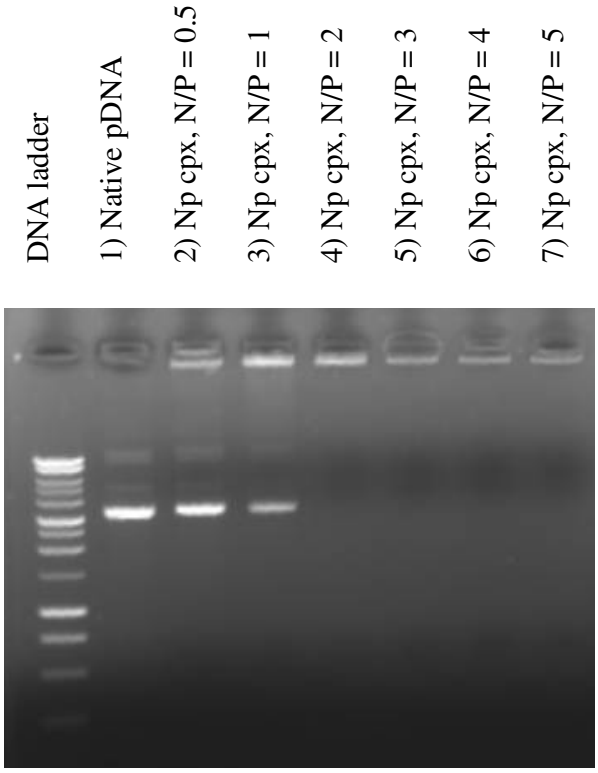

Figure 4.1. Result of AGE showing the electrophoretic mobility of plasmid DNA (1) in the native form and (2-7) in the form of pDNA/nanoparticle complex form prepared at various N/P ratios from 0.5 to 5 as specified. The pDNA was run through a 0.8% gel, stained with EtBr (0.5μg/mL) and visualized using an UV transilluminator.

Figure 4.2 shows the effect of pDNA/nanoparticle complex formation using nanoparticles with PEI contents of 43% (Figure 4.2A), 38% (Figure 4.2B) and 26% (Figure 4.2C) respectively. It can be observed that the pDNA was completely complexed by the nanoparticles of 43% and 38% of PEI at the N/P ratios of 3 and 4 respectively (NP/pDNA ratio (w/w) = 0.914 and 1.39 respectively). However, nanoparticles with 26% of PEI content show a weak ability in pDNA condensation and cannot completely condense the pDNA at the N/P ratio of 9.

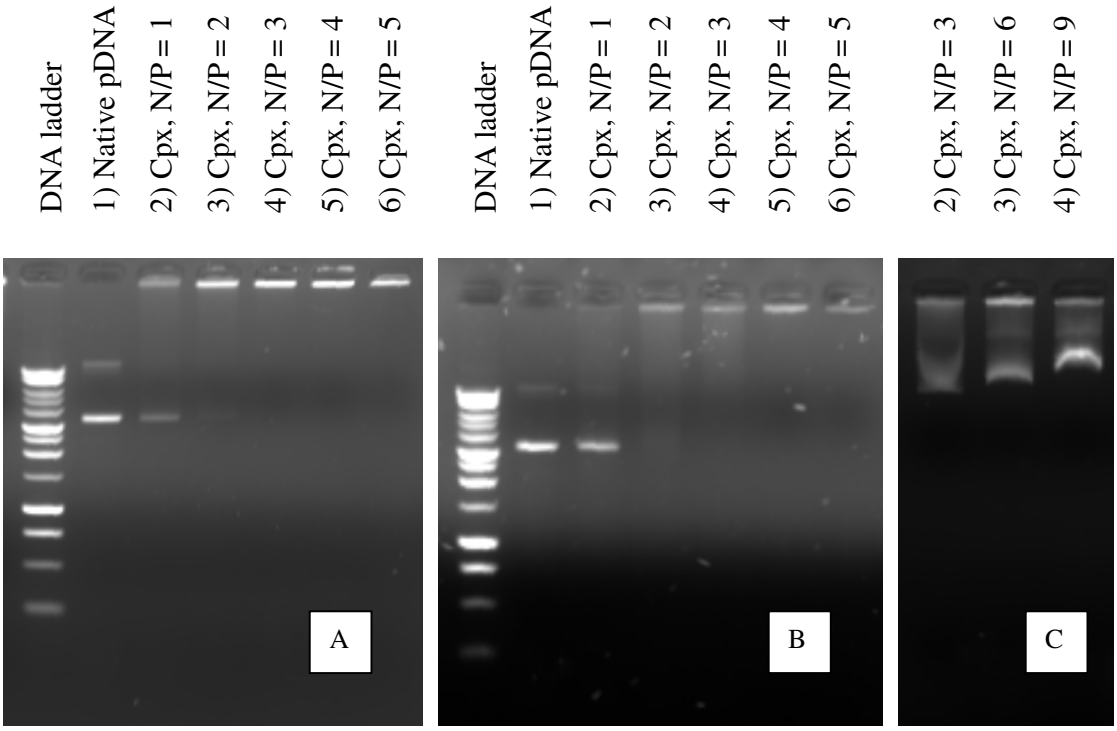

Figure 4.2. Result of AGE showing the electrophoretic mobility of plasmid DNA (1) in the native form and (2-6) in the form of pDNA/nanoparticle complex prepared at various N/P ratios from 1 to 9 as specified. The pDNA was run through a 0.8% gel, stained with EtBr (0.5µg/mL) and visualized using an UV transilluminator. **A)** Nanoparticles with 43% of PEI content; **B)** Nanoparticles with 38% of PEI content; and **C)** Nanoparticles with 26% of PEI content.

Theoretically, the nanoparticles should be able to condense the pDNA at an N/P ratio of 1. Based on the results above, the nanoparticles fully condensed the pDNA at a minimum N/P ratio of 2. In, addition, the DNA condensing ability of the nanoparticles decreased with decreasing PEI contents of the nanoparticles. This is because the effect of ethanol treatment is more obvious in nanoparticles with higher PEI contents. The PEI chain extension is more complete and more PEI chains are concentrated at the particle surface. This can be proved by the difference of zeta potentials of the nanoparticles having different PEI contents (see Section 3.4). As a result, the gelatin/PEI nanoparticles with a higher PEI content can fully condense pDNA at a lower N/P ratio.

Moreover, although the DNA condensation ability of the nanoparticles with higher PEI content is higher, the PEI shells are also thicker. Only those PEI at the superficial layer of the nanoparticles are available for gene complexation. The PEI in the inner part is wasted.

4.3.2 Complexations of siRNA with gelatin/PEI nanoparticles

Figure 4.3 displays the effect of siRNA/nanoparticle complex formation using nanoparticles with PEI contents of 43% (Figure 4.4A) and 38% (Figure 4.3B) respectively. . The absence of bands in the middle level at lanes 6-7 of Figure 4.4A and lanes 4-7 of Figure 4.4B indicated that there is no free siRNA. It can be concluded that the siRNA was completely complexed by nanoparticles with 43% and 38% of PEI at N/P ratios of 5 and 6 respectively (NP/siRNA ratio (w/w) = 1.52 and 2.06 respectively).

By comparing the N/P ratios of the pDNA complexations, it can be concluded that the N/P ratios required for siRNA condensation are greater than those for the pDNA, which were 3 and 4 at the same PEI contents. This was because after purification, the pDNA was redissolved in Milli-Q H_2O, whereas the siRNA, which was commercially bought, was dissolved in buffer and contain some salts. So, part of the positive charge of the PEI shells was neutralized by the salts and the electrostatic interaction between the nanoparticles and the siRNA molecules were less effective. Therefore, a higher N/P ratio was required for complete siRNA condensation.

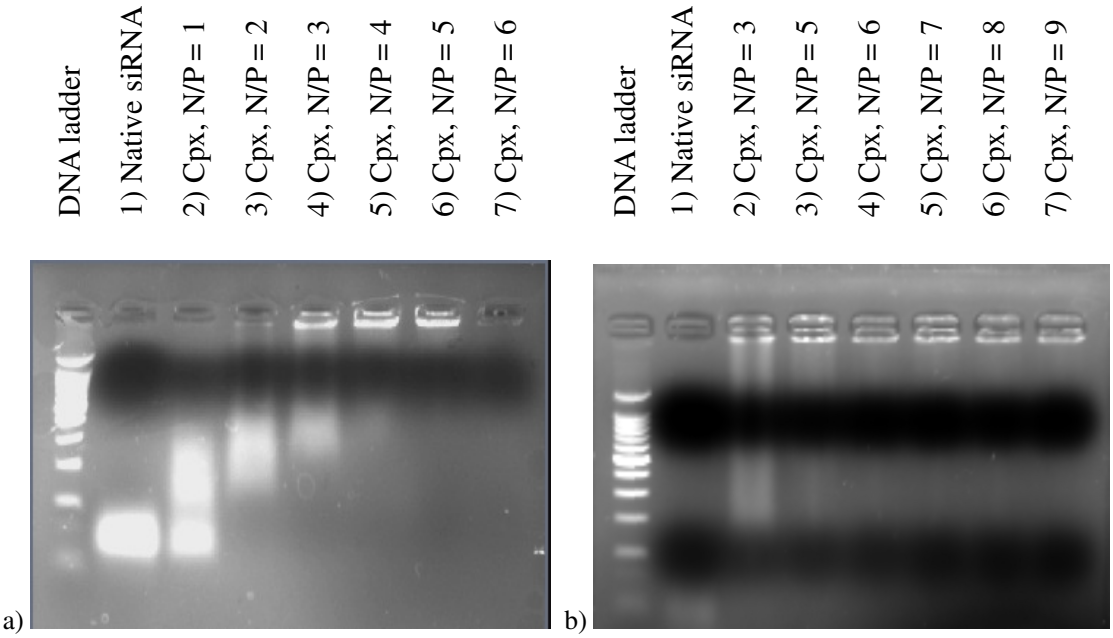

Figure 4.3. Result of AGE showing the electrophoretic mobility of siRNA (1) in the native form and (2-7) in the form of siRNA/nanoparticle complex form, prepared at various N/P ratios from 1 to 9 as specified. The pDNA was run through a 2.0% gel, stained with EtBr (0.5μg/mL) and visualized using an UV transilluminator. A) nanoparticles with PEI content = 43%, B) nanoparticles with 38% PEI content.

4.3.3 Release of pDNA from gelatin/PEI Nanoparticles

Figure 4.4 shows the AGE results of the release of pDNA from the nanoparticles using poly(L-aspartic acid) (pAsp). Plasmid DNA and nanoparticles were allowed to form complexes with an N/P ratio of 2 (NP/pDNA ratio (w/w) = 0.5341). After that, pAsp with COO^-:P ratio = 100:1 and 150:1 was added to each of the complex. pAsp is an anionic polymer that contains rich carboxylic groups. It was added in large excess by polyelectrolyte exchange reaction to compete with pDNA to release pDNA from the nanoparticles. However, the presence of bands in the top (wells) of lanes 5 and 6 shows that some of the pDNAs were still complexed with the nanoparticlese; whereas the presence of bands at the middle levels shows that some of the pDNAs have been released. The amount of pAsp added was not enough to completely release the pDNA. So, the release analysis was repeated by increasing the amount of pAsp added and extending the incubation time.

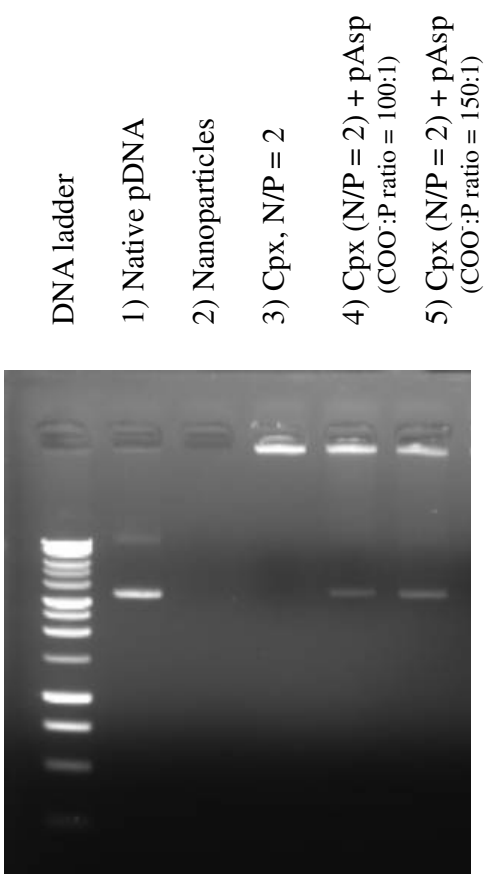

Figure 4.4. AGE (0.8% gel; 0.5µg/mL EtBr) study of the release of pDNA from pDNA/nanoparticle complex by poly(L-aspartic acid) (pAsp) showing the electrophoretic mobility of (1) the native pDNA, (2) nanoparticles, (3) pDNA/nanoparticle complex and (4-5) complex with pAsp addition as specified. The complexation time was 30 min at room temperature. After that, the complex was added with pAsp and incubated for 2 hours at room temperature.

Figure 4.5 shows the same study with increasing amount of pAsp added and extending the incubation time. In Figure 4.5a, the amounts of pAsp added for pDNA release were increased to COO^-:P ratio = 500:1 and 1000:1 respectively. In Figure 4.5b, the incubation time of pDNA release was increased to 15 h (overnight) with increasing amount of pAsp added. The results were similar to that of the previous one. The presence of bands at the top (wells) of lanes 5 and 6 shows that after increasing the pAsp to COO^-:P ratio = 1000:1 and extending the incubation time of pDNA release to 15 h, the pDNA could not be fully released; whereas the presence of bands in the middle levels shows that some of the pDNAs have been released.

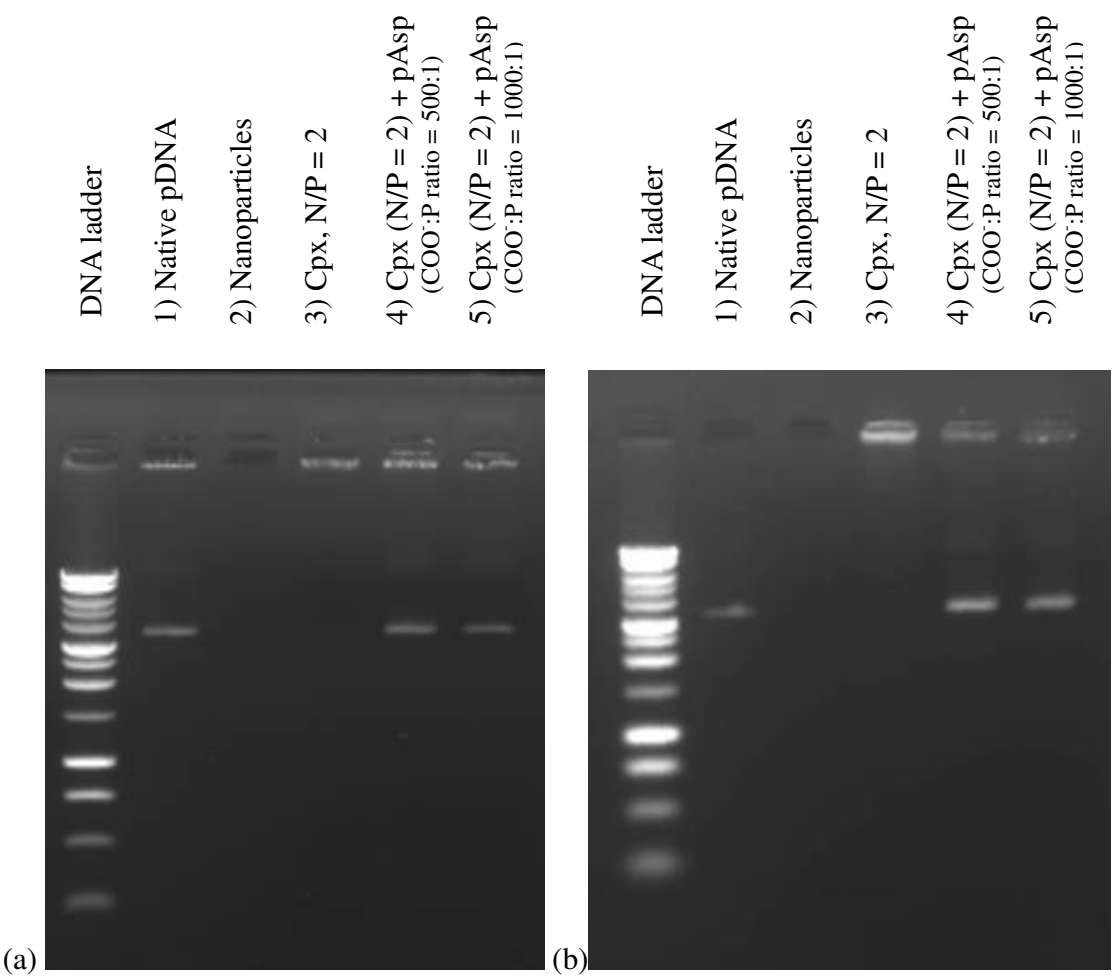

Figure 4.5. AGE (0.8% gel; 0.5μg/mL EtBr) study of the release of pDNA from pDNA/nanoparticle complex by adding poly(L-aspartic acid) (pAsp),showing the electrophoretic mobility of (1) the native pDNA, (2) nanoparticles, (3) pDNA/nanoparticle complex and (4-5) complex with pAsp addition as specified. The complexation time was 30 min at room temperature. After that, the complex was added with pAsp and incubated for (a**) 2 hours** at room temperature, (b) **15 hours** at room temperature.

Figure 4.6 shows the AGE results of the release of pDNA from the nanoparticles with lesser PEI contents using pAsp. Figures 4.6a and 4.6b display the release of pDNA from nanoparticles with 43% and 38% PEI contents respectively. Plasmid DNA and nanoparticles were allowed to form complexes with N/P ratio of 5. After that pAsp with COO^-:P ratio of 100:1 to 500:1 was added to each of the complex. For both kind of nanoparticles, most of the pDNAs were released by adding 100 times molar excess of COO-:P groups of poly(aspartic acid). This was because the pDNA release was more successful at the N/P ratio of 5 than that of 2 as the N/P 5 pDNA/nanoparticle complex had a higher excessive positive surface charge. Therefore, the complexes have higher stability in aqueous form. Meanwhile the net positive surface charge of the complex with the N/P ratio of 2 was lower and the complex was easier to form aggregates. Therefore, the release of pDNA at N/P ratio 2 was hindered when anionic charged pAsp was added.

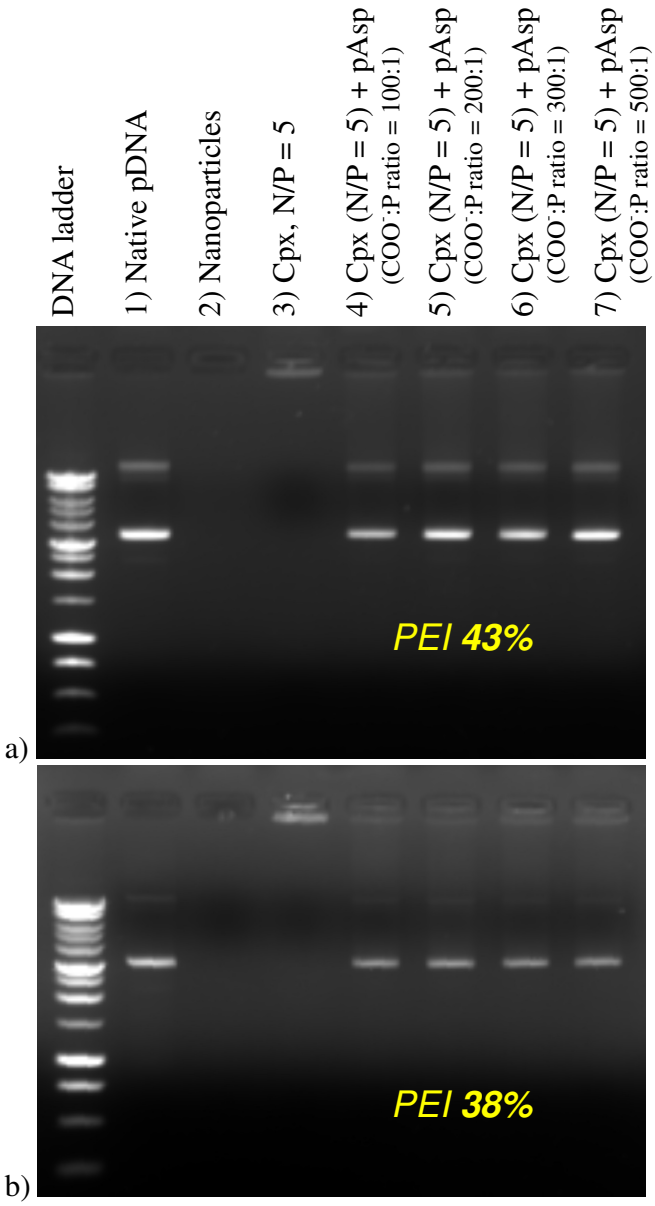

Figure 4.6. AGE (0.8% gel; 0.5µg/mL EtBr) study of the release of pDNA from pDNA/nanoparticle complex by adding pAsp showing the electrophoretic mobility of (1) the native pDNA, (2) nanoparticles, (3) pDNA/nanoparticle complex with N/P ratio of 5 and (4-7) complex with pAsp addition as specified. The complexation time was 30 min at room temperature. After that, the complex was added with pAsp and incubated for 2 h at room temperature. (a) nanoparticles with **43% PEI content** (b) nanoparticles with **38% PEI content**.

N/P ratio denotes for the PEI nitrogen-to-DNA phosphate ratio between PEI and DNA. Theoretically, the amount of nitrogen groups should be equal to or larger than the amount of phosphate groups in order to fully condense DNA molecules, i.e. the N/P ratio should be equal to or larger than 1. But for DNA/nanoparticle complex with N/P ratio of 1, the complex is almost neutral in surface charge and is ease to form aggregate. The high the N/P ratio, the DNA molecules are more tightly condensed and better protected by the excessive positive charge of PEI. And the complex can be stabilized in dispersion form.
In DNA release experiments, large amount of pAsp was added to compete with DNA for PEI. At a higher N/P ratio, higher amount of pAsp was required to release the condensed DNA.

4.3.4 Release of siRNA from gelatin/PEI nanoparticles

Figures 4.7a and 4.7b show the AGE results of the release of siRNA from the gelatin/PEI nanoparticles with 43% and 38% PEI contents, respectively. The siRNA and nanoparticles were allowed to form complexes with N/P ratios of 5 and 6 accordingly. After that, pAsp with COO^-:P ratio of 50:1 to 100:1 was added to each N/P ratio complex. For both kind of nanoparticles, the absence of siRNA band on the well of lanes 4-6 of Figure 4.7 indicates that most of the pDNA were released by adding 50 times molar excess of COO-:P groups of poly(aspartic acid).

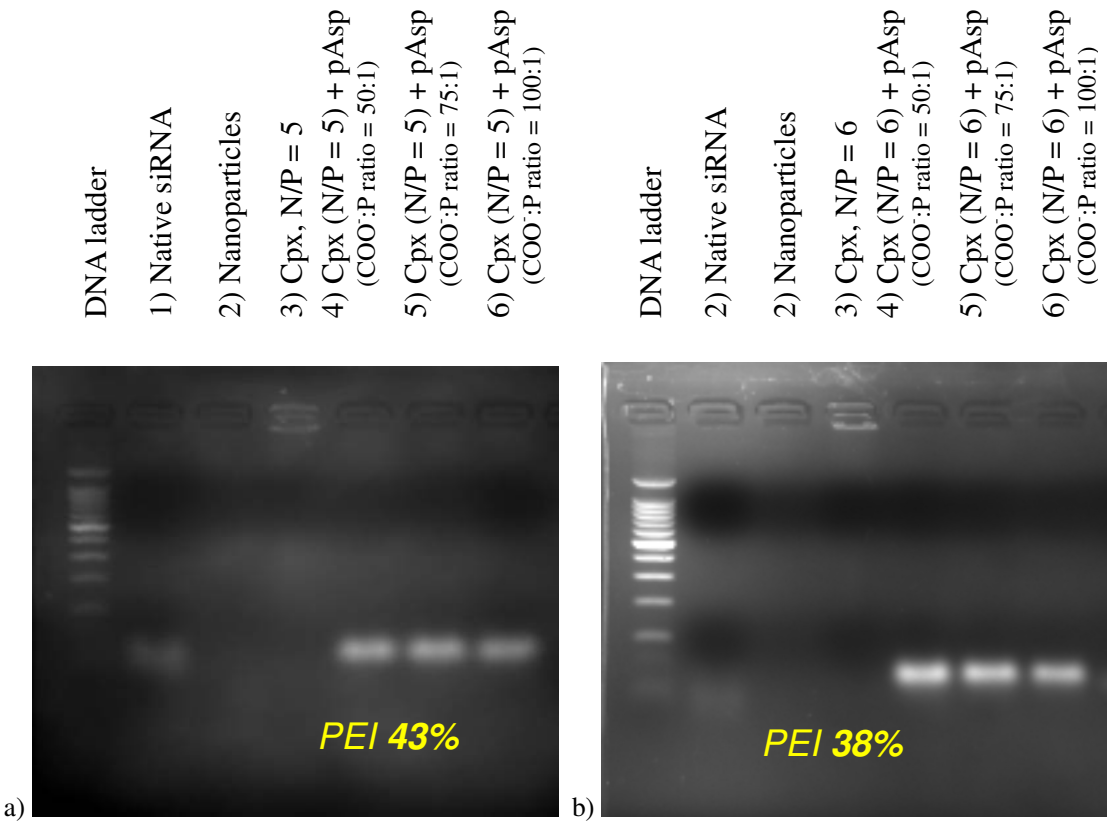

Figure 4.7. AGE (2.0% gel; 0.5μg/mL EtBr) study of the release of siRNA from siRNA/nanoparticle complex by adding pAsp showing the electrophoretic mobility of (1) the native siRNA, (2) nanoparticles, (3) siRNA/nanoparticle complex and (4-6) complex with pAsp addition as specified. The complexation time was 30 min at room temperature. After that, the complex was added with pAsp and incubated for 2 h at room temperature. (a) nanoparticles with **43% PEI content** (b) nanoparticles with **38% PEI content**.

Comparing the results of the pDNA and siRNA release using poly(aspartic acid), it is found that siRNA is much easier to be released than pDNA because the molecular mass of pDNA is much larger than that of siRNA while their negative charge densities are similar. The pDNA and siRNA are 5256 bps and 25 bps long respectively, i.e., the siRNA

is about 210 times shorter than the pDNA. On the other hand, both pDNA and siRNA contain 2 negatively charged phosphate groups per base pair. Therefore, the pDNA is stronger in competing the positively charged amine groups of the PEI shell. As a result, more pAsp is required to release pDNA from the nanoparticles.

4.3.5 Protection of pDNA against enzymatic degradation

Native plasmid DNA is susceptible for enzymatic degradation by DNase in blood circulation. Therefore, protecting DNA from enzymatic degradation is required for an efficient gene transfection. In this study, DNase I was chosen as the model DNA digesting enzyme to analyze the protecting ability of the gelatin/PEI nanoparticles.

The AGE results of native and condensed pDNA digestions are shown in Figures 4.8 and 4.9 respectively. The degrees of enzymatic digestions of the native and condensed pDNA are compared. As shown in Figure 4.8, the two bands present in lane 1, which are located at the upper and lower positions respectively, are the nicked and supercoiled pDNA. The higher band intensity of the supercoiled pDNAs suggests that most of the untreated native pDNAs were in intent closed circular form and minor portion of the pDNA were in nicked circular form. However, after treatment with 0.05 U of DNase I, the band intensity of the supercoiled pDNA decreased while those of the nicked pDNA increased (Lane 2). This means that some of the pDNAs were in one point digestion on one of the DNA strands. In addition, the smear presence in the lower part of lane 2 indicated that some of the pDNA was degraded in fragments with lower molecular mass. When the pDNA was

treated with 0.2 U of DNase I, the nicked and supercoiled bands were almost unobservable. This means that most of the native pDNA was degraded by 0.2 U of DNase I.

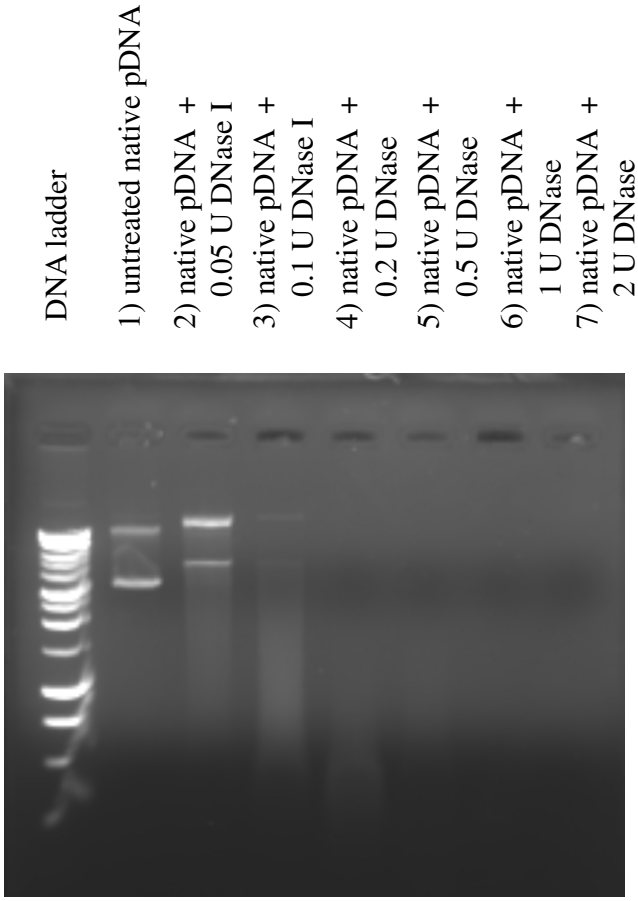

Figure 4.8. AGE (0.8% gel; 0.5μg/mL EtBr) study of the digestion of native pDNA showing the electrophoretic mobility of (1) the untreated native pDNA, (2-7) native pDNA treated with different activities of DNase I as specified. The native pDNAs were digested by DNase I for 10 min.

Figure 4.9 displays the AGE results of the digestions of the condensed pDNA. Upon condensation by gelatin/PEI nanoparticles, the strong band intensity of the supercoiled pDNA and the absence of smear in lane 4 imply that no significant pDNA degradation is observed when the pDNA was treated with 0.5 U of DNase I. From lanes 5 to 10, the band intensities of the supercoiled pDNA decrease while the degree of smears increase. It shows that when the DNase activity is increased from 1-12 U, the degree of DNA degradation increases slowly but the degradation is not complete up to 12 U as the 2 light bands of nicked and supercoiled pDNA are still present.

It can be suggested that the gelatin/PEI nanoparticles give effective protection to the pDNA by reducing the degree of DNase I degradation. When the pDNA is in the native form, the pDNA is fully exposed to the DNase I and can easily be degraded. When the pDNA is condensed onto the surface of the nanoparticles, the surface area of the pDNA is greatly reduced and much less susceptible to be attacked by the enzyme. However, as the pDNA is condensed on the surface of the nanoparticles, there is still some opportunity for pDNA degradation.

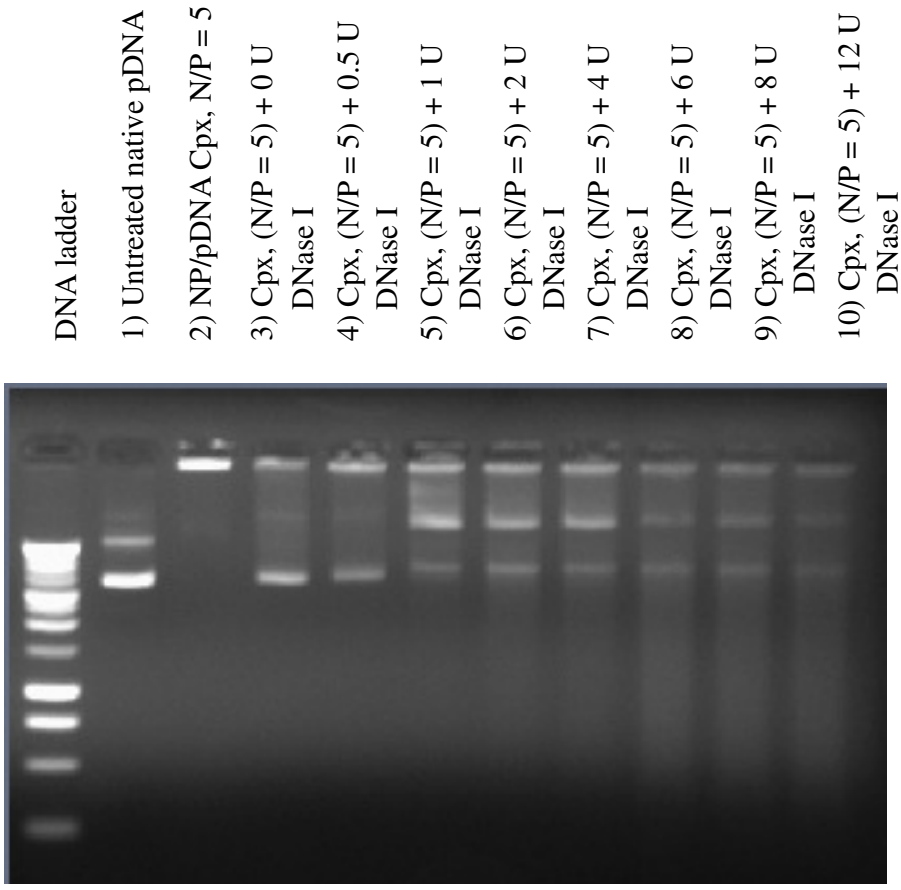

Figure 4.9. AGE (0.8% gel; 0.5μg/mL EtBr) study of the digestion of condensed pDNA showing the electrophoretic mobility of (1) the untreated native pDNA, (2) nanoparticle/pDNA complex with N/P ratio of 5, (3-10) nanoparticle/pDNA complex with N/P ratio of 5, treated with different activities of DNase I as specified. The pDNA/nanoparticle complexes were digested by DNase I for 10 min. After enzyme inactivation, the condensed pDNA was released by adding pAsp and incubated for 2 hours at room temperature.

4.3.6 Protection of siRNA against enzymatic degradation

Native siRNA, similar to the native plasmid DNA, is also susceptible to enzymatic degradation by RNase inside the cells, in blood circulations and body fluids. Therefore protecting the siRNA from enzymatic degradation is required for an efficient gene transfection. In this study, RNase A was chosen as the model siRNA digesting enzyme to analyze the protecting ability of the gelatin/PEI nanoparticles.

The AGE results of native and condensed siRNA digestions are shown in Figures 4.10 and 4.11 respectively. The degrees of enzymatic digestions of the native and condensed siRNA are compared. As shown in Figure 4.10, the siRNA band intensity in lane 2 is lighter than that of lane 1. This implies that the siRNA treated by 1 μg of RNase A was partially degraded. The absence of siRNA band in lane 3 suggests that the majority of siRNA was degraded by 5 μg of RNase A.

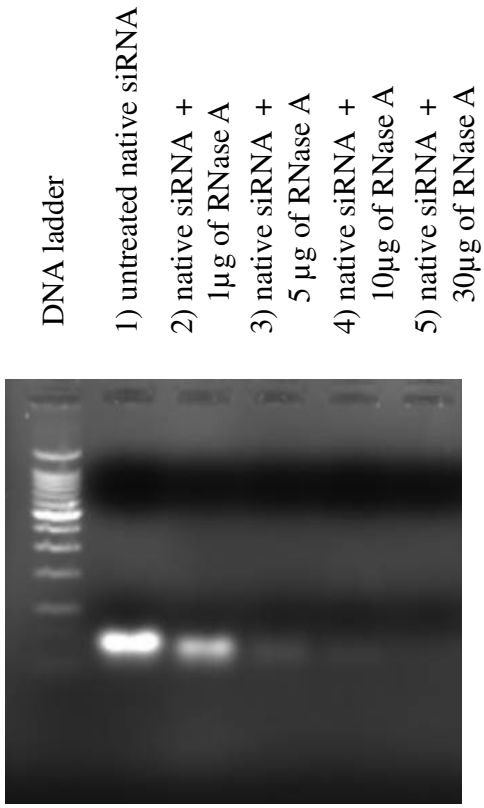

Figure 4.10. AGE (2.0% gel; 0.5µg/mL EtBr) study of the digestion of native siRNA showing the electrophoretic mobility of (1) the untreated native siRNA, (2-7) native siRNA treated with different activities of RNase A as specified. The native siRNA was digested by RNase A for 10 min.

Figure 4.11 shows the AGE results of condensed siRNA digestions. Upon condensation by gelatin/PEI nanoparticles, the siRNA band intensity is still quite strong, implying that when the siRNA was treated with 5 µg of RNase A, the majority of the siRNA were still in intact form. In lanes 4 to 7, the band intensities of the siRNA decrease, indicating that when the RNase A was increased from 5 to 30µg, the degree of siRNA degradation increased slowly and almost no intact siRNA was observed when the siRNA was treated

with 50 μg of RNase A. The gelatin/PEI nanoparticles also give effective protection to the siRNA by reducing the degree of RNase A degradation through condensing the siRNA on the surface of the nanoparticles.

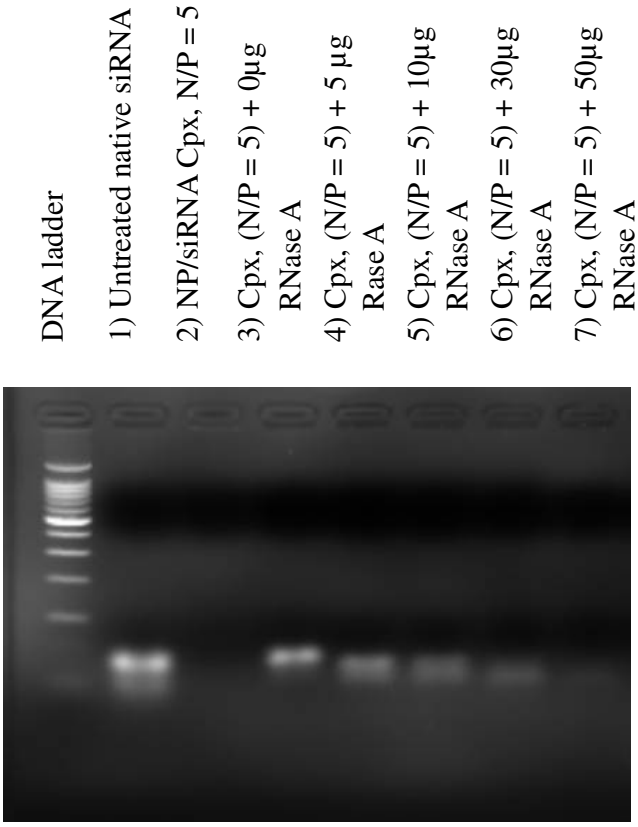

Figure 4.11. AGE (2.0% gel; 0.5μg/mL EtBr) study of the digestion of condensed siRNA showing the electrophoretic mobility of (1) the untreated native siRNA, (2) nanoparticle/siRNA complex with N/P ratio of 5, (3-7) nanoparticle/siRNA complex with N/P ratio of 5, treated with different amounts of RNase A as specified. The siRNA/nanoparticle complexes were digested by RNase A for 10 min. After enzyme inactivation, the condensed siRNA was released by adding pAsp and incubated for 2 hours at room temperature.

The core-shell nanoparticles are less stable in buffer solution when comparing with DI water. It is because the presence of salts can partially neutralize the positive charge of the nanoparticles and the effect is depended on the salt concentration. In DNA complexation studies, the nanoparticles were dispersed in Milli-Q water where the salt screening effect is minimized. Whereas in *in vitro* studies, the nanoparticles were dispersed in water for gene condensation. After that, the siRNA/nanoparticle complexes were diluted with serum free DMEM. The major kinds of salts present in the medium were sodium chloride and sodium bicarbonate with concentration of 0.11 M and 0.044 M respectively. Other components included 5 other kinds of inorganic salts (concentrations ranging from 0.0002 mM to 5 mM), 15 kinds of amino acids (concentrations ranging from 0.08 mM to 4 mM), 8 kinds of vitamins (concentrations ranging from 0.001 to 0.04mM), D-glucose (concentration 5.56 mM) and phenol red (concentration 0.04 mM). In these concentrations of salts, certain degree of screening effect of the electrostatic interaction can be happened. However, the nanoparticles used were in large excess to compromise the reduction of change density due to the screening effect. The N/P ratios used were from 10 to 30. In addition, serum can also contribute the screening effect and cause particle destabilization. Therefore, during transfection of cell culture, the cells were incubated in serum free medium to reduce the screening effect. After removal of nanoparticles, the medium were changed back to FBS containing medium.

4.4 Conclusions

The plasmid DNA and siRNA condensation, protection and release properties of the nanoparticles were analyzed.

In the complexation studies, the gelatin/PEI core-shell nanoparticles could fully condense plasmid DNA at the N/P ratios of 2 to 4 depending on the PEI contents of the nanoparticles. In addition, the nanoparticles could fully condense siRNA at the N/P ratios of 5 to 6, also depending on the PEI contents of the nanoparticles. It was found that the higher the PEI contents of the nanoparticles, the lower was the fully condensing N/P ratio and the higher was the complexation ability.

In the release experiments, the nanoparticles were allowed to form complexes with pDNA and siRNA respectively with an N/P raito of 5. After adding large excess of poly(L-aspartic acid) (pAsp), both pDNA and siRNA could be released from the nanoparticles and their integrities were maintained. The amount of pAsp required for pDNA release was higher than that of the siRNA. The plasmid DNA was released after adding 100 times molar excess of pAsp while the siRNA was released after adding 50 times molar excess of pAsp.

The pDNA and siRNA's protection ability of the nanoparticles against enzymatic degradations was also determined. The nanoparticles showed good ability in reducing both pDNA degradation by DNase I and siRNA degradation by RNase A through

condensing the pDNA and siRNA on the nanoparticle surface. Most of the native pDNA was degraded when treated with 0.2 U of DNase I. When the pDNA was condensed by the nanoparticles, some intact pDNA was still present when treated with 12 U of DNase A. Similarly, most of the native siRNA was degraded when treated with 5 μg of RNase A. When the aiRNA was condensed by the nanoparticles, some intact siRNA was still present when treated with 30μg of RNase A.

4.5 References

1. Wizard Plus SV Minipreps DNA Purification System Technical Bulletin, TB225: http://www.promega.com/tbs/tb225/tb225.pdf
2. Junghun Suh, Hyun-jong Paik and Byung Jeun Hwang, "Ionization of poly(ethylenimine) and poly(allylamine) at various pH's" *Bioorganic Chemistry 22* **(1994)** 318-327.

4.6 Appendix

A. Calculation of the N/P ratios of the nanoparticle-to-pDNA or siRNA complex:

	pDNA	siRNA
Concentration (determined by UV/VIS spectrophotometer)	0.049 µg/µL	0.514 µg/µL
Volume equal to 0.3 µg of pDNA or siRNA	0.3 / 0.049 = 6.12 µL	0.3 / 0.514 = 0.58 µL
In 1 ug of DNA, there are 0.00303 umol of "P		
No. of mole of phosphate "P" in 0.3 µg of pDNA or siRNA	0.00303 x 0.3 = 0.909 pmole	0.00303 x 0.3 = 0.909 pmole

For N/P ratio of 2:

No. of mole of nitrogen "N" added = 0.909 pmole x 2 = 1.818 pmole

Molecular weight (Mw) of the repeating unit of branched PEI = 43.1 g/mole

(Calculation of the molecular weight of the repeating unit of branched PEI:)

Amine	Primary (1^o)	Secondary (2^o)	Tertiary (3^o)
Molecular structure	($-CH_2-CH_2-NH_2$)	($-CH_2-CH_2-NH-$)	($-CH_2-CH_2-N-$)
Molecular weight	44.1	43.1	42.1
Mole ratio in branched PEI [2]	1	2	1
Average Mw of the repeating unit of branched PEI	44.1x1 + 43.1x2 + 42.1x1 = 43.1 g/mole		

Weight of branched PEI added = 1.818 x 43.1 = 78.4 pg or 0.0784 µg

Concentration of gelatin/PEI nanoparticle dispersion: 0.42% (w/v) or 4.2 mg/mL

PEI content of the gelatin/PEI nanoparticles: 43%

PEI concentration of the nanoparticle dispersion: 4.2 x 43% = 1.81 mg/mL

After 45 times of dilution, the PEI concentration of the nanoparticle dispersion is:

40.2 µg/mL or 0.0402 µg/µL

Volume of nanoparticle dispersion added = 0.0784 / 0.0402 = 1.95 µL

Weight of nanoparticles: 0.0784 µg / 43% = 0.182 µg

Weight ratio of nanoparticle-to-pDNA or siRNA = 0.182 : 0.3 = 0.607

Table of volume of pDNA, nanoparticles dispersion and water added for different N/P ratios for pDNA complexation studies.

N/P ratio	0.5	1	2	3	4	5	6	9
Volume of pDNA (µL)	6.12	6.12	6.12	6.12	6.12	6.12	6.12	6.12
No. of mol of phosphate "P"(pmol)	0.909	0.909	0.909	0.909	0.909	0.909	0.909	0.909
No. of mol of nitrogen "N"(pmol)	0.4545	0.9090	1.818	2.727	3.636	4.545	5.454	8.181
Weight of PEI (µg)	0.0196	0.0392	0.0784	0.1175	0.1567	0.1959	0.2351	0.3526
Weight of NP (µg)	0.0420	0.0841	0.1681	0.2522	0.3363	0.4204	0.5044	0.7566
Volume of NP (0.0402 µg/µL) (µL)	0.49	0.98	1.95	2.93	3.90	4.88	5.85	8.78
Volume of H_2O (µL)	8.39	7.90	6.93	5.95	4.98	4.00	3.03	0.10
Total volume (µL)	15	15	15	15	15	15	15	15
NP/pDNA or NP/siRNA ratio (w/w)	0.152	0.303	0.607	2.43	1.21	1.52	2.43	7.28

B. The calculations of the mole ratio of phosphate P-to-pAsp COO^- group:

Amount of pDNA and siRNA added:

	pDNA	siRNA
In 1 ug of DNA, there are 0.00303 umol of "P		
No. of mole of phosphate "P" in 0.3 µg of pDNA or siRNA	0.00303 x 0.3 = 0.909 pmole	0.00303 x 0.3 = 0.909 pmole

If pAsp is in 100 times molar excess of COO^- group to the phosphate groups,

No. of mole of COO^- group added = 0.909 pmole x 100 = 90.9 pmole

Molecular weight (Mw) of the repeating unit of pAsp = 114 g/mole

Molecular structure of the repeating unit of poly(L-aspartic acid):

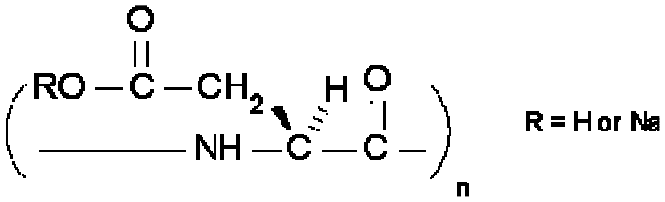

If R = H, molecular weight = 114 g/mole

Weight of pAsp added: 90.9 x 114 = 10,363 pg or 10.4 µg

Concentration of pAsp solution = 16 mg/mL

Volume of pAsp solution added = 10.4 / 16 = 0.65 µL

Table of volume of pAsp added for different COO^-:P ratios for pDNA and siRNA release:

Molar ratio (COO^-:P)	50	75	100	150	200	500	1000
No. of mole of COO^- (pmole)	45.5	68.2	90.9	136	182	455	909
Weight of pAsp (ug)	5.19	7.77	10.4	15.5	20.7	51.9	104
Volume of pAsp (16mg/ml)	0.32	0.49	0.65	0.97	1.30	3.24	6.48

5 *In Vitro* siRNA delivery using gelatin/PEI core-shell nanoparticles

5.1 Materials

The human HeLa cell line (human cervix adenocarcinoma cell) was purchased from the American Type Culture Collection (ATCC, Maryland). Dulbecco's modified Eagle's medium (DMEM) with low glucose, fetal bovine serum (FBS, US, certified), penicillin-streptomycin (P/S) and trypsin-EDTA (0.25% trypsin, 1mM EDTA4Na) were purchased from Gibco BRL (Grand Island, NY). Human Argininosuccinate synthetase targeting small interfering ribonucleic acid (ASS-siRNA), Block-It alexa fluoro red fluorescent (Alexa red siRNA) and Lipofectamine 2000 were obtained from Invitrogen (San Diego, CA). The synthetic ASS-siRNA has a sense strand (5´-AGCAGCUGAGCUCAAACCGGACCUG-3´ and antisense strand 5´-CAGGUCCGGUUUGAGCUCAGCUGCU-3´. RNeasy Mini Kit was purchased from Qiagen (Hilden). Reverse transcription system and GoTaq green master mix were purchased from Promega (Madinson, WI). Fluorescein isothiocyanate isomer I (FITC), and 3-(4,5-dimethylthiazol-2-yl)-2,5-diphenyltetrazolium bromide (MTT) were purchased from Sigma-Aldrich (St. Louis, MO). Custom oligonucleotides were purchase from Sigma and used as PCR primer. All other reagents were in analytical grade.

5.2 Methods

5.2.1 Argininosuccinate synthetase (ASS) gene silencing studies by reverse transcription-polymerase chain reaction (RT-PCR)

HeLa cells were seeded at 5 x 10^4 cells/well of density in 24-well plates (Iwaki) supplemented with 500 µL of DMEM containing 10% FBS and 1% P/S. The cells were incubated at 37°C in a 5% CO_2 humidified incubator for overnight before transfection. Complexes of ASS-siRNA and gelatin/PEI nanoparticles were prepared with 25 pmole of siRNA at different nitrogen-to-phosphate (N/P) ratios in 20 µL of Milli-Q water. The mixtures were incubated at room temperature for 30 min. After that, the complexes were diluted to 100 µL by adding 80 µL of serum free DMEM. Complex of ASS-siRNA and Lipofectamine 2000 and native siRNA were also prepared. Each solution was dissolved in 100 µL of FBS-free medium. The complex of siRNA and Lipofectamine was prepared according to the manufacturer's recommendation. Before transfections, the medium of the cell cultures was removed and changed to 400 µL of FBS-free medium. To start transfections, the complex mixtures were added dropwisely to the cultures followed by 5 h of incubation at 37°C. (The final concentration of each of the siRNA-containing sample was 50 pmole/mL) After washing the cells by PBS and changing the culture medium to 500 µL of fresh FBS-containing medium, the cultures were further incubated for 22 h.

The total RNA of the cells was extracted using the RNeasy Mini Kit according to the

protocol supplied by the manufacturer's manual for animal cell cultures. Briefly, after cell lysis, the total RNA was adsorbed to a silica matrix, washed with the recommended buffer buffers and eluted with 20 µL of RNase-free water by centrifugation. The concentrations of total RNA were quantified by a GeneQuant pro UV/VIS spectrophotometer (Amersham Bioscience).

The cDNA conversion was performed using reverse transcription system according to the manufacturer's recommendations. For each sample, 0.3 µg of total RNA was subjected for cDNA conversion in a PTC-200 Peltier thermal cycler (MJ Research). The RNA was firstly incubated at 70 ^{o}C for 10 min. After that, the following components were added to each sample: $MgCl_2$ (25 mM, 4 µL); reverse transcription 10X buffer (2 µL); dNTP mixture (10 mM, 2 µL); recombinant RNasin® ribonuclease inhibitor 0.5 µL) and AMV reverse transcriptase (high concentration, 15 U); oligo$(dT)_{15}$ primer. The total volume of each sample was made up to 20 µL by adding nuclease free water. The following protocol was then applied: 42^{o}C for 15 min; 95^{o}C for 5 min and 4^{o}C for 5 min.

Polymerase chain reaction (PCR) was then performed in a PTC-200 Peltier thermal cycler (MJ Research) for amplification. For ASS-gene amplification, 2 µL of the cDNA product, 0.4 µL of ASS primer (sense strand 5'-GGGGTCCCTGTGAAGGTGACC-3'; anti-strand 5'-CGTTCATGCTCACCAGCTC-3'), and 10 µL of the 2X green master mix were mixed. Nuclease-free water was then added up to 20 µL of final volume. For GAPDH (house keeping) gene amplification, 0.1 µL of GAPDH primer (sense strand 5'-TGAACGGGAAGCTCACTGG-3'; anti-strand 5'-TCCACCACCCTGTTGCTGTA-3')

was used instead of ASS primer. The reaction conditions of ASS gene amplifications consisted of enzyme activation at 95^{o}C for 3 min followed by 35 cycles at 94^{o}C for 30 s (denaturation), 57^{o}C for 40 s (annealing) and 72^{o}C for 30 s (extension). For GAPDH gene amplifications, the reaction cycle was 25 instead of 35. The reactions were ended by a final extension at 72^{o}C for 10 min followed by refrigeration at 4^{o}C for 5 min. Finally, the resulting PCR products were analyzed by agarose gel electrophoresis (AGE, 0.8% gel) and visualized by ethidium bromide staining. The PCR products for ASS gene and GAPDH gene were 448 bp and 306 bp in length respectively. The intensities of the DNA products were captured and analyzed by the Lumi-Imager F1 (Roche). The percentage knock-down of ASS expressions were calculated by the following equations:

The ASS gene encoding mRNA level was calculated as:

$$I_{ASS} / I_{GAPDH} \qquad \text{(Equation 1)}$$

where I_{ASS} is the band intensity of ASS gene and I_{GAPDH} is the band intensity of GAPDH (house keeping) gene.

$$\text{Percentage knock down} = 100\% - [(I_{ASS} / I_{GAPDH})_s / (I_{ASS} / I_{GAPDH})_c] \qquad \text{(Equation 2)}$$

where $(I_{ASS} / I_{GAPDH})_s$ was the ASS gene encoding-mRNA level of the HeLa cells after treatment and $[(I_{ASS} / I_{GAPDH})_c$ was ASS gene encoding-mRNA level of the HeLa cells without treatment (control).

5.2.2 FITC-labeling of gelatin/PEI nanoparticles

The gelatin/PEI nanoparticles (43% of PEI content) were fluorescently labeled with FITC for visualization in confocal microscopy and flow cytometry. 2.3 mg of the nanoparticles (0.3 mL of nanoparticle dispersion, 7.6 mg mL of concentration) were mixed with 0.1 mL of FITC solution (10 mg/mL in ethanol) and 0.6 mL of borate buffer (0.1 M H_3BO_3, pH 8.5). The micture was stirred gently at room temperature for 5 h in dark (covered the reaction vial with aluminum foil). The weight ratio of PEI (in nanoparticles) to FITC was equal to 1:1. The unreacted FITC was removed by overnight dialysis against autocalved Milli-Q water in a dialysis tubing (MWCO 50 kDa) in dark. The FITC-nanoparticles was stored at 4°C in dark. The reaction scheme between FITC and PEI was illustrated in Figure 5.1.

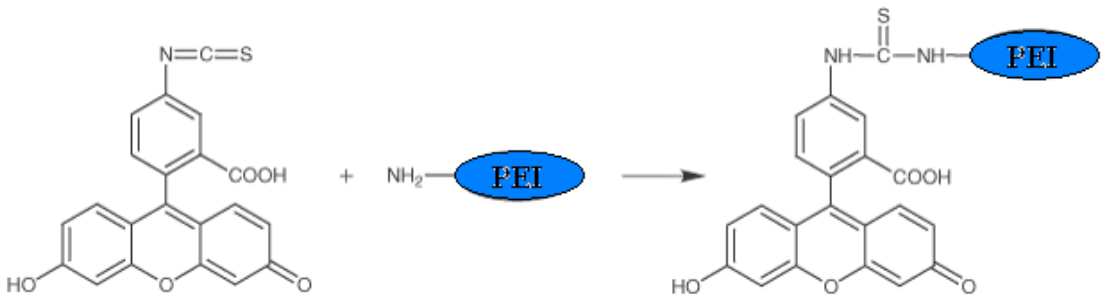

Figure 5.1. Schematic illustration of the reaction between FITC and the amine group of PEI.

5.2.3 Internalization studies of siRNA and gelatin/PEI nanoparticles by confocal laser scanning microscopy (CLSM)

The cellular internalization and intracellular distributions of the gelatin/PEI nanoparticles and siRNA/nanoparticles complexes were examined using LSM 510 META confocal microscope (Zeiss, USA) equipped with 20X and 40X objectives. HeLa cells with 1 X 10^4 and 2 X 10^4 of cell density were seeded in 8-wells chamber slides supplemented with 400 µL of DMEM (10% FBS, 1% P/S) overnight at 37°C in 5% CO_2. Complexes of red-siRNA and FITC-gelatin/PEI nanoparticles were prepared with 25 pmole of Alexa red-siRNA at N/P ratios ranging from 10 to 50 in 20 µL of Milli-Q water. The mixtures were incubated at room temperature for 30 min in dark. After that, the complexes were diluted to 100 µL by adding 80 µL of plain DMEM. Native siRNA solution and nanoparticles dispersions having same concentrations with those of the complexes were also prepared in 100 µL of serum-free medium. The medium of the cells were changed to 300 µL of the fresh serum free DMEM and the FITC-nanoparticles/(Alexa red-siRNA) complex were added. (The final concentration of each of the siRNA-containing sample was 62.5 pmole/mL) For experiments with a longer transfection time, the cells and nanoparticles were incubated for 5 h at 37°C in 5% CO_2 for transfection. After that, the medium was replaced by 400 µL of the fresh serum-containing DMEM (10% FBS, 1% P/S). The cells were post-transfected for 18 h at 37°C in 5% CO_2. For experiments with a short transfection time, the transfection time and post-transfection time were 2.5 h and 2.5 h respectively. For observation of confocal LSM microscopy, the medium was removed and the cells were fixed by 4% paraformaldehyde for 20 min. The chambers were removed.

The antifade solution was added and a cover slip was covered on the slide for microscopic observation. FITC green fluorescence was excited at 488 nm and its emission was collected by green filter (505 – 550 nm band pass). While for the red-siRNA, red fluorescence was excited at 555 nm, and their emission was collected by red filter (>560 nm band pass).

5.2.4 Cellular uptake efficiency studies by flow cytometry

The efficiencies of cellular uptakes of gelatin/PEI nanoparticles and siRNA/nanoparticles complexes were analyzed by FACSAria Cell Sorter (BD Biosciences, USA). The HeLa cells were seeded in 6-well plates at a density of 6 X 10^5 of HeLa cells per well in 2.5mL of FBS-containing DMEM (10% FBS, 1% P/S) overnight at 37^{o}C with supplement of 5% CO_2. Complexes of Alexa red-siRNA and gelatin/PEI nanoparticles were prepared with 125 and 250 pmole of Alexa red-siRNA at N/P ratios of 10 and 30 in 200 μL of Milli-Q water. (The final concentrations of siRNA were 50 and 100 pmole/mL)The mixtures were incubated at room temperature for 30 min in dark. After that, the complexes were diluted to 500 μL by adding 300 μL of FBS-free DMEM. Native siRNA solution and nanoparticles dispersions, having same concentrations with that of the complexes (nanoparticles concentrations 4.6 – 27 ppm), were also prepared in 500 μL of the serum-free medium in dark. The medium of the cells were changed to 2.5 mL of the fresh serum free DMEM and the FITC-nanoparticles/(Alexa red-siRNA) complex were added. For transfections, the cells and nanoparticles were incubated for 5 h at 37^{o}C in 5% CO_2 in dark. After that, the medium was replaced by the fresh serum containing DMEM (10%

FBS, 1% P/S). The cells were post-transfected for 22 h at 37°C in 5% CO_2 in dark. After that, the medium was removed and the cells were trypsinized and resuspended in shealth fluid for measurement. The cells were sorted based on the fluorescent signals by FACSAria Cell Sorter using FITC (green) filter as nanoparticles detection and PI (red) filter for siRNA detection. For each of the measurement, the fluorescence signals of 10^4 cells were counted.

5.2.5 Cytotoxicity studies of gelatin/PEI nanoparticles by MTT assay

The cytotoxicity of the gelatin/PEI nanoparticles were determined by MTT assay and were compared with that of the free PEI polymer. In addition, the complexes of ASS-siRNA/nanoparticles with several N/P ratios were also determined and the cytotoxicities were compared with that of the complex of siRNA/Lipofectamine.

HeLa cells were seeded at 10^4/well in 96-well plates using 100 μL of serum containing DMEM (10% FBS, 1% P/S) overnight at 37°C with supplement of 5% CO_2. Various concentrations of gelatin/PEI nanoparticles dispersions and PEI solution, ranging from 5 to 80 ppm were prepared in FBS-free DMEM. For the siRNA/nanoparticles complex, N/P ratios ranging from 10 to 30 and siRNA/lipofectamine complex were also prepared in FBS-free DMEM. For each of the complexed sample, the amount of siRNA added was varied from 1 to 15 pmole/well (10 – 150 pmole/mL in concentration). The medium of the cells was removed and washed by PBS followed by addition of 100 μL of the PEI solution, nanoparticles, siRNA/nanoparticle complex or siRNA/lipofectamine complex

dispersions. The cells were incubated for 5 h at 37°C in 5% CO_2. The medium of the cells were changed to 100 µL of the fresh FBS-containing DMEM and the cells were further incubated for 22 h at 37°C. 10 µL of the MTT solution (5 mg / mL in PBS) was added to each well and the cells were incubated for another 4 h at 37°C for development of formazan crystals. Subsequently, 100 µL of SDS-HCl solution (0.1 mg / mL in 0.01 M HCl) was added to each well followed by overnight incubation at 37°C to dissolve the formazan completely. The absorbances at 570 nm were measured by 680 microplate reader (Bio-Rad, USA) with subtraction of background absorbance at 655 nm.

The percentage of cell viabilities was calculated based on the following equation:

$$\text{Percentage of cell viability} = (A_{sample} / A_{control}) \text{ X } 100\%$$

where A_{sample} is the absorbance of the nanoparticles or PEI treated cells and $A_{control}$ is the absorbance of the untreated cells.

Each of the samples was done in triplicate.

5.2.6 Studies of cell death caused by siRNA induced ASS deficiency accompany with arginine deiminase (ADI), analyzed by MTT assay

HeLa cells were seeded at 5 X 10^3/well in 96-well plates using 100 µL of serum containing DMEM (10% FBS, 1% P/S) overnight at 37°C with supplement of 5% CO_2. After transfecting with fixed amount of native siRNA, siRNA/nanoparticle complex or siRNA/lipofectamine complex for totally 27 h as described above, the medium were changed to ADI containing medium with ADI concentrations ranging from 0 – 0.0025 U/mL. The cells were incubated for another 3 days at 37°C. The viability of the cells was then determined by adding MTT solution and SDS-HCl solution as described above.

5.3 Results and discussions

5.3.1 Effect of N/P ratio of the nanoparticle/siRNA complex on the knockdown efficiency of the ASS gene

The function of siRNA is to degrade the target mRNA at post-transcriptional level in order to reduce the level of the protein in cells without affecting the expression of other genes. The rationale of the experiments is to determine the ASS encoding-mRNA levels of the HeLa cells treated with native siRNA, siRNA/(gelatin/PEI nanoparticle) complexes and siRNA/Lipofectamine complex and compare the mRNA levels of them with the untreated ones. The mRNA levels of the target gene (ASS) are standardized with the mRNA levels of the house keeping gene (GAPDH). At the same level of GAPDH-mRNA, the lower the level of ASS-mRNA, the better is the specific gene silencing effect.

In the experiments, the complexed and native siRNA were delivered to the HeLa cells for transfections. After that, the total RNA (including the genes of interest) of each of the samples were purified and converted to complementary DNA (cDNA). However, only the genes of interest were amplified and visualized by agarose gel electrophoresis and analyzed based on their bands intensities. The ASS-DNA concentrations of each sample were normalized by dividing them with GAPDH-DNA, i.e,

$$I_{ASS} / I_{GAPDH} \qquad \text{(Equation 5.1)}$$

where I_{ASS} is the band intensity of ASS gene and I_{GAPDH} is the band intensity of GAPDH gene. The percentage knock down of ASS gene of the treated cells was then compared

with the untreated ones (control), i.e,

$$\text{Percentage knock down} = 100\% - [(I_{ASS} / I_{GAPDH})_s / (I_{ASS} / I_{GAPDH})_c] \quad \text{(Equation 5.2)}$$

where $(I_{ASS} / I_{GAPDH})_s$ was the ASS gene encoding-mRNA level of the HeLa cells after treatment and $(I_{ASS} / I_{GAPDH})_c$ was ASS gene encoding-mRNA level of the HeLa cells without treatment.

Figure 5.2 shows the gel images of agarose gel electrophoresis of the RT-PCR products with ASS primer added (Figure 5.2a) and GAPDH primer added (Figure 5.2b). Figure 5.2a shows the band intensities of ASS gene while Figure 5.2b shows those of the GAPDH gene. In Figure 5.2b, most of the samples show similar concentrations of GAPDH gene except the sample siRNA/nanoparticle complex with N/P ratios of 6 and 30, which had slightly higher concentrations. In Figure 5.2a, the band intensity of ASS gene decreases with increasing N/P ratios of siRNA/nanoparticle complex from 3 to 30, showing the decreasing trend of ASS gene expression. The band intensity of the sample treated with siRNA/lipofectamine was similar to that treated with siRNA/nanoparticle complex with an N/P ratio of 15.

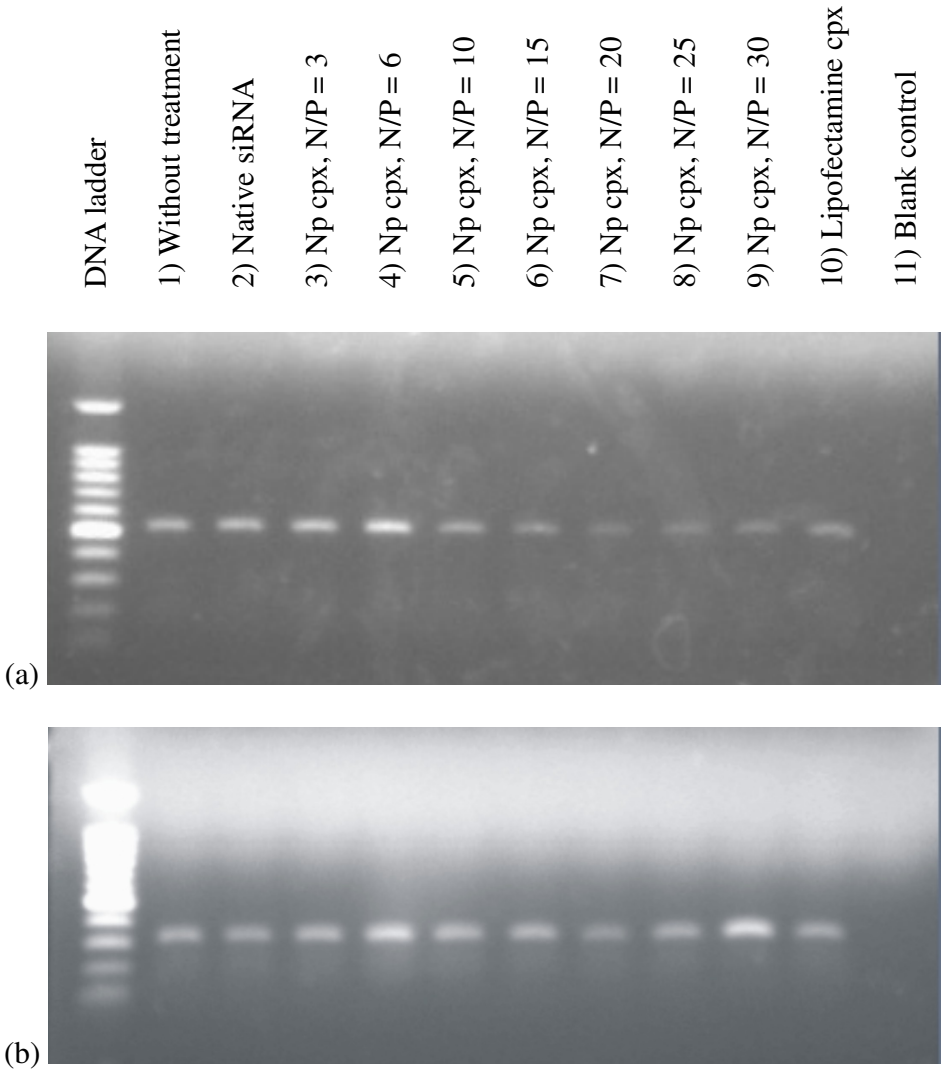

Figure 5.2. Agarose gel electrophoresis of the RT-PCR products with (a) ASS primer added and (b) GAPDH primer added. Prior to RT-PCR, the HeLa cells were (1) untreated, treated with (2) native ASS-siRNA, (3-9) siRNA/nanoparticle complex with various N/P ratios from 3 to 30 and (10) siRNA/Lipofectamine complex (11). Nuclease free water was added instead of RNA for RT-PCR for blank control (zero concentration of RT-PCR product).

The ASS gene silencing efficiencies of the native and complexed siRNA were quantified using Equations 5.1 and 5.2. The percentage knock down of the ASS gene of the samples were statistically analyzed and the results are illustrated in Figure 5.3. All of the cells treated with complexed ASS-siRNA showed lower ASS-mRNA levels than those treated with native siRNA. In addition, most of the cells treated with siRNA/nanoparticle complexes had a higher ASS gene knockdown effect than those treated with siRNA/lipofectamine complex. Among those siRNA/nanoparticle complexes with different N/P ratios, the percentage knockdown increases from about 30% to 70% when the N/P ratios of the complexes increase from 3 to 30 and shows highest gene knockdown percentage at N/P ratio 30. Further increase of complex N/P ratio to 50 resulted in a drop of knockdown percentage to about 50%.

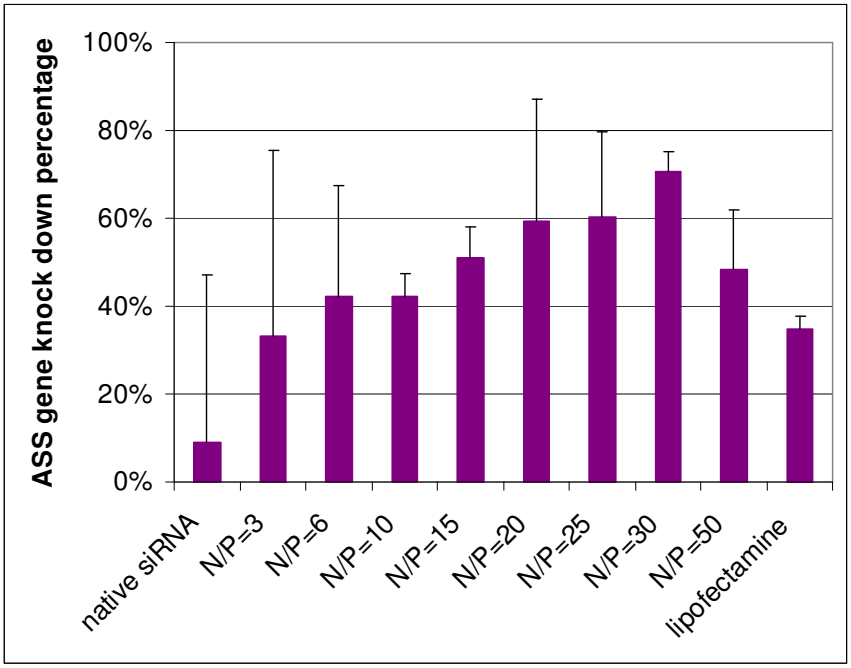

Figure 5.3. Normalized knock down percentages of ASS gene of the HeLa cells transfected with native siRNA, siRNA/nanoparticle complex with various N/P ratios from 3 to 50 (N/P = 3 to 50) and siRNA/Lipofectamine complex (lipofectamine).

In previous studies about the delivery of plasmid DNA using poly(methyl methacrylate)/polyethylenimine (PMMA/PEI) core-shell nanoparticles, the highest gene transfection efficiency for luciferase activity was obtained when the HeLa cells were treated with nanoparticle/pDNA complex with an N/P ratio of 5,[2] which is a relatively low N/P ratio. Unlike pDNA delivery, the gene knockdown efficiency after siRNA transfection is the highest at N/P ratio of 30, which is a relatively high N/P ratio. The difference between pDNA and siRNA delivery can be explained by two reasons.

Firstly, the degree of cytotoxicity is lower at lower N/P ratios of the complexes (see Section 5.3.3). Majority of the cells continue the process of mitosis and this result in a relatively large increase of cell numbers. The amount of internalized siRNA will be halved upon each cycle of cell division. This causes dilution of the internalized siRNA in each cell and a reduction of the gene knockdown effect. Conversely, when the N/P ratios of the siRNA/nanoparticle complexes increase, the nanoparticle concentrations also increase, which causes a higher degree of cytotoxicity (see Section 5.3.3). Majority of cells then stop dividing. So, there is little increase in cell numbers. In this circumstance, the siRNA dilution effect is mild so the gene knockdown effect is little reduced.

Secondly, gene transcription occurs in the nuclei, where mRNA is produced. After that, mRNA is transported to the cytoplasm where gene translation takes place and the encoding protein is synthesized. Therefore, mRNA is present in the nuclei, cytoplasm and the perinuclear region. However, Kim *et al* and Lavigne *et* al suggested that siRNA must

be localized in the cytoplasm, where siRNA action occurs, in order to maintain an effective siRNA intracellular concentration for gene silencing.[3-4] For the gelatin/PEI nanoparticles mediated siRNA delivery data that we have obtained, the siRNA molecules were mainly distributed in the perinuclear region and cytoplasm before mitosis while they were distributed in the nuclei after mitosis. (see Section 5.3.2). In addition, the normal mitotic activity is reduced when the cells are transfected with siRNA/nanoparticle complex with higher N/P ratios. As a result, most of the internalized siRNA remained at the perinuclear region and the cytoplasm had a higher gene knockdown percentage.

5.3.2 Intracellular distributions of siRNA and gelatin/PEI nanoparticles

The cellular uptake and intracellular distributions of the gelatin/PEI nanoparticles and siRNA after treating with native Alexa red-siRNA, FITC-labeled gelatin/PEI nanoparticles and their complexes were analyzed by confocal laser scanning microscopy. Their confocal images were shown in Figures 5.4 to 5.10. The Alexa red-siRNA gave red fluorescence signal while the gelatin/PEI nanoparticles gave green fluorescence signal.

Cellular entry of gelatin/PEI nanoparticles

Figure 5.4 manifests the confocal images of the HeLa cells treated with the FITC-labeled gelatin/PEI nanoparticles. The concentrations of the nanoparticles were the same as those of the siRNA/nanoparticles complexes of N/P ratio of 10 (Figure 5.4A), 20 (Figure 5.4B) and 30 (Figure 5.4C). The cells were transfected for 5 h followed by 18 h of post-transfection incubation, which is similar to the incubation time used in gene silencing studies. Most of the cells treated with the FITC-labeled nanoparticles gave green fluorescence signals which indicated that the nanoparticles were able to be internalized into nearly all of the cells. The exact figures of the percentage of cellular uptake were determined by flow cytometry. The cellular entry of the nanoparticles is due to adsorptive endocytosis of the cells. Moreover, the nanoparticles are observed to be distributed non-specifically at the cytoplasm and the perinuclear regions.

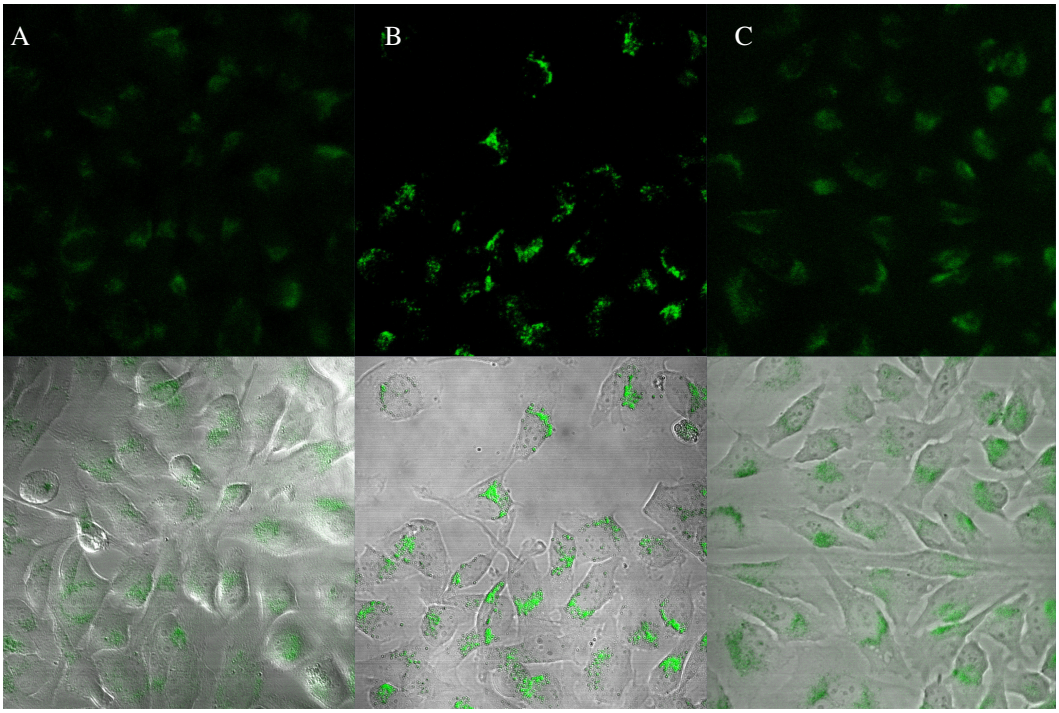

Figure 5.4. Confocal microscopy images of HeLa cells treated with various concentrations of FITC-gelatin/PEI nanoparticles. (A) 5.1 ppm, (B) 10.2 ppm and (C) 15.3 ppm of nanoparticle dispersions. Green fluorescence channel of FITC-nanoparticles (upper) and combination of differential inference contrast (DIC) images and green fluorescence channel (lower). The HeLa cells were transfected with a longer transfection time (5 h of transfection and 18 h of post-transfection) and were observed using 40X amplification.

The intracellular distribution of the nanoparticles was further confirmed by the series of optical sections of the HeLa cells treated with the FITC-labeled gelatin/PEI nanoparticles (Figure 5.5). The optical sections of different optical planes were captured by moving the objective of the microscope from top to bottom. Based on the images, the fluorescence

signals of the nanoparticles were highest at the middle of the focal planes (18 – 26 µm) and decreased when moving to the top and bottom of the cells.

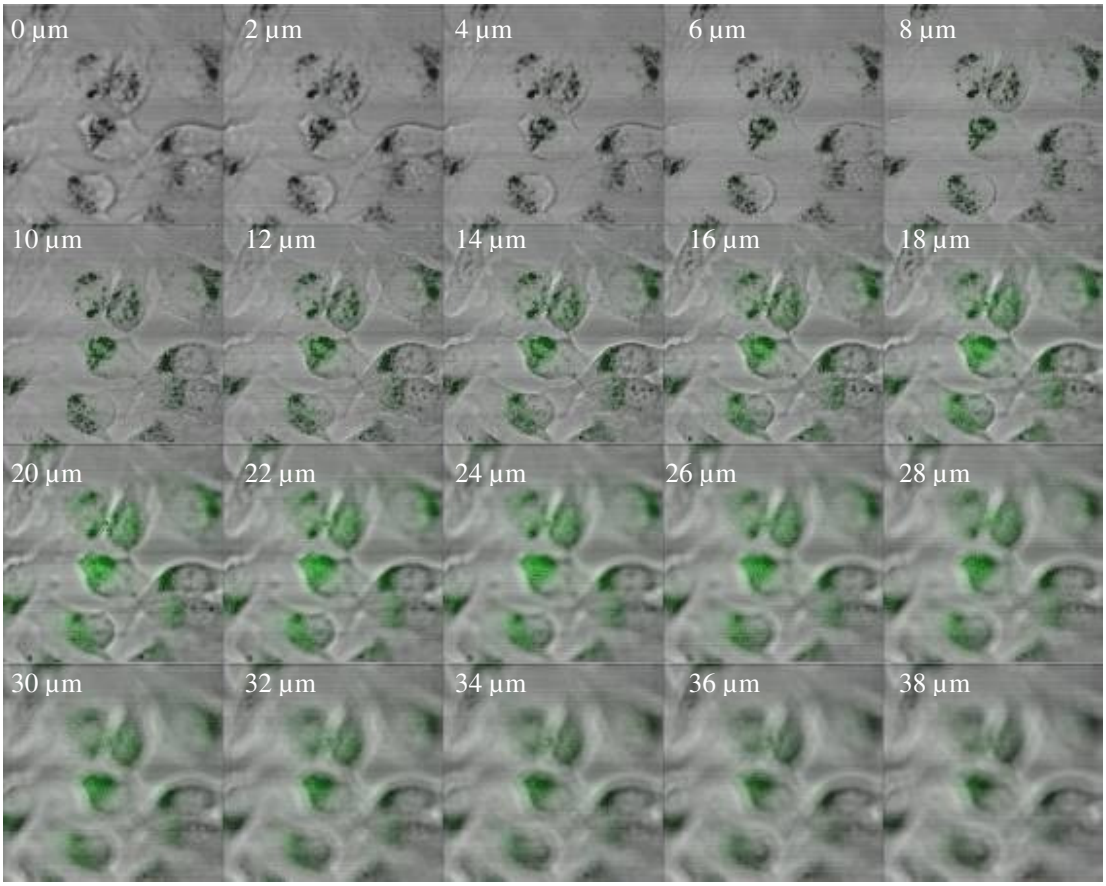

Figure 5.5. Series of optical sections of confocal microscopy images of HeLa cells treated with FITC-gelatin/PEI nanoparticles (15.3 ppm of particle dispersion). The images were in combination of DIC images and green fluorescence channel and were observed using 40X amplification.

Cellular entry of siRNA

Figure 5.6 exhibits and compares the confocal micrographs of the HeLa cells treated with native Alexa red-siRNA (Figure 5.6B) and (Alexa red-siRNA)/(FITC-gelatin/PEI nanoparticles) complexes (Figure 5.6C – D). The micrographs of the untreated cells were also taken as the control reference (Figure 5.6A). The upper row shows the red fluorescence images while the lower row shows the differential inference contrast (DIC) images.

The treated HeLa cells were transfected for 5 h followed by 18 h of post-transfection incubation. The red fluorescence signal treated with native siRNA at Figure 5.6B is similar to those of the untreated cells at Figure 5.6A that no cell-localized red fluorescence was detected. This indicates that most of the native siRNA could not be internalized into the cells by itself. Oppositely, for the cells treated with the complexes of siRNA/nanoparticles with both N/P ratios of 10 and 40, strong red fluorescence signals were observed at most of the cells. This indicates that native siRNA is not able to enter into the cells unless forming complexes with the nanoparticles. In addition, the nanoparticles can deliver the complexed siRNA molecules effectively to nearly all of the cells.

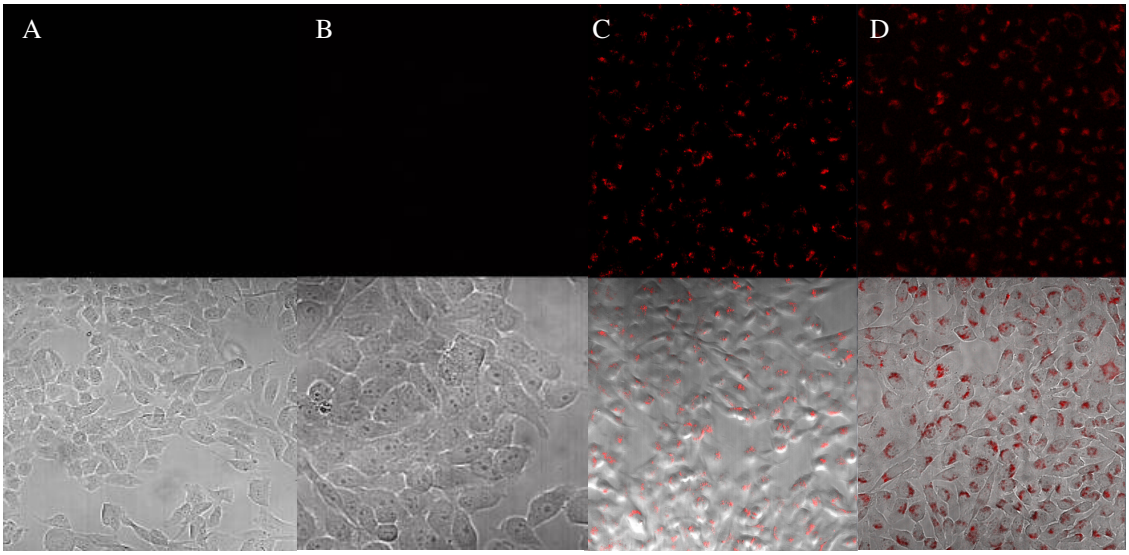

Figure 5.6. Confocal microscopic images of HeLa cells (A) without treatment and after treated with (B) native Alexa red-siRNA and (Alexa red-siRNA)/FITC-nanoparticles complexes with (C) N/P ratio of 10 and (D) N/P ratio of 40. Red fluorescence channel of Alexa red-siRNA (upper row) and combination of DIC images and red fluorescence channel (lower row) and were observed with 20X amplification. The HeLa cells were transfected with a longer transfection time (5 h of transfection and 18 h of post-transfection).

Fluorescence signals at different N/P ratios

Figure 5.7 signifies the confocal images of the HeLa cells treated with various N/P ratios of the (Alexa red-siRNA)/(FITC-gelatin/PEI nanoparticles) complexes. The N/P ratios of those complexes were 10 (Figure 5.7A), 20 (Figure 5.7B) and 30 (Figure 5.7C) respectively.

The red and green fluorescence signals represent the presence of siRNA and gelatin/PEI nanoparticles respectively while the yellow fluorescence signals represent the overlap of the siRNA and the nanoparticles. This is observed that at the image of cells treated with complex having N/P ratio of 10 (Figure 5.7A), the reddish yellow fluorescence signal was in dominant. When at that of N/P ratios of 20 and 30 (Figure 5.7B and C respectively), yellowish green and green fluorescence signals were in dominant respectively. Therefore, it can draw a conclusion that the amount of nanoparticles inside the cells increased when the fed N/P ratio increased.

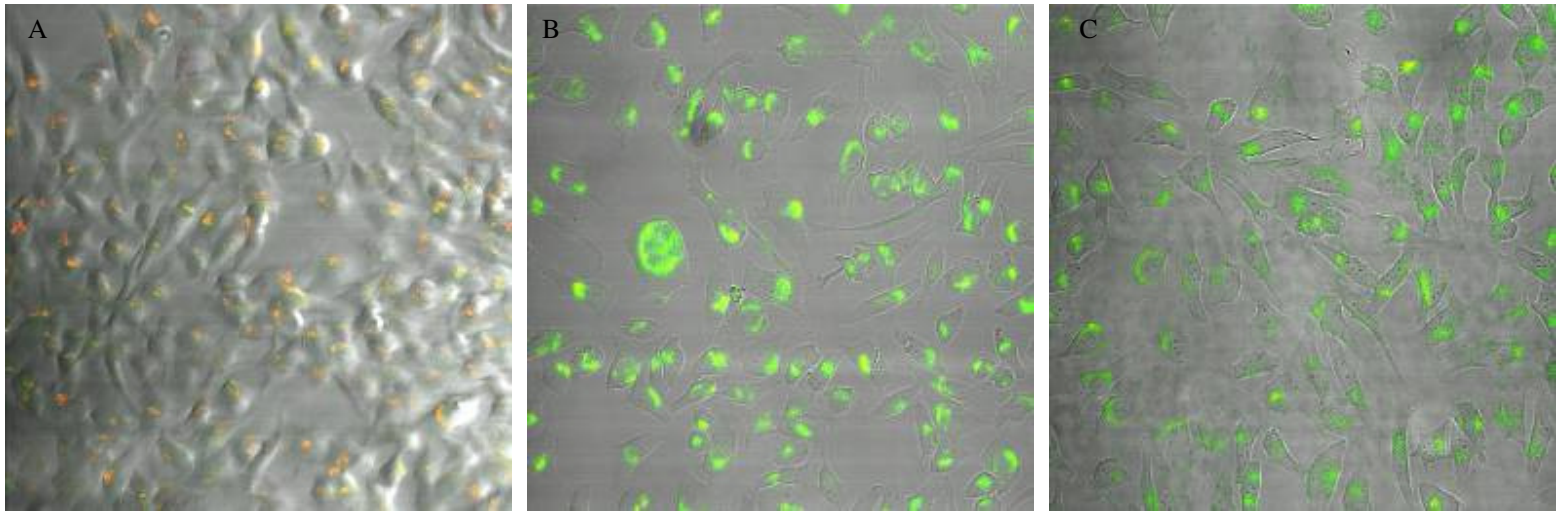

Figure 5.7. Confocal microscopic images of HeLa cells after treated with (Alexa red-siRNA)/FITC-nanoparticles complexes with (A) N/P ratio of 10, (B) N/P ratio of 20, and (C) N/P ratio of 40. Combination of DIC images, green and red fluorescence channels was shown and the images were observed with 20X amplification. The HeLa cells were transfected with a longer transfection time (5 h of transfection and 18 h of post-transfection).

Intracellular distribution of siRNA and gelatin/PEI nanoparticles

After treated with the siRNA/nanoparticle complexes, the intracellular distributions of the siRNA and gelatin/PEI nanoparticles inside the HeLa cells can also be observed from the confocal micrographs. Based on Figure 5.7, the Alexa red-siRNA/FITC-nanoparticle complex were found in the perinuclear region and the cytoplasm of part of the cells. However, the complexes were also found in the nuclei of other cells. The distributions of the complexes at different deepness of these two kinds of cells were further analyzed by capturing the series of optical sections.

Figures 5.8 and 5.9 display the confocal micrographs of the series of optical sections of the HeLa cells, which were transfected with (Alexa red-siRNA)/FITC-nanoparticle complex, illustrating the fluorescence images at different optical planes. At Figure 5.8, the red fluorescence of the siRNA is located at the nucleus (circular region in the middle) and the fluorescence intensity is the strongest at the focal planes corresponded to 4 – 8 μm slices, i.e. the top part of the cell. Whereas, the green fluorescence of the nanoparticles is distributed at the cytoplasm with the strongest intensity at the focal planes corresponded to 20 – 26 μm slices, i.e. the middle and bottom parts of the cell. Therefore, it can be inferred that the siRNA has been dissociated from the nanoparticles and have entered into the nucleus.

Figure 5.9 shows the confocal micrographs of the series of optical sections of the HeLa cells transfected with Alexa red-siRNA/FITC-nanoparticle complex. The fluorescence

signals are different from that of Figure 5.8 that red fluorescence signal is not observed. However, yellow and green fluorescence are present at the pericuclear region and cytoplasm of the cells and the strongest intensity was at the focal planes corresponded to the 10 – 14 μm slices, i.e. the middle part of the cells. This indicated that the siRNA was in complexed form. The nanoparticles can still provide protection to the siRNA in the cytoplasm to prevent degradation of the siRNA molecules.

The intracellular distributions of the siRNA and nanoparticles between the two kinds of cells were different. This is because the cells at Figures 5.8 and 5.9 were divided cells and non-divided cells respectively. Before mitosis, the siRNA/nanoparticle complexes were located at the perinuclear region and undergo endosomal escape via the sponge effect of the branched PEI shells. After that, the siRNA molecules were released from the nanoparticles. During mitosis, the nuclear envelop disassembles and provide an opportunity for the siRNA molecules to enter into the nuclei [4-5] while the nanoparticles were remain at the cytoplasm. The small sizes of the siRNA molecules (25 bp long) also facilitate the entry into nuclei by passive diffusion.

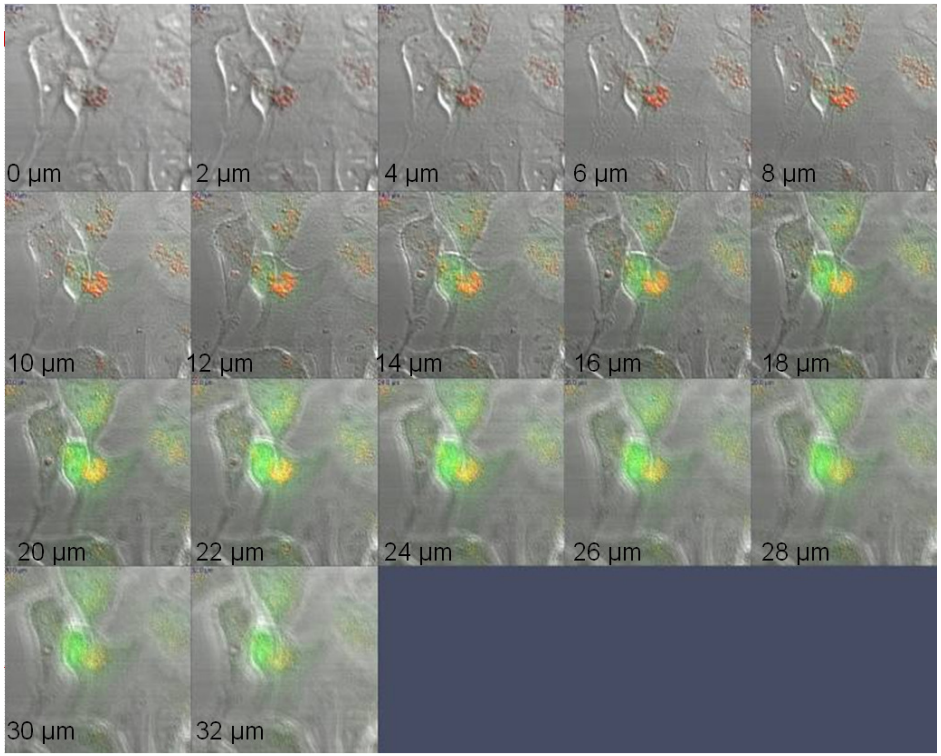

Figure 5.8. Series of optical sections of confocal microscopy images of HeLa cells treated with (Alexa red-siRNA)/FITC-nanoparticles complexes (N/P ratio of 10).

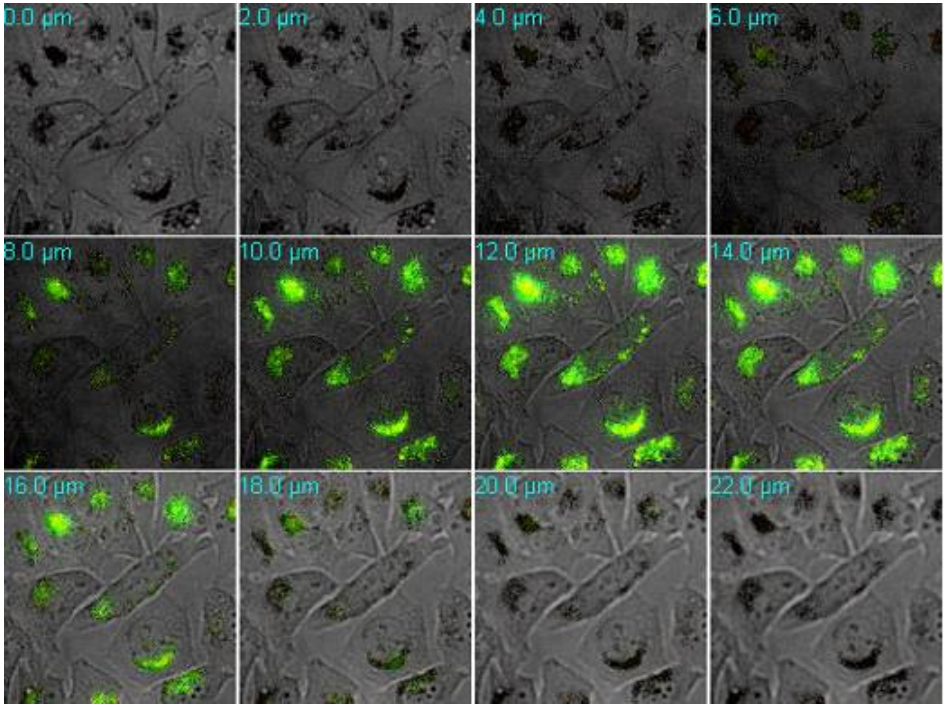

Figure 5.9. Series of optical sections of confocal microscopy images of HeLa cells treated with (Alexa red-siRNA)/FITC-nanoparticles complexes (N/P ratio of 20).

Cellular entry at different transfection time

Figure 5.10 compares the confocal micrographs of the HeLa cells treated with the siRNA/nanoparticle complex with two different transfection times with the same N/P ratio (N/P ratio of 10). The HeLa cells on the left hand side were treated with a longer transfection time of 23 h (5 h of transfection and 18 h of post-transfection incubation) while the cells on the right hand side were treated with a shorter transfection time (2.5 h of transfection and 2.5 h of post-transfection incubation). The red and green fluorescence signals were observed in the cells treated with shorter transfection time but the intensities were weaker than those treated with longer transfection time. This indicates that the complexes can be internalized into the cells after 2.5 h of incubation and the cellular internalization will be continued if the incubation time is extended.

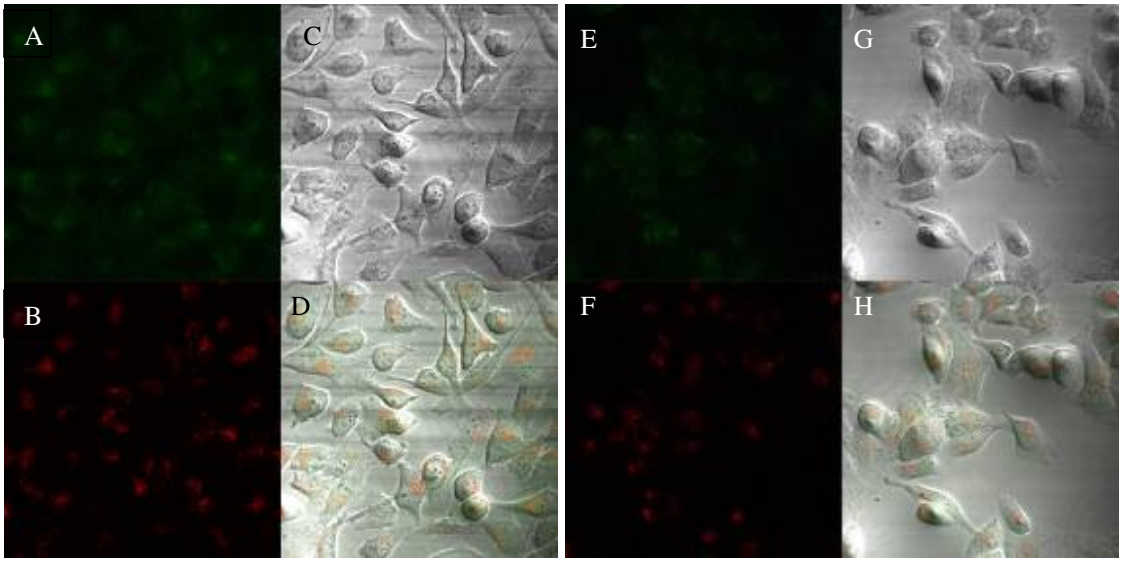

Figure 5.10. Confocal microscopy images of HeLa cells after treating with (Alexa red-siRNA)/FITC-nanoparticles complexes with N/P ratio of 10 (A-D) with a longer transfection time (5 h of transfection and 18 h of post-transfection incubation) and (E-H) a shorter transfection time (2.5 h of transfection and 2.5 h of post-transfection incubation). A & E display green fluorescence channel of FITC-gelatin/PEI nanoparticles; B & F display green fluorescence channel of Alexa redd-siRNA; C & G display the DIC images; D & H display the overlay of the DIC and fluorescence images.

5.3.3 Cellular uptake efficiency of siRNA and gelatin/PEI nanoparticles

The cellular uptake efficiencies of the native siRNA, gelatin/PEI nanoparticles and siRNA/nanoparticles complexes were compared by counting the percentage of HeLa cells that contain the red and green fluorescence signals of the Alexa red-siRNA and FITC-(gelatin/PEI nanoparticles) respectively using flow cytometry. The HeLa cells were treated with native Alexa red-siRNA, FITC-nanoparticles and siRNA/nanoparticle complexes respectively with a total

transfection time of 27 h (5 h of transfection and 22 h of post-transfection incubation). The untreated HeLa cells were served as the control.

The cells were sorted based on their fluorescence intensity. The flow cytometry histogram profiles express the number of cells counted as a function of fluorescence intensity. The higher the fluorescence intensity of the cells, the higher degree of rightward shifting is the profile. Flow cytometry histogram profiles of the HeLa cells illustrating the fluorescence signals of FITC-nanoparticles and Alexa red-siRNA were shown in Figures 5.11 and 5.12 respectively. For counting the percentage of fluorescence positive cells, a gate was firstly set at the highest fluorescence intensity of the untreated cells. The presence of fluorescence signals will cause rightward shifting of the samples' profiles .The percentage of the cell profile that is gated will be counted as fluorescence positive. In addition, the percentage of cells that contained siRNA and nanoparticles were summarized in Table 5.1. Two concentrations of siRNA, which were the same as and doubled of the concentration used in gene silencing study, were used to analyze the cellular uptake efficiency.

Cellular uptake efficiency of gelatin/PEI nanoparticles

Figure 5.11 summarizes the FITC fluorescence signals of the flow cytometry histogram profiles of the HeLa cells treated with various concentrations of FITC-nanoparticles and complexes of (Alexa red-siRNA)/FITC-nanoparticles. The cells treated with the nanoparticles and complexes were resulted in very similar rightward shiftings of the profiles. The higher the concentrations of the nanoparticles, the higher are the extent of the rightward shifting of the profiles comparing

with the control. The percentage of green fluorescence signal positive cells treated with the nanoparticles and complexes, which were gated in regions M2 and M3 respectively, were also summarized in Table 5.1. It can be seen that both nanoparticles and siRNA/nanoparticle complexes show similar percentage of cellular entry of nanoparticles. When the concentration of the nanoparticles was increased from 4.6 to 9.2 ppm, the percentage of cellular uptake increased from about 60% to 90%. The percentage of cellular uptake at 9.2 ppm of the nanoparticles is already very high and further increment of nanoparticle concentration have limited space of improvement of cellular uptake, where the percentages of cellular uptake at 13.7 ppm and 27.4 ppm of nanoparticles were 95% and 99% respectively. The percentages of cellular entry of that of the complexes with the same nanoparticle concentrations were 2-3% lower than that of the nanoparticles. The similar percentages of cellular entry between the cells treated with nanoparticles and siRNA/nanoparticle complex at the same nanoparticle concentration is because both nanoparticles and siRNA/nanoparticle complex mediate adsorptive endocytosis by the positive surface charge. For the siRNA/nanoparticle complex, the nanoparticles are in large excess (N/P ratios of 10, 20 and 30). There is very little change of surface charge of the particles after complexing with the siRNA. So, there is negligible effect to the cellular uptake percentages.

However, the improvement of cellular uptake also accompanies with the increase of cytotoxicity. (see Section 5.4.3 and Figure 5.13) The percentage of viable cells dropped from 100% to 60% when the amount of the nanoparticles added was increased from 5 ppm to 27 ppm. A conclusion can be drawn that the HeLa cells treated with 9.2 ppm of nanoparticles had relatively high internalization efficiency (~90%) and low degree of cytotoxicity (>90% of living cells).

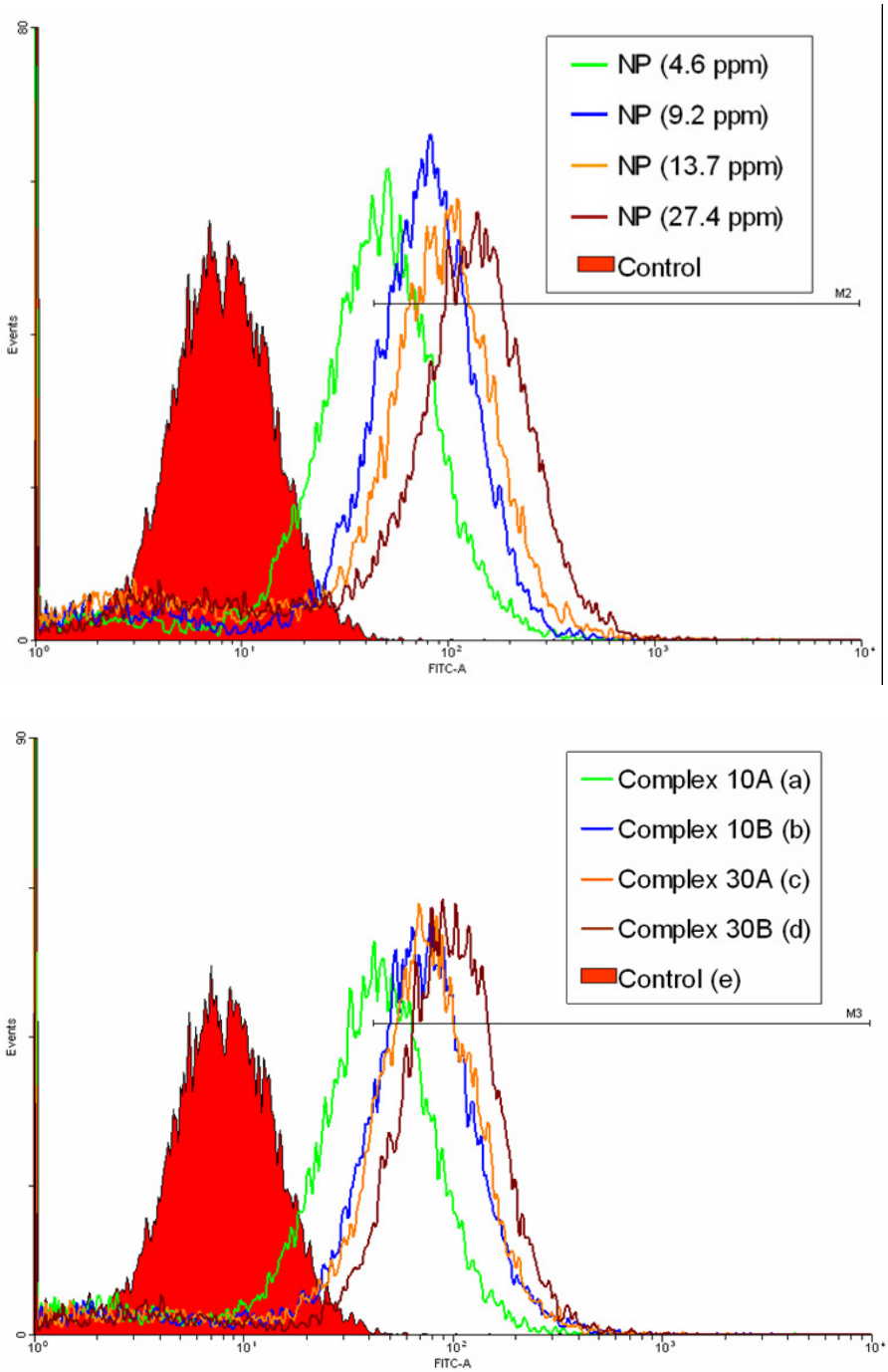

Figure 5.11. Flow cytometry histogram profiles showing green fluorescent signal of HeLa cells treated with various concentrations of (upper graph) FITC-nanoparticles and (lower graph) (Alexa red-siRNA)/(FITC-nanoparticle) complexes. Both graphs: (green) 4.6 ppm of

nanoparticles; (blue) 9.2 ppm; (orange) 13.7 ppm and (brown) 27.4 ppm. Lower graph: (a) siRNA/nanoparticle complex with N/P ratio of 10 (siRNA 50 pmole/mL and nanoparticles 4.6 ppm); (b) complex with N/P ratio of 10 (siRNA 100 pmole/mL and nanoparticles 9.2 ppm; (c) complex with N/P ratio of 30 (siRNA 50 pmole/mL and nanoparticles 13.7 ppm) and (d) complex with N/P ratio of 30 (siRNA 100 pmole/mL and nanoparticles 27.4 ppm). (e)The untreated control group is shown in red filled graph. The siRNA concentrations were the same as that used in gene silencing study (a & c) and double of the concentrations used in gene silencing study (b & d). M2 and M3 represent gated regions (fluorescence intensity 40 – 10,000).

Cellular uptake efficiency of siRNA

Figure 5.12 summarizes the Alexa red-siRNA fluorescence signals of the flow cytometry histogram profiles of the HeLa cells treated with various concentrations of (Alexa red-siRNA)/FITC-nanoparticle complex with N/P ratios of 10 and 30. The positions of the histogram profiles of the cells treated with native siRNA were similar to that of the control. Whereas, all of the cells treated with the complexes were resulted in different extents of rightward shiftings of the profiles comparing with that of the untreated cells, indicating that the nanoparticles can promote different degree of cellular internalization of siRNA.

In addition, the percentage of red fluorescence signal positive cells treated with the complexes gated from region M1 were also summarized in Table 5.1. The cells treated with native siRNA only had negligible percentage of cellular entry. For the cells treated with 50 pmole/mL of siRNA, which is the same as that used in gene silencing studies, the percentage of siRNA-

positive cells treated with the siRNA/nanoparticle complexes with N/P ratios of 10 and 30 were 41% and 84% respectively. The percentage of cellular entry at N/P ratio 30 was about 2 times higher than that of N/P ratio 10. This was because the concentration of the nanoparticle of N/P ratio 10 is not high enough for high percentage of cellular uptake. At that nanoparticle concentration, only less than 60% of the cells contained FITC signals of the nanoparticles. Whereas, at N/P ratio 30, the nanoparticle concentration was high enough that over 90% of the treated cells contained FITC signal of the nanoparticles. As a result, over 80% of the cells internalized with the siRNA.

When the siRNA concentrations were double and the N/P ratios of the complexes were kept at 10 and 30, the cellular entries were further increase to 84% and 95% respectively. The cellular uptake at N/P ratio 10 was further increased for about 50% as the nanoparticle concentration was 2 times higher. More siRNA can be brought into the cells. Unlike the previous one, the cellular uptake at N/P ratio 30 had only about 10% increase when the nanoparticle concentration was doubled. This is because the original percentage cellular uptake is already high. Further increase of nanoparticle concentration has limited area for uptake increament.

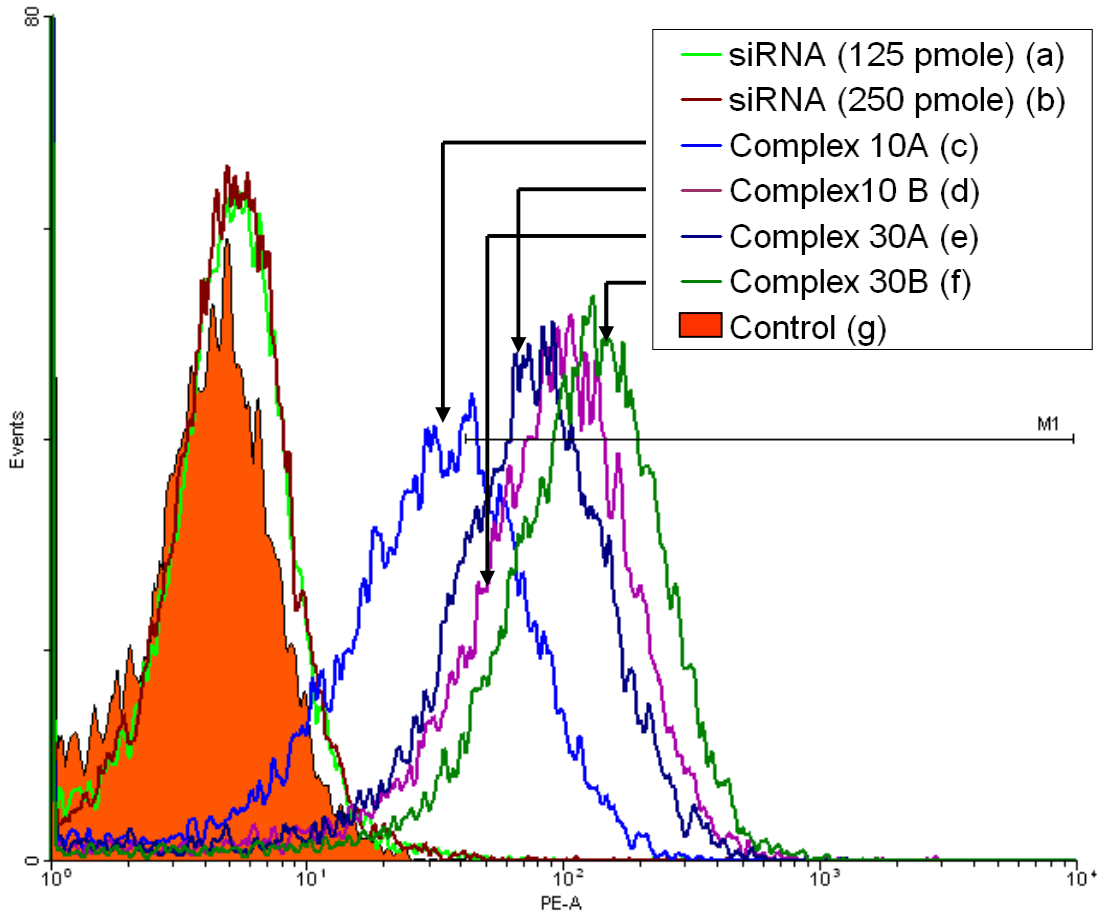

Figure 5.12. Flow cytometry histogram profiles showing red fluorescent signal of HeLa cells treated with (a, b) native Alexa red-siRNA, (c, d) (Alexa red-siRNA)/FITC-nanoparticles complexes with N/P ratio of 10 and (e, f) N/P ratio of 30. The untreated control group is shown in red filled color (g). The siRNA concentrations were the same as that used in gene silencing study (a, c & e) and double of the concentrations used in gene silcening study (b, d & f). M1 represents gated regions (fluorescence intensity 45 – 10,000).

Table 5.1. Percentages of HeLa cells that contained Alexa red-siRNA and FITC-nanoparticles after treating in various conditions (without treatment, treated with native Alexa red-siRNA, FITC-nanoparticles and siRNA/nanoparticle complexes respectively).

Treatment condition	% of cells containing FITC-nanoparticles (P2)	% of cells containing Alexa red-siRNA (P3)
Control (no treatment)	0.1	0.0
siRNA A (50 pmole/mL)*	0.0	0.0
siRNA B (100 pmole/mL)	0.1	0.1
NP (4.6 ppm)	60.3	0.0
NP (9.2 ppm)	89.5	0.0
NP (13.7 ppm)	95.3	0.0
NP (27.4 ppm)	98.9	0.5
Cpx A, N/P ratio 10 (siRNA 50 pmole/mL; NP 4.6 ppm)*	58.3	40.5
Cpx B, N/P ratio 10 (siRNA 100 pmole/mL; NP 9.2 ppm)	87.4	89.2
Cpx C, N/P ratio 30 (siRNA 50 pmole/mL; NP 13.7 ppm)*	91.9	83.6
Cpx D, N/P ratio 30 (siRNA 100 pmole/mL; NP 27.4 ppm)	96.0	94.7

* The siRNA concentrations were the same as that used in gene silencing study

5.3.4 Cytotoxicity studies of nanoparticle mediated transfections

Cytotoxicityt of gelatin/PEI nanoparticles

The cytotoxicities of the gelatin/PEI nanoparticles and free PEI polymer were compared using MTT assay. The HeLa cells were treated with different concentrations of the gelatin/PEI nanoparticles (PEI contents 43% and 38%) and free PEI polymer (25 kD) for 27 h followed by addition of MTT solution. The percentages of cell viability were determined by measuring the degree of conversion from MTT to formazan crystals by the cells. The results are shown in Figure 5.13. Based on Figure 5.13a, the IC_{50} concentration of the free PEI polymer is about 8 ppm. Whereas, the IC_{50} concentrations of the nanoparticles with PEI contents of 43% and 38% are 33 ppm and 50 ppm respectively. The reduction of cytotoxicity is because of the presence of gelatin. Figure 5.13b was obtained by neglecting the gelatin and only focusing on the PEI portion. The IC_{50} concentrations of the nanoparticles with PEI contents of 43% and 38% were 15 ppm and 17 ppm of PEI respectively. Therefore, it can be verified that the cytotoxicty of the PEI is reduced by about 2 times after covalent grafting. In addition, gelatin does not contribute to additional cytotoxicity.

It is believed that covalently immobilizing PEI to the surface of nanoparticles can reduce the contact surface area between PEI and the cellular membrane and lessen the cytotoxicity. It was also found that the higher the PEI contents of the nanoparticles, the higher is the cytotoxicity, owing to the higher surface charges (zeta potentials) of the nanoparticles. Generally, the cytotoxicity is contributed by the positive charge of the cationic polymers and nanoparticles. The

positive surface charge of nanomaterials facilitates cellular endocytosis with compensation of destabilization of cell membranes and cellular disruption.

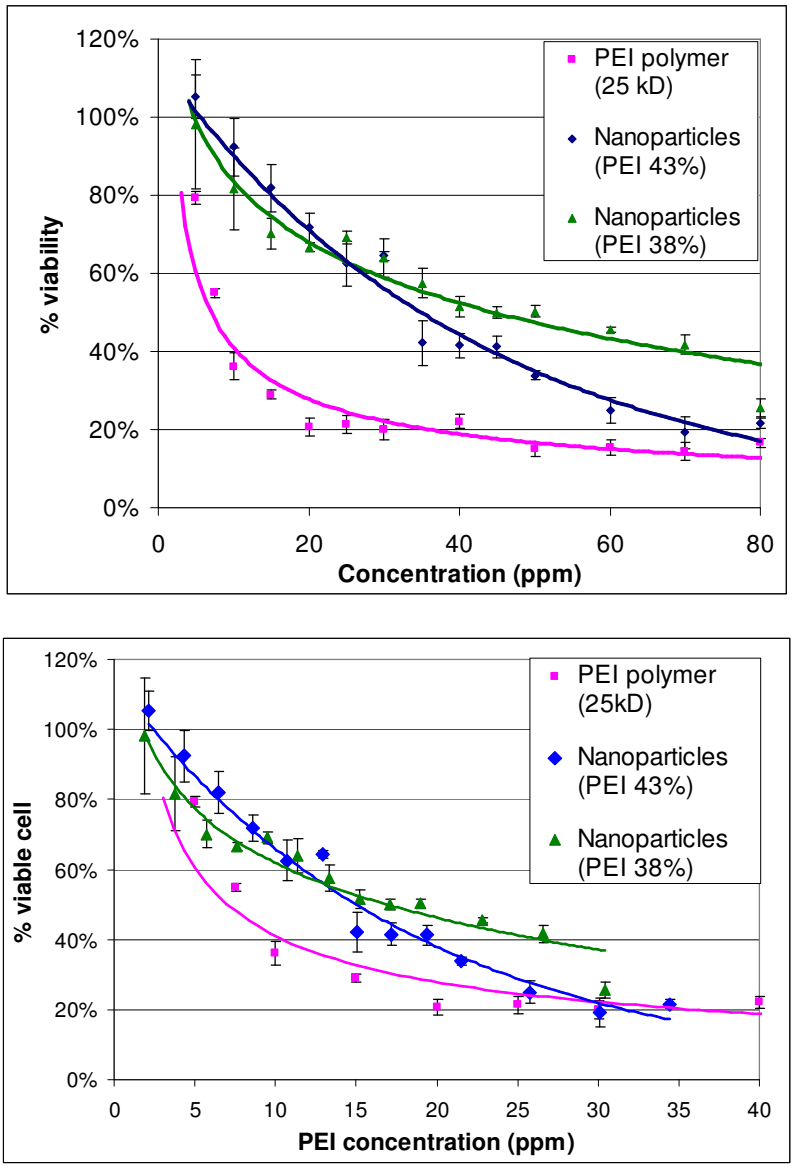

Figure 5.13. The percentage of viable cells after treated with various concentrations of the gelatin/PEI nanoparticles with (♦) 43% of PEI contents and (▲) 38% of PEI content; and (■) free PEI polymer (25 kD). Percentage of viable cells as a function of (upper graph) nanoparticles concentration and PEI polymer concentration and (lower graph) were shown as a function of PEI concentration.

Cytotoxicity of siRNA/(gelatin/PEI nanoparticle) complexes

The cytotoxicities of the (gelatin/PEI nanoparticle)/siRNA complexes with various N/P ratios were analyzed by MTT assay and were compared with native siRNA and liopfectamine/siRNA complex. The gelatin/PEI nanoparticles with 43% of PEI content was used for siRNA complexation and the HeLa cells were transfected for totally 27 h prior to MTT assay.

Based on Figure 5.14, manifesting the percentages of viable cells after treated with different concentrations of native and complexed siRNA, the native siRNA does not show any observable cytotoxicity up to 150 pmole/mL, which is 3 times of that used in transfection studies. However, reduction of percentage of viable cells is found by increasing the concentrations of the lipofectaime/siRNA complex and nanoparticle/siRNA complexes. When comparing the nanoparticle/siRNA complexes with different N/P ratios, there is an overall increasing trend of cytotoxicity by increasing the N/P ratios from 10 to 30.

The siRNA concentration of 50 pmole/mL was used in the transfection studies. At this concentration, the percentages of viable cells after treated with lipofectamine/siRNA complex, nanoparticle/siRNA complexes with N/P ratios of 10, 15, 20 and 30 are 97%, 87%, 92%, 86% and 72% respectively. For further studying the effect of cell death due to ADI treatment, siRNA concentration with relatively low cytotoxicity (over 80% of viable cells) was chosen. Since the cytotoxicity of those treated with N/P ratio 30 of nanoparticle/siRNA complex was too high, the siRNA concentration of 25 pmole/mL will be used instead. For other samples, 50 pmole/mL of siRNA was used.

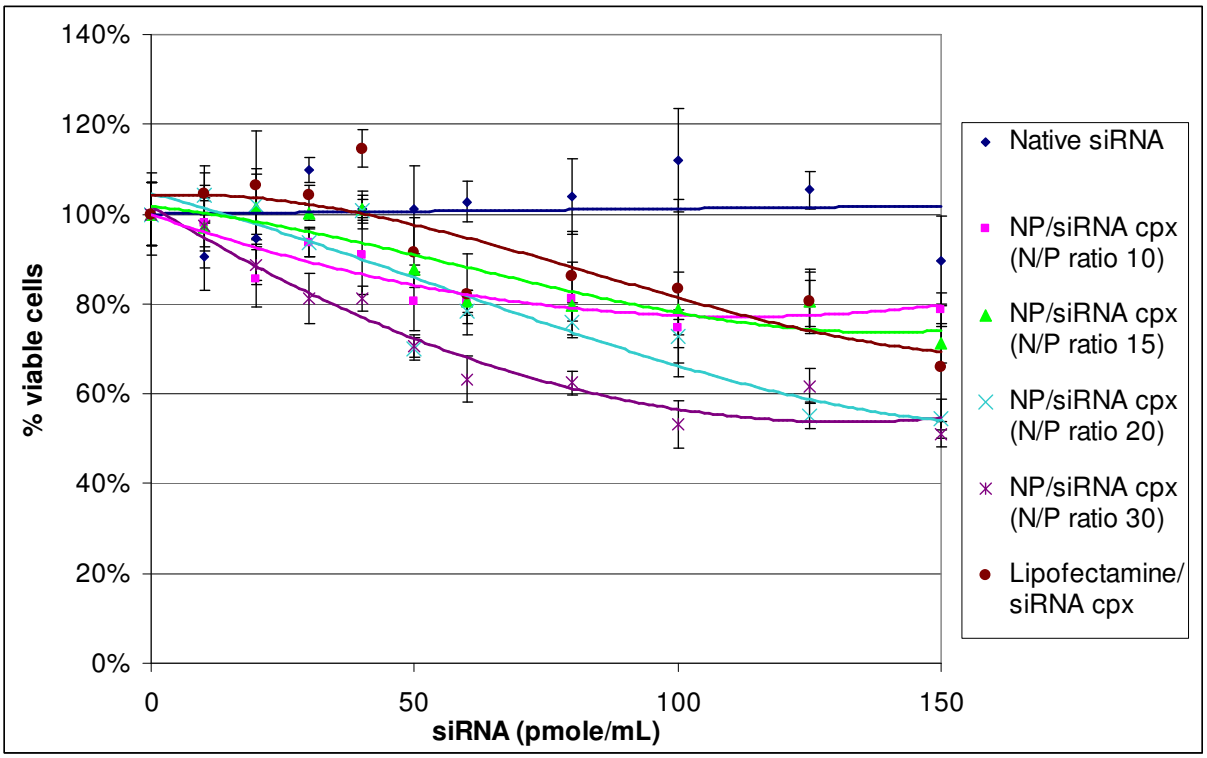

Figure 5.14. The percentage of viable cells after treated with various concentrations of (♦) native siRNA, nanoparticle/siRNA complexes with (■) N/P ratios of 10, (▲) N/P ratio of 15, (x) N/P ratio of 20, (*) N/P ratio of 30 and (●) lipofectamine/siRNA complex. Percentages of viable cells were shown as a function of siRNA concentration.

5.3.5 Cell death after transfected with (gelatin/PEI nanoparticle)/siRNA complexes followed by addition of arginine deiminase (ADI)

As mentioned by Kim *et al,* Touz *et al* and Park *et al*, arginine deiminase (ADI) is found to be able to induce cell death of the cancer cell lines which were ASS negative or were made to be ASS deficicent.[6-8] In the experiments, the HeLa cells were firstly transfected with fixed amount of nanoparticle/siRNA complexes and lipofectamine/siRNA complex to the HeLa cells for totally 27 h to reduce the ASS level of the cells. In addition, other cells were also added with fixed amount of native siRNA for compare. After that, various concentrations of ADI, ranging from 0 to 0.0025 U/mL, were added. The cells were further incubated for 3 days to allow cell death induced by arginine depletion. The final percentages of cell death were analyzed by MTT assay. The results are illustrated in Figure 5.14.

Based on Figure 5.14, addition of ADI caused similar extents of cell death for both siRNA treated and untreated cells. For the control and the cells treated with native siRNA, the percentages of viable cells drop gradually from over 100% to about 75% when the amount of ADI added was increased to 0.0018 U/mL. For the cells treated with nanoparticle/siRNA complexes or lipofectamine/siRNA complex but ADI was not added, different degree of cytotoxicity appeared and the percentage viabilities are lower than 100%. The degree of cytotoxicity in ascending order is lipofectamine, nanoparticle with N/P ratio 10, nanoparticle with N/P ratio 30 (concentration was halved) and nanoparticle with N/P ratio 20. For these four samples, there are about 30% of further reductions of viable cells when the ADI concentration was increased to 0.002 U/mL.

It shows that when comparing with the cells treated with ADI only, the cells treated with both native and condensed siRNA did not cause obvious further reduction of viable cells. The failure is possible to be due to the short interfering time inside the cells. Especially, the viability of the cells was measured after 3 days of ADI administration. The internalized siRNA may be degraded or cannot perform mRNA degradation after such long period of time.

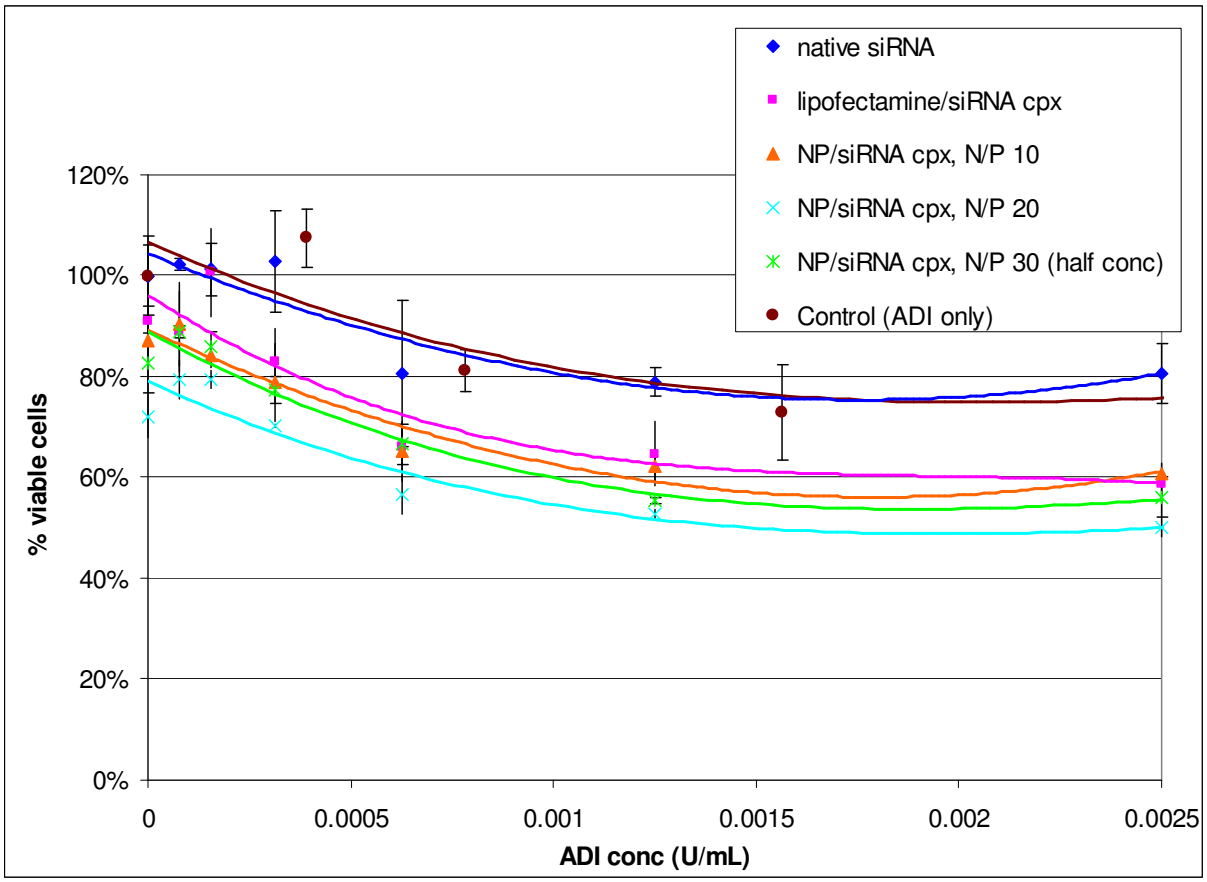

Figure 5.15. The percentage of viable cells after (●) untreated or treated with fixed concentrations of (♦) native siRNA, nanoparticle/siRNA complexes with N/P ratios of (▲) 10, (x) 20 and (*) 30 and (■) lipofectamine/siRNA complex followed by adding 0 – 0.0025 U/mL of ADI. Percentage of viable cells are shown as a function of ADI concentration.

5.4 Conclusions

A series of *in vitro* experiments have been carried out to investigate the effectiveness of gelatin/PEI nanoparticles in delivering ASS-siRNA to the HeLa cells. The nanoparticles, which have 43% of PEI content, were chosen.

The confocal laser scanning microscopy revealed that the nanonparticles themselves were able to be internalized into the cells and distributed non-specifically at the cytoplasm and the perinuclear region. In addition, the internalization of the native siRNA was found to be rare. Upon complexing with the nanoparticles, the siRNA was present in most of the transfected cells. It was also found that the nanoparticles were present in the cytoplasm and the perinuclear region while the siRNA was either found inside the nuclei or in the perinuclear region. It is believed that the siRNA was in condensed form and be protected by the nanoparticles before mitosis. Whereas, the siRNA was released from the nanoparticles and entered to the nuclei after the process of cell division.

The internalization efficiencies of the nanoparticles and siRNA were also analyzed by flow cytometry. Similar to the results of confocal studies, the percentage of cellular entry of the native siRNA was negligible. However, its cellular entry was greatly promoted by forming complexes with the gelatin/PEI nanoparticles. The higher the concentration of the nanoparticle used for complexation, the high the percentage of siRNA entry. The percentages of cellular entry of the nanoparticle/siRNA complexes with N/P ratios of 10 and 30 were 41% and 84% respectively. However, the improvement of cellular uptake also accompanies with the increase of cytotoxicity.

Combining the results of flow cytometry and cytotoxicity studies, the percentage of viable cells dropped from 100% to 60% when the amount of the nanoparticles added was increased from 5 ppm to 27 ppm. The cells incubated with 13.7 ppm of nanoparticle concentration gave high percentage of cellular entry (about 95%) with mild degree of cytotoxicity (over 90% of viability).

The ASS gene silencing efficiency of the nanoparticle-complexed siRNA was also studied by reverse transcription-polymerase chain reaction (RT PCR). The HeLa cells were treated with the nanoparticle/siRNA complexes with N/P ratios of 3 to 50. When the N/P ratios of the complexes increased from 3 to 30, the percentage of gene knockdown rise from about 30% to 70%. Whereas, the ASS-gene knockdown percentages of the cells treated with native siRNA and lipofectamine/siRNA complex were only about 10% and 35% respectively. This means that the nanoparticle medicated siRNA delivery gave as high as 2 times higher of gene silencing efficiency than those lipofectamine medicated siRNA delivery.

Although when comparing with the treatment of arginine deiminase (ADI), an anti-cancer drug, there is obvious further cell death when the ASS targeting siRNA is delivered to the cells before ADI treatment, it is believed that its due to the short interference effect of the siRNA itself.

5.5 References:

1. Hwan Park, Jun-Beom Lee, Young-Jun Shim, Yong-Jae Shin, Seong-Yun Jeong, Junseo Oh, Gil-Hong Park, Kee-Ho Lee, and Bon-Hong Min, "Arginine deiminase enhances MCF-7 cell radiosensitivity by inducing changes in the expression of cell cycle-related proteins" *Molecules and Cells,* **2008** 25(2) 305-311.

2. Yuen Shan Siu, "Gene delivery using core-shell nanoparticles", M. Phil thesis, The Hong Kong Polytechnic University, Hong Kong (2006).

3. Carole Lavigne, Alain R. Thierry, "Specific subcellular localization of siRNAs delivered by lipoplex in MCF-7 breast cancer cells", *Biochimie* **2007** 89 1245-1251.

4. Sun Hwa Kim, Ji Hoon Jeong, Tae-il Kim, Sung Wan Kim, and David A. Bull, "VEGF siRNA delivery system using arginine-grafted bioreducible poly(disulfide amine)", *Molecular Pharmaceutics* **2009** 6(3) 718–726.

5. Roosmarijn E. Vandenbroucke, Bart Lucas, Joseph Demeester, Stefaan C. De Smedt and Niek N. Sanders, "Nuclear accumulation of plasmid DNA can be enhanced by non-selective gating of the nuclear pore", *Nucleic Acids Research*, **2007** 35(12) e86.

6. S. Brunner, T. Sauer, S. Carotta, M. Cotten, M. Saltik and E. Wagner, "Cell cycle dependence of gene transfer by lipoplex, polyplex and recombinant adenovirus", *Gene Therapy* **2000** 7 401–407.

7. Randie H. Kim, Jodi M. Coates, Tawnya L. Bowles, Gregory P. McNerney, Julie Sutcliffe, Jae U. Jung, Regina Gandour-Edwards, Frank Y.S. Chuang,Richard J. Bold, and Hsing-Jien Kung, "Arginine deiminase as a novel therapy for prostate cancer induces autophagy and caspase-independent apoptosis", *Cancer Research* **2009** 69(2) 700-708.

8. Maria Carolina Touz, Andrea Silvana Rópolo, Maria Romina Rivero, Cecilia Veronica Vranych John Thomas Conrad, Staffan Gunnar Svard and Theodore Elliott Nash, "Arginine deiminase has multiple regulatory roles in the biology of *Giardia lamblia*", *Journal of Cell Science* **2008** 121(17) 2930-2938.

6. Conclusions

The gelatin/PEI core-shell nanoparticles have been synthesized successfully. Firstly, the gelatin microgels were formed by thermal denaturation. After that, the branched polyethylenimine (PEI) polymers were grafted to the gelatin microgels through coupling reaction using *N*-Ethyl-*N*′-(3-dimethylaminopropyl)carbodiimide hydrochloride (EDC·HCl) as coupling reagent. The resultant nanoparticles having PEI contents ranging from 26% to 64% were obtained by varying the reaction pH and amount of PEI added. The core-shell nanostructure of the gelatin/PEI nanoparticles were induced after ethanol treatments. The hydrodynamic diameters of the resultant nanoparticles were 260 – 320 nm depended on the PEI content with narrow size distribution. The surface charges of the nanoparticles were between +20mV to +60 mV at physiological pH depended on the PEI contents of the nanaoparticles and ethanol treatments. The particle size and surface charges can be controlled by the percentage of ethanol solution used and times of ethanol treatments. The scanning electron microscopy (SEM) verified that the gelatin/PEI nanoparticles had spherical shape and uniform size. The transmission electron microscopy (TEM) revealed the core-shell nanostructure of the nanoparticles. The biodegradability of the gelatin microgels and gelatin/PEI nanoparticles were studied by sodium dodecyl sulfate

polyacrylamide gel electrophoresis (SDS-PAGE). It suggested that the gelatin/PEI nanoparticles had a lower degradation rate than those of the gelatin microgels, contributed by the protection of the PEI shell.

In the second part, the gelatin/PEI nanoparticles were used to condense the plasmid DNA (pDNA) and small interfering RNA (siRNA) for gene delivery. It was found that the nanoparticles were able to condense the pDNA and siRNA at N/P ratio of 2 and 5 respectively. The lower the PEI contents of the nanoparticles, the higher the N/P ratio for complete DNA condensation. In the release experiments, the nanoparticles were allowed to form complexes with pDNA and siRNA respectively with N/P ratio of 5. After adding with large excess of poly(L-aspartic acid) (pAsp), both pDNA and siRNA can be released from the nanoparticles and their integrities were retained. The nanoparticles also show good pDNA and siRNA protection ability against enzymatic degradation by gene condensation. The degree of digestion of the condensed genes is much lower than those of the native genes.

In the third part, the effectiveness of gelatin/PEI nanoparticles in delivering ASS-siRNA to the HeLa cells was investigated by *in vitro* studies. The ASS gene silencing efficiency of the nanoparticle-complexed siRNA was studied by reverse

transcription-polymerase chain reaction (RT-PCR). The HeLa cells treated with the nanoparticle/siRNA complex with N/P ratio of 30 gave about 70% of ASS gene knockdown without affecting the house keeping gene (GAPDH). Whereas, the ASS-gene knockdown percentages of the cells treated with native siRNA and lipofectamine/siRNA complex were only about 10% and 35% respectively. The confocal laser scanning microscopy (CLSM) revealed that the nanonparticles themselves were able to be internalized into the cells and distributed non-specifically in the cytoplasm and the perinuclear region while internalization of the native siRNA was rare. The internalization efficiencies of the nanoparticles and siRNA were also analyzed by flow cytometry. Similar to the results of confocal studies, the percentage of cellular entry of the native siRNA was negligible. However, its cellular entry was greatly promoted by forming complexes with the gelatin/PEI nanoparticles. The percentages of cellular entry of the siRNA after complexation with N/P ratios of 10 and 30 were 41% and 84% respectively. However, the improvement of cellular uptake also accompanies with the increase of cytotoxicity. The cytotoxicity of the gelatin/PEI nanoparticles was determined by MTT assay. It was found that the nanoparticles showed reduction of cytotoxicity comparing with the same amount of PEI polymers. Although when comparing with the treatment of arginine deiminase (ADI), an anti-cancer drug, there was no further obvious cell death when the ASS targeting

siRNA was delivered to the cells before ADI treatment, it is believed that it is due to the short duration interference effect of the siRNA itself.

It can be concluded that the biodegradable gelatin/PEI nanoparticles with well-defined core-shell nanostructure have been synthesized and well characterized. The particle sizes and surface charges of the resultant nanoparticles are well controlled and have been optimized so that the nanoparticles is able to been applied at gene carriers. The nanoparticles can condense, protect the gene molecules and deliver the genes to the nuclei or cytoplasm of the cells with high efficiency. After internalization, the siRNA can still perform down-regulation of specific gene and the gene silencing effect is much higher than those using lipofectamine as gene carrier. Therefore, the gelatin/PEI core-shell nanoparticles that we have developed have a potent potential to be the effective gene carriers.